

AMERICAN UNIVERSITY OF BEIRUT

UNDERSTANDING SELF-ASSEMBLY BEHAVIOR AND
NANOCAPSULE FORMATION OF POLY(ETHYLENE OXIDE)-
BLOCK-POLY(PROPYLENE OXIDE)-*BLOCK*-
POLY(ETHYLENE OXIDE): APPLICATION AS VEHICLE FOR
CURCUMIN DELIVERY AND FLUORESCENCE SENSING

By

LINDA MOHAMMED BECHNAK

A thesis
submitted in partial fulfillment of the requirements
for the degree of Master of Arts
to the Department of Chemistry
of the Faculty of Arts and Sciences
at the American University of Beirut

Beirut, Lebanon

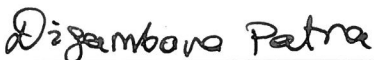
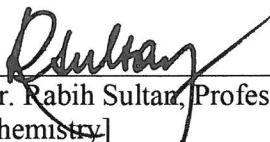
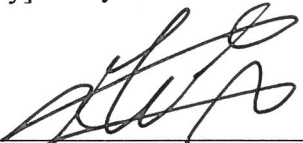
February 2018

AMERICAN UNIVERSITY OF BEIRUT

UNDERSTANDING SELF-ASSEMBLY BEHAVIOR AND
NANOCAPSULE FORMATION OF POLY(ETHYLENE OXIDE)-
BLOCK-POLY(PROPYLENE OXIDE)-*BLOCK*-
POLY(ETHYLENE OXIDE): APPLICATION AS VEHICLE FOR
CURCUMIN DELIVERY AND FLUORESCENCE SENSING

by
LINDA MOHAMMED BECHNAK

Approved by:

	[Signature]
[Dr. Digambara Patra, Associate Professor] [Chemistry]	Advisor
	[Signature]
[Dr. Rabih Sultan, Professor] [Chemistry]	Member of Committee
	[Signature]
[Dr. Mohamad Hmadeh, Assistant Professor] [Chemistry]	Member of Committee

Date of thesis/dissertation defense: [February 5, 2019]

AMERICAN UNIVERSITY OF BEIRUT

THESIS, DISSERTATION, PROJECT RELEASE FORM

Student Name:

Bechnak Linda Mohammed
Last First Middle

Master's Thesis
Dissertation

Master's Project

Doctoral

I authorize the American University of Beirut to: (a) reproduce hard or electronic copies of my thesis, dissertation, or project; (b) include such copies in the archives and digital repositories of the University; and (c) make freely available such copies to third parties for research or educational purposes.

I authorize the American University of Beirut, to: (a) reproduce hard or electronic copies of it; (b) include such copies in the archives and digital repositories of the University; and (c) make freely available such copies to third parties for research or educational purposes

after :One --- year from the date of submission of my thesis, dissertation, or project.

Two --- years from the date of submission of my thesis, dissertation, or project.

Three years from the date of submission of my thesis, dissertation, or project.

[Signature]

Signature

February 7, 2019

Date

This form is signed when submitting the thesis, dissertation, or project to the University Libraries

ACKNOWLEDGEMENTS

First of all, I would like to express my deepest appreciation to my advisor and mentor Dr. Digambara Patra for his patience and support throughout all my master's journey. During the past three years he assisted me in every single way a Dr. might use to support his students. He guided me on the academic level, helped me develop new research projects, enriched my scientific knowledge and taught me how to be patient. Moreover, there were hard times where I had reached crossroads and hopelessness. Each time he supported me to continue and never give up. I thank him for being such a thoughtful and patient Dr whom without I would not have accomplished my thesis.

I would like to acknowledge Professors Rabih Sultan and Mohammad Hemadeh for the knowledge and experience they shared with me in my undergraduate courses and during my graduate life. Also, I would like to thank them for the useful comments and advice they provided me for the thesis. I would like to express a special thanks to Professor Rabih Sultan who was also the graduate advisor throughout my master's period. He provided me with academic guidance and necessary advice to accomplish my graduate courses and thesis.

A special thanks to the Doctors Rony Khnayzer and Christian Khalil from the Department of Natural Sciences at Lebanese American University for their cooperation and help in the photodynamic therapy part.

A special thanks goes to CRSL members; Ms. Rania Chatila, Mr. Joan Youness, Mr. Chadi Assaf, and Mr. Samer El Khalil for their technical support and assistance.

A heartfelt thanks to the research assistant in our laboratory, Ms. Riham El Kurdi, for being a supportive, energetic, helpful, and creative RA. She gave me experience, useful tips and advice which helped me ace my research projects.

I would like to thank my friend and roommate Fatima Hussein who supported me. During the three years, I spent the happiest moments and aced the hardest times with her. A heartfelt thanks to my friends Zahraa Saleh and Alaa Khaled. Without their support, our shared happy moments and laughter, I could not ace my undergraduate and graduate life at AUB. A special thanks also to my colleagues in the Chemistry department.

Finally, I would like to dedicate this work to my dear family, my father, mother and siblings. No words can express my heartfelt gratitude and sincere appreciation for your constant encouragement, wholehearted support and inspiration at all the stages of my life. I hope I met all your trust and faith in me which helped in reaching this level. Thanks to my older sister who was always there for me, giving me advice and supporting me. The last and heartiest thank you is to my mom. Without your endless genuine caring, support, and prayers for me, I could not have achieved success with good health and aced hard times.

AN ABSTRACT OF THE THESIS

Linda Mohammed Bechnak for Master of Science
Major: Chemistry

Title: Understanding Self-assembly Behavior and Nanocapsule Formation of Poly(ethylene oxide)-*block*-poly(propylene oxide)-*block*-poly(ethylene oxide): Application as Vehicle for Curcumin Delivery and Fluorescence Sensing

F108 is a water-soluble non-ionic triblock copolymer. It belongs to the class of block copolymers, so called pluronics or poloxamers. These copolymers have dual character: hydrophilic and hydrophobic which establishes these molecules as amphiphilic species that can self-assemble in aqueous media into micelles having a hydrophobic core and a hydrophilic surface. Micellization occurs above a certain concentration, known as critical micelle concentration (CMC) and/or above a certain temperature, called critical micelle temperature (CMT). There has been extensive research on the utility of these micellar structures in different fields. On the other hand, extensive research is being held on curcumin, known for its therapeutic effects. However, this efficiency is still limited due to its low water-solubility and oral bioavailability. Therefore, various methods were developed to enhance solubility of curcumin. Moreover, due to its responsive fluorescence properties, curcumin is being extensively used as a probe to target specific systems.

In this work, properties of F108 are studied in solution using fluorescence technique and curcumin as the molecular probe. Fluorescence of curcumin has been tracked in solutions of different concentrations of F108. The CMC and CMT have been found to be 23.2 μM and 35 $^{\circ}\text{C}$ respectively. Furthermore, fluorescence quenching technique, using Cetylpyridinium Bromide (CPB), has established the position of curcumin. Effect of ionic strength and bile salt on the CMC and CMT values of F108 is evaluated through curcumin probing. CMC has decreased with the increase in the concentration of the three salts except for NaC. The effect has been arranged in decreasing order as follows: NaDC > NaCl > NaC. On the other hand, the effect of the three salts on the CMT of F108 has been found to be less remarkable, with a 1-fold decrease for NaCl and NaDC and almost no change for NaC. Lastly, quenching results, using CPB which has proved to be a better quencher, have established that curcumin is located at the stern layer of the micelle.

Curcumin is well known for its therapeutic efficiency that is yet limited by its poor solubility in water and low oral bioavailability. To overcome these limitations, we attempt to stabilize curcumin through encapsulating it in F108 nanocapsules having a 1:1 drug to copolymer ratio. Under scanning Electron Microscopy (SEM), they have appeared as spherical particles of size between 270 and 310 nm. Besides, the interaction between curcumin and F108 is assessed by thermogravimetric analysis (TGA), X-ray diffraction

(XRD), and Fourier Transform Infrared Spectroscopy (FTIR). The XRD has indicated a change in curcumin's structure upon encapsulation. Moreover, the FTIR has verified interaction with F108 at the hydroxyl and carbonyl sites. In addition, the degradation pattern of 1:1 nanocapsules has indicated stability up till ~ 250 °C. Toxicity assays of curcumin and nanocapsules is assessed using two types of cancerous cells, A549 and A375 cells, in the presence and absence of irradiated light. Results have indicated an enhancement in the phototoxicity of curcumin upon encapsulation.

Furthermore, we have investigated the dependence of encapsulation of curcumin on the drug to copolymer ratio. Therefore, a variation of the previous nanocapsules is synthesized where the curcumin to F108 ratio is 1:40. XRD patterns and calculation of the degree of crystallinity have revealed change in packing of curcumin with higher change in the 1:40 ratio. Moreover, in the FTIR spectra have indicated a type of hydrogen bonding and dipole interaction between curcumin and F108. Drug loading was measured using UV-visible spectroscopy. Results have demonstrated an enhancement in curcumin loading from 14.9 % to 79.1 % in the 1:40 nanocapsules. Furthermore, fluorescence and absorbance profiles of curcumin in both nanocapsules have indicated location of curcumin in more hydrophobic microenvironment in the 1:40 ratio. The relative fluorescence yield has increased by 6 times in the 1:40 nanocapsules, which renders them as more sensitive probes to be used later on in our sensing study. Therefore, based on the functionality of curcumin as a fluorescent transducer, encapsulated curcumin is used in biomedical application as DNA and RNA sensing. Detection limits are detected as 50 μM and 60 μM for DNA and RNA respectively. The interaction between the nanocapsules and our targeted molecules is further approved by zeta potential studies. Furthermore, the real interaction of DNA with the encapsulated curcumin is confirmed by the interaction of the adenine and cytosine nucleotides. This has been verified through zeta potential measurements. Moreover, our prepared nanocapsules has presented a high percentage recovery of DNA and RNA (96-101%). Finally, stability results have illustrated a high photostability of encapsulated curcumin, indicating that our nanocapsules can be considered as a stable sensor during measurement time.

CONTENTS

ACKNOWLEDGMENTS.....	v
AN ABSTRACT OF THE THESIS	vi
LIST OF ILLUSTRATIONS	xi
LIST OF TABLES	xiv

I. INTRODUCTION	1
A. Block Copolymers.....	1
1. Background	1
2. Structure	2
3. Nomenclature	3
4. Micellization of Pluronics (the hydrophobic effect).....	3
5. Thermodynamics of micellization	4
6. Morphologies of Micelles.....	7
7. Factors that affect properties of Micelles	8
8. Fluorescence probing as a new method to study micellization behavior	11
9. Polymeric micelles as drug delivery systems	12
B. Curcumin	14
1. Background	14
2. Structure	15
3. Photophysical properties of curcumin	16
4. Applications.....	16
5. Limitations of Curcumin	20
6. Means to overcome limitations of curcumin	20
C. Fluorescence	22
1. Principal of fluorescence	23
2. Quenching	24
D. Aims	25

II. UNDERSTANDING SELF-ASSEMBLY BEHAVIOR OF POLY(ETHYLENE oxide)-*BLOCK*-POLY(PROPYLENE oxide)- *BLOCK*-POLY(ETHYLENE oxide)..... 27

A.	Introduction	27
B.	Materials and Methods	28
1.	Materials.....	28
2.	Sample preparation.....	28
3.	Instrumentation.....	30
C.	Results and discussion.....	31
1.	Self-assembly and critical micelle concentration	31
2.	Self-assembly and critical micelle temperature.....	41
3.	Location of probe molecule, curcumin.....	48
4.	Formation of F108 micelles in solution.....	52
D.	Conclusion:.....	52

III. NANOCAPSULE FORMATION OF POLY(ETHYLENE oxide)-*BLOCK*-POLY (PROPYLENE oxide)-*BLOCK*- POLY(ETHYLENE oxide) FOR CURCUMIN DELIVERY 53

A.	Introduction	53
B.	Materials and Methods	55
1.	Materials.....	55
2.	1:1 Nanocapsules preparation.....	55
3.	Sample preparation.....	56
4.	Instrumentation.....	57
5.	Spectroscopic method.....	58
C.	Results and Discussion.....	58
1.	Formation of nanocapsules.....	58
2.	Interaction between curcumin and F108 within the Nanocapsules	59
3.	Photodynamic therapy	62
D.	Conclusion.....	67

IV. NANOCAPSULE FORMATION OF POLY(ETHYLENE oxide)- <i>BLOCK</i> -POLY (PROPYLENE oxide)- <i>BLOCK</i> -POLY(ETHYLENE oxide) FOR FLUORESCENCE SENSING	69
A. Introduction	69
B. Materials and Methods	70
1. 1:40 Nanocapsules preparation.....	70
2. Sample preparation.....	70
3. Instrumentation.....	72
4. Spectroscopic method.....	73
C. Results and discussion.....	73
1. Formation of nanocapsules.....	73
4. Interaction within Nanocapsules	74
5. Drug loading.....	78
6. Optical properties of curcumin within Nanocapsules.....	79
7. DNA and RNA sensing	82
D. Conclusion.....	92
V. Conclusion.....	94
VI. References.....	99

ILLUSTRATIONS

Figure I. 1 Structure of triblock copolymers.....	2
Figure I. 2 illustration of typical morphologies formed by amphiphilic block copolymers in solution (red region represents hydrophobic core and blue is for hydrophilic surface)..	8
Figure I. 3 Chemical structures of curcumin tautomers.....	16
Figure I. 4 Jablonski diagram	23
Figure II. 1 Fluorescence emission spectra of curcumin (3.33 μ M) at different concentrations of F108	32
Figure II. 2 Fluorescence intensities of curcumin at 512 nm plotted versus concentration of F108.....	33
Figure II. 3 Fluorescence emission spectra of curcumin (3.33 μ M) at different concentrations of F108 in the presence of 1 mM NaCl.....	34
Figure II. 4 Fluorescence intensities of curcumin at 512 nm plotted versus concentration of F108 and 3.33 μ M curcumin in the presence of A. 1 mM, B. 10 mM, C. 100 mM, and D. 150 mM NaCl	35
Figure II. 5 CMC variation with increasing concentration of sodium chloride.....	36
Figure II. 6 Fluorescence emission spectra of curcumin obtained at different concentrations of F108 and 3.33 μ M curcumin in the presence of 0.25 mM NaC	37
Figure II. 7 Structures of sodium cholate (left) and sodium deoxycholate (right)	38
Figure II. 8 Fluorescence intensities of curcumin at 512 nm versus concentrations of F108 in the presence of 3.33 μ M of curcumin and A. 0.25 mM, B. 0.5 mM, and C. 5 mM NaC.....	38
Figure II. 9 Fluorescence emission spectra of curcumin at different concentrations of F108 in the presence of 0.25 mM NaDC	39
Figure II. 10 Fluorescence intensities of curcumin at 512 nm versus concentrations of F108 in the presence of A. 0.25 mM, B. 0.5 mM, and C. 1 mM NaDC	40
Figure II. 11 Fluorescence emission spectra of 3.33 μ M curcumin obtained at a fixed concentration of F108 and different temperatures.....	43
Figure II. 12 Fluorescence emission spectra of 3.33 μ M curcumin obtained at a fixed concentration of F108 and different temperatures.....	43
Figure II. 13 Fluorescence emission spectra of 3.33 μ M curcumin obtained at a fixed concentration of F108 and different temperatures.....	45
Figure II. 14 Fluorescence emission spectra of 3.33 μ M curcumin obtained at a fixed concentration of F108 and different temperatures.....	45
Figure II. 15 Fluorescence emission spectra of 3.33 μ M curcumin obtained at a fixed concentration of F108 and different temperatures.....	46
Figure II. 16 Fluorescence intensities of curcumin at 512 nm versus temperatures at different concentrations of sodium cholate	46
Figure II. 17 Fluorescence emission spectra of curcumin at different temperatures in the presence of 0.25 mM sodium deoxycholate	47

Figure II. 18 Fluorescence intensities of curcumin at 512 nm versus temperature at different concentrations of sodium deoxycholate.....	47
Figure II. 19 Fluorescence emission spectra of curcumin obtained at different concentrations of CPB.....	50
Figure II. 20 Emission intensity of curcumin at 512 nm versus concentration of CPB	50
Figure II. 21 F_0/F versus concentration of CPB (Stern volmer plot).....	51
Figure II. 22 Fluorescence emission spectra of curcumin at different concentrations of KI. Inset is the emission intensity plotted at 512 nm versus KI concentrations.....	51
Figure II. 23 Schematic illustration of curcumin-F108 micelle formation.....	52
Figure III. 3 11 XRD patterns.....	59
Figure III. 1 Schematic illustration showing the formation of 1:1 nanocapsules.....	58
Figure III. 2 SEM images of 1:1 nanocapsules.....	58
Figure III. 3 XRD patterns.....	59
Figure III. 4 FTIR spectra of free curcumin, F108 and 1:1 nanocapsules.....	61
Figure III. 5 TGA patterns for F108, curcumin and 1:1 nanocapsules.....	62
Figure III. 6 Effects of light on compound activity as measured on A549 and A375 cells. (a) Curcumin using A549 cells, (b) curcumin using A375 cells, (c) nanocapsules using A549 cells, (d) nanocapsules using A375 cells, (e) polymer F-108 using A549 cells, (f) polymer.....	64
Figure III. 7 DNA damage assessment using the comet assay on negative control (pure cells), positive control ($KMnO_4$ solution), nanocapsules and curcumin in the dark (blue) and upon light irradiation (red). The concentration of nanocapsules and curcumin were at the IC_{50} in the dark. Statistical significance was reported versus the negative control as follow: * $P \leq 0.05$ and ** $P \leq 0.01$	66
Figure IV. 1 Calibration curve of curcumin	71
Figure IV. 2 Schematic illustration showing the formation of 1:40 nanocapsules.....	73
Figure IV. 3 SEM images of 1:1 nanocapsules (left) and 1:40 nanocapsules (right) with inset showing magnification of particles.....	74
Figure IV. 4 XRD comparing the 1:1 to 1:40 nanocapsules along with curcumin and F108	75
Figure IV. 5 FTIR spectra of 1:1 and 1:40 nanocapsules, curcumin, and F108.....	77
Figure IV. 6 TGA patterns of 1:1 and 1:40 nanocapsules, curcumin, and F108.....	78
Figure IV. 7 Absorption spectra	80
Figure IV. 8 Fluorescence emission spectra at excitation wavelengths 425 nm	81
Figure IV. 9 Relative fluorescence yields of the prepared nanocapsules compared to free curcumin.....	81
Figure IV. 10 Fluorescence emission spectra of 1:40 nanocapsules at different DNA concentrations (left) and linear correlation of the intensities at 540 nm versus DNA concentration	86

Figure IV. 11 Zeta potential curves for 1:40 nanocapsules (top), DNA (middle), and mixture of nanocapsules and DNA (bottom).....	87
Figure IV. 12 Fluorescence emission spectra of 1:40 nanocapsules at different RNA concentrations (left) and linear correlation of the intensities at 540 nm versus RNA concentration	88
Figure IV. 13 Nucleotide analysis	88
Figure IV. 14 zeta potential curves of 1:40 nanocapsules (top), adenine (middle) and their mixture (bottom).....	89
Figure IV. 15 zeta potential curves of 1:40 nanocapsules (top), cytosine (middle), and their mixture (bottom).....	90
Figure IV. 16 Photostability measurements.....	92

TABLES

Table II.1 CMC values at different concentrations of sodium chloride, sodium cholate and deoxycholate.....	40
Table II.2 CMT values at different concentrations of sodium chloride, sodium cholate and deoxycholate.....	48
Table III.1 Calculated IC ₅₀ of curcumin, nanocapsules and the polymer F-108 on A549 and A375 cell lines. Each value represents the average of three independent experiments performed on the same day and using the same batch of cells.....	65
Table IV.1 DNA sensing in literature.....	91
Table IV.2 DNA recovery table.....	91
Table IV.3 RNA recovery table.....	91

CHAPTER I

INTRODUCTION

A. Block Copolymers

1. Background

Self-assembly processes involving amphiphilic molecules have attracted numerous interest in nanoscience and nanotechnology¹⁻² because of their unique property to form thermodynamically stable self-assemblies and modify interfacial and surface properties.³ Hartley introduced the word *amphiphile* referring to a large class of compounds with two distinct moieties that are covalently bonded and have different affinity for the same solvent.⁴ These molecules possess two blocks: one is soluble in polar solvents such as water while the other is soluble in non-polar solvents such as esters, ethers and hydrocarbons. Typical examples of amphiphiles are lipids and surfactants. Generally speaking, surfactants or surface-active agents have low molecular weight and are composed of a hydrophilic head and a hydrophobic tail;⁵ the head can be either charged or uncharged and the tail might be composed of one or more hydrocarbon, fluorocarbon, or dimethylsiloxane. Surfactants can be classified into four categories based on the nature of their head: cationic, anionic, non-ionic and zwitterionic surfactants. Cationic surfactants are comprised of a positively charged head like fatty amine salts. Anionic surfactants have a negatively charged head such as carboxylate and sulfonates. Non-ionic surfactants possess an oligo(ethylene oxide) chain as a hydrophile. Zwitterionic surfactants consist of a head with both negative and positive charges along with a long hydrocarbon tail. Surfactants

have attracted much attention because of their surface activity.⁶ At very low concentrations, they can remarkably alter the air-water or oil-water interface, and this can serve many surface chemistry functions offered by surfactants, such as solubilization,⁷ emulsification,⁸ foaming,⁹ and cosmetics.¹⁰ Over recent years, block copolymers have attracted a considerable attention as a new category of amphiphiles which proved to benefit a plethora of applications including drug delivery,¹¹ tissue engineering,¹² nanoparticles synthesis,¹³ mesoporous materials,¹⁴ and many other applications. Block copolymers belong to the class of non-ionic surfactants and are considered as macromolecular amphiphiles of high molecular weight.⁴

2. Structure

A representative class of block copolymers which have proved to be beneficial in numerous applications are poloxamers, known commercially as pluronics. These are water-soluble non-ionic triblock copolymers. These block copolymers exhibit an amphiphilic assembly: a hydrophobic polypropylene oxide (PPO) chain terminated by two hydrophilic polyethylene oxide (PEO) chains; hence, the general structure is an A-B-A structure: PEO-PPO-PEO (Figure I.1).¹⁵

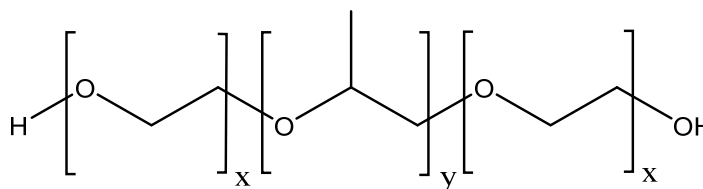


Figure I. 1 Structure of triblock copolymers

3. Nomenclature

Nomenclature of pluronics includes a numeric code preceded by a letter which expresses its phase. The letter “L” stands for the liquid, “F” for flakes or solid, and “P” for paste. The numeric code defines the PPO and PEO structure of the copolymer. The first one or two digits multiplied by 300 indicate the approximate molecular weight of the PPO block in Da whereas the last digit signifies the percentages of ethylene oxide. For example, ‘F-127’ is a solid copolymer with an approximate PPO molecular weight of 12600 and 70% ethylene oxide.¹⁶

4. Micellization of Pluronic (the hydrophobic effect)

Owing to the dual structure of pluronics and the difference in solubility between their two blocks, they can spontaneously self-assemble into various organized structures, the most prominent ones being spherical micelles with a hydrophobic core and hydrophilic corona.¹⁷ However, this self-assembly process known as ‘*micellization*’ occurs only above a certain polymer concentration known as critical micelle concentration (CMC) and above a certain temperature at which micelles form, critical micelle temperature (CMT).¹⁸ This self-association process is driven by the hydrophobic effect. This term was first coined by Charles Tanford in 1970s referring to the nonpolar molecules that have tendency to form aggregates in water.¹⁹ An ambiguity in understanding this phenomenon is still present due to the many intermolecular forces involved. Some has attributed micellization process to the strong hydrophobic attractive forces that exist between the nonpolar chains in aqueous media. Others have opposed this by saying it is completely the opposite; the origins of these interactions are rooted in the strong attractive forces (hydrogen bonding) between water

molecules. Thus, hydrophobic effect is clearly defined as the tendency of water molecules to decrease the alkyl chain/water contacts that increase the free energy of the solution. As the copolymer concentration increases in the solution and as more copolymers adhere to the air/solution interface, the unfavorable interactions between the hydrophobic blocks and water continue to grow, which cause the free energy of the system to increase. To avoid a further increase in the free energy, water molecules reduce these alkyl chains/water contacts by pushing the insoluble lipophilic blocks to aggregate to form micelles having an oily core where PPO blocks are in contact with each other. The head groups (PEO) form a shell at the surface of this core to further decrease the alkyl chains/water contact.⁴

5. Thermodynamics of micellization

For a better understanding of self-assembly processes, it is crucial to study their thermodynamics. This requires the discussion of the equilibrium aspects of micellization as well as some thermodynamic quantities such as entropy (ΔS), enthalpy (ΔH), and Gibbs free energy (ΔG). A productive insight on the thermodynamics of micellization was obtained by Alexandridis et al. in the early 1990s.^{18, 20-21} In principle, there are two mechanisms or models through which micellization can proceed: open and closed association mechanisms. The former takes place through a series of equilibria including monomers, dimers, trimers, up to n-mers. Yet, the latter is characterized by a dynamic equilibrium between dispersed copolymers (monomers) and the aggregated structures (micelles).²² It has been proved by Alexandridis et al. that block copolymer micellization occurs through the closed association model.¹⁸ Indeed, it is well established that micelles are thermodynamically stable species.²³ However, an important question arises in the

thermodynamics of micellization: which term, the enthalpic or entropic term, contributes more to the thermodynamic stability of micelles? As mentioned above, to reduce the free energy of the system upon the increase in the unfavorable interactions between the PPO chains and water molecules, water molecules tend to aggregate the nonpolar blocks together, forming micelles. To answer this question, there are two approaches that can analyze the thermodynamics of micelle formation: the phase separation model and mass-action model. In the phase separation model, micelles, formed at CMC, exist as a separate phase in the solution. It is also assumed that the concentration of free monomers in equilibrium with micelles is equal to the CMC value. In the mass-action model, it is considered that the free monomers and micelles are in an association-dissociation equilibrium. For both models, the free energy of micellization for non-ionic block copolymers i.e. the Gibbs free energy change for 1 mole of amphiphile to transfer from solution to the micellar phase is

$$\Delta G^\circ = RT \ln(X_{cmc}) \quad (1)$$

where R is the gas constant, T is the absolute temperature, and X_{cmc} is the critical micelle concentration in mole fractions.

If aggregation number, that is the number of surfactant units (monomers) constituting a micelle, is assumed to be independent of temperature according to the mass action model and applying the Gibbs Helmholtz equation ($G = H - TS$), the standard enthalpy of micellization, ΔH° , can be expressed as²⁴

$$\Delta H^\circ = -RT^2 \left[\frac{\partial \ln(X_{cmc})}{\partial T} \right]_p = R \left[\frac{\partial \ln(X_{cmc})}{\partial \left(\frac{1}{T}\right)} \right]_p \quad (2)$$

Finally, the standard entropy of micellization can be written as

$$\Delta S^\circ = \frac{(\Delta H^\circ - \Delta G^\circ)}{T} \quad (3)$$

Some studies have shown that for block copolymer micellization, the following equation applies²⁵

$$\frac{\partial \ln(X_{cmc})}{\partial \left(\frac{1}{T}\right)} = \frac{\partial \ln(X)}{\partial \left(\frac{1}{T_{cmt}}\right)} \quad (4)$$

Where T_{cmt} is the critical micellization temperature and X is the block copolymer concentration in mole fractions; thus, equation 2 becomes

$$\Delta H^\circ = R \left[\frac{\partial \ln(X)}{\partial \left(\frac{1}{T_{cmt}}\right)} \right] \quad (5)$$

Thermodynamic quantities ΔG° , ΔH° , and ΔS° for various pluronics at their critical micellization temperature were calculated by Alexandridis and his collaborators.¹⁸

ΔH° values were positive indicating that micellization is endothermically unfavorable process. However, the negative standard Gibbs free energies, ΔG° , values show that micelles are thermodynamically stable moieties formed spontaneously. It can be concluded that the negative free energies are exclusively a result of the positive entropy contribution. Therefore, micellization is an entropy driven process. This contradicts the aggregation process in which dispersed monomers form highly ordered clusters (micelles), which is entropically unfavorable. However, solvation effect of water molecules plays an important role in increasing the entropy.¹⁹ The non-polar chains of block copolymers are

not dissolved in water due to their inability to hydrogen-bond with water molecules. Thus, without breaking hydrogen bonds, water molecules in their vicinity arrange themselves to a more ordered assembly to form a cavity in which the nonpolar molecules can be solvated. This results in an entropy decrease which disfavors the process to occur. However, the loss of entropy becomes very large to the extent that favors the restoration of the previous hydrogen-bonding structure of water, which will lead to an increase in the entropy outweighing the entropy loss resulting from the aggregation process of monomers into micelles. Hence, the driving force behind micellization is entropic.²²

6. Morphologies of Micelles

Micelles of diverse morphologies can be obtained when block copolymers self-assemble in solution.¹⁷ Furthermore, polymeric assemblies are more stable compared to small-molecule aggregates. Due to this versatility, they offer greater opportunities that can meet the requirements of a wide range of applications. For instance, in the synthesis of mesoporous materials, morphology of the micelle plays an important role in the determination of the pore structure of the material. Several conditions can dictate the destined structure of the micelle, including the HLB balance (hydrophobic/hydrophilic ratio) or copolymer composition, polymer concentration, solvent concentration and nature, and other properties.²⁶ Following the same principle of surfactants, a dimensionless factor, p , can predict the final morphology of the micelle in solution. This parameter, $p = v/a_0l_c$, is a packing parameter, where v and l_c are the volume and length of the hydrophobic segment respectively and a_0 is the area of the polar head. According to the value of p , pluronics can self-assemble into a variety of nanostructures, such as spherical micelles, cylindrical or

worm-like structures, polymersomes and flat bilayers, lamellae, vesicles, etc. Spherical micelles are considered the pre-requisite morphology for other aggregates. Figure I.2 illustrates all the possible morphologies in relation to the p value.¹⁷

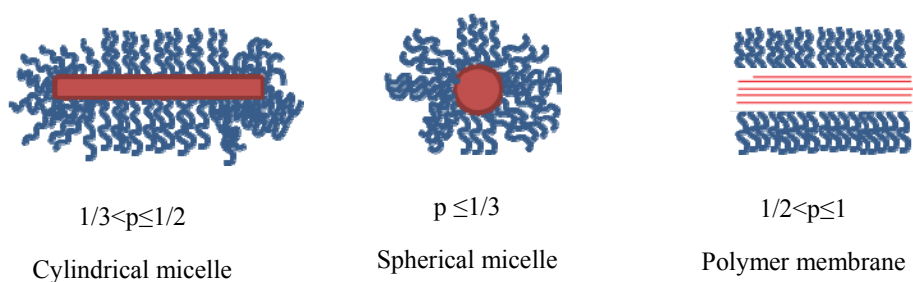


Figure I. 2 illustration of typical morphologies formed by amphiphilic block copolymers in solution (red region represents hydrophobic core and blue is for hydrophilic surface)

7. *Factors that affect properties of Micelles*

Several physical factors can alter the structures and properties of copolymer aqueous solution. Effects of temperature,²⁷ copolymer concentration and molecular weight,¹⁸ added salts,²⁸ and other features on the structure and hydrophobic/hydrophilic character of the PEO-PPO-PEO block copolymers have been studied extensively.

a. Effect of copolymer concentration and temperature

Some studies have revealed a strong dependence of CMC and CMT on the solution temperature. For instance, using Differential Scanning Calorimetry (DSC), Alexandridis et al. have shown that CMT of L64 decreased when the copolymer concentration increased from 1wt% to 10 wt%.²⁰ The observations made here were in a good agreement with an

earlier work for Alexandridis et al. where dye solubilization method was employed to investigate the effect of temperature and copolymer concentration on the CMC and CMT values for 12 pluronics having a broad range of molecular weights (2900-14600). Indeed, it was detected that the CMT values decreased with the increase in copolymer concentration, and the CMC values decreased with temperature.¹⁸ Later, Alexandridis et al. used surface tension measurements for 7 pluronics covering molecular weights from 3400 to 14600 to further examine the effect of temperature, concentration, molecular weight, and PPO/PEO composition on the molecular characteristics of pluronics. For that purpose, surface tension data for P103, P104, F108, P105, P85, and P65 were plotted semi-logarithmically with respect to the copolymer concentration at two temperatures, 25 and 35 °C. Results showed a decrease in the CMC with temperature for the 7 pluronics.²¹ This is in compliance with the previous conclusions from dye-solubilization technique where it clearly showed that CMC decreased with temperature. In 2005, Mata et al. have confirmed temperature-induced micellization by using FTIR spectroscopy to monitor the temperature dependence of the key infrared bands of L64. The wave number shift of the C-O-C band, exhibited by the PPO block of pluronics, was tracked for different concentrations of L64 in aqueous media as a function of temperature. In this study, DSC and FTIR were also employed to assure that CMT values of L64 decreased with the increase in copolymer concentration from 1 to 25 %w/v.²⁹

b. Effect of molecular composition

Micellization is not only temperature and concentration dependent. However, it shows a strong reliance on the molecular weight and composition of the pluronic molecule.

Alexandridis et al. have also shown that PPO and PEO composition of the pluronic can highly affect the CMC and CMT values. Their study showed that for P65, P84, and P123, having same hydrophilic (PEO) composition but different hydrophobic (PPO) segment, polymers with the largest PPO weight (P123) formed micelles at lower temperatures and concentrations i.e. at lower CMC and CMT values. To investigate the effect of the PEO segment, a group of pluronics having same PPO weight but varying PEO content showed an increase in the CMC and CMT values as the number of PEO units increased from 40, 50 to 80%. However, the effect of PEO on the CMC and CMT is less pronounced than that of the PPO, indicating that PPO is the chief feature of micellization, which is in fact a key contributor to the hydrophobic effect. Moreover, it was shown that for copolymers with the same PPO/PEO ratio and different molecular weight, those with the higher molecular weight undergo micellization more readily, or at lower CMTs and CMCs.²¹

c. Effect of added salt

Furthermore, many studies have illustrated the influence of added salts on the aggregation behavior of pluronics. It has been confirmed that pluronics in salt-containing solutions demonstrated remarkable aggregation properties. After plotting surface tension data for P65 in water and 2M NaCl as a function of copolymer concentration at 30 °C, Jain et al. have reported that in the absence of salt, this copolymer did not aggregate up to the highest concentration studied (1% w/v) where the plot has not shown any break point in surface tension. This absence of aggregation is mainly due to the high hydrophilic character of P65 (50%). In contrast, in 2M NaCl, two break points over a wide range of concentration in the surface tension graph, where the second break corresponding to the CMC occurred at

0.08% w/v i.e. at a lower CMC value.²⁸ Using surface tension measurements, Desai et al. have also reported a considerable lowering of the CMC value, concentration at the second break, of F88 upon increasing the sodium chloride concentration from 1.0 to 2.0 M.²⁷

8. Fluorescence probing as a new method to study micellization behavior

Recently, steady-state fluorescence measurements using the emission of fluorescence probes have emerged as a powerful tool to investigate the effect of temperature, concentration and added salts on the micellization properties of pluronics. In 2008, Patel et al. were interested in studying the changes in aggregation characteristics of pluronic F88 upon modifying the concentration, temperature, and adding potassium chloride. Steady-state fluorescence technique was employed using pyrene as a fluorescence probe because it has a characteristic emission spectrum of five bands that are strongly dependent on the polarity of the medium; the ratio, I_1/I_3 which is the intensity of the first to the third band, was taken as an indication of the polarity of the medium. Results of polarity ratio in varying concentration of F88 plotted as a function of solution temperature have shown a drastic decrease in the CMT value at higher F88 concentration. Another plot for polarity ratio of pyrene for 2.5% F88 in solutions with increasing salt concentration has clearly demonstrated that micellization occurs more readily i.e. at lower CMTs when the salt concentration is larger. Temperature-induced and salt-induced micellization were further confirmed through viscosity measurements which have shown a gradual decrease in relative viscosity for F88 solutions with increasing temperatures and amounts of salts. This is primarily due to the more compact structures of micelles as compared to the F88 unimers.³⁰ As a conclusion, several studies have used multiple techniques to establish

micelle formation in solution and the alteration of their properties when several conditions were modified.

9. Polymeric micelles as drug delivery systems

One of the most powerful properties of poloxamers is their capacity to form these thermodynamically stable species (micelles) whose aqueous solution properties are highly dependent on concentration, temperature, solvent characteristics, and added salts or other additives. Depending on the solution conditions, poloxamers can be amenable to multiple therapeutic drug delivery formulations, leading to various thermodynamically-stable drug-encapsulating structures such as cubosomes, thermo sensitive gels, ellipsoids, micelles, rods, etc. Each structure has its unique adsorption and associative characteristics which allow it to target a specific disease, work with a certain drug, or function at a different delivery rate and routes.³¹ The hydrophobic core of these structures is central to their utility as it offers a medium to solubilize hydrophobic drugs having low-aqueous solubility and thus low oral bioavailability.³² Dorn et al. was the first to observe and report formation of drug loaded pluronic micelles.³³ Advantages that render poloxamers as a suitable choice for many clinical applications aside from their supremacy in fundamental research and industrial applications as foaming agents, stabilizers, emulsifiers, and detergents include: high commercial availability, wide array of molecular weights and compositions, and approval for the use in pharmaceutical industry by the FDA for pharmaceutical and medical applications and by the US and British pharmacopoeia.³¹ SP1049C, which is a formulation incorporating doxorubicin (Dox) in the mixed micelles of pluronics L61 and F127, was the first micellar formulation to reach clinical evaluation as an anti-cancer therapeutic. The

pharmacokinetics and biodistribution profiles of Dox have shown that Dox fused in micelles demonstrated more efficient accumulation in the tumors compared to the free drug. Furthermore, this analysis indicated that Dox formulated with SP1049C in the tumor had delayed peak levels and higher residence time as compared to the free Dox. Dox, paclitaxel or other drugs in pluronics formulations also showed improvement of drug anticancer effect in *in vivo* tumor models.³⁴ Up till recent years, many researchers have been thoroughly highlighting the utilization of “smart” drug nanocarriers developed with pluronic copolymers in numerous drug formulations and treatment pathways for several diseases. In 1988 Saettone et al. manifested that for a series of poloxamers with different molecular weights and characteristics, solubility of the cycloplegic drug, tropicamide, displayed a linear increase upon increasing the copolymer concentration.³⁵ In 1989, Kabanov et al. recognized a 5-fold improvement in solubility of haloperidol, a neuroleptic drug, when encapsulated in P85.³⁶ Furthermore, the solubility of the HRT drug, estriol, was enhanced with the increase in temperature and L64/salt concentration.³⁷ In 2006, enhanced oral bioavailability in *in vitro* of camptothecin was shown by Sugin et al. when this hydrophobic drug was encapsulated in F127, F68, and P85 delivery vehicles.³⁸ Moreover, Kwon et al. have also reported that drugs encapsulated in Pluronic micellar systems are more efficient at tumor cells as compared to the free drug. This can be attributed to the enhanced circulation time of drug-loaded micelles and slower rate of dissociation of drugs in micelles in the blood circulation system.³⁹ Recently, results on solubilization of carbamazepine (CBZ) using pluronic delivery vehicles and its interactions with the block copolymer solutions were presented by Kadam et al. in 2009. CBZ is a long-established antiepileptic drug, yet its bioavailability is highly limited by low-water solubility.

Therefore, Kadam et al. have conducted a systematic study to investigate the solubilization capacity of P103, P123, P84, and F127 for this drug. Results have shown that the amount of solubilized CBZ increased with the increase in P103 and P84 concentration. However, the effect was more pronounced for P103 because it is more hydrophobic. This dissolution enhancement was observed for P123 and F127 as well. Effect of temperature on solubilization was also investigated. A slight increase in solubility of CBZ was detected when temperature was increased.⁴⁰ Results here were in a good agreement with previous results from Saito et al. on estriol.⁴¹ Fioritto et al. also got similar outcomes on the dissolution of Furosemide.⁴² In conclusion, a thorough review of the literature clearly demonstrates that solubility, therapeutic effects, stability, and drug pharmacokinetics and biodistribution profiles of low molecular mass drugs can be extremely boosted when combined into pluronic micelles.

B. Curcumin

1. Background

Curcuma longa is a perennial plant that belongs to the ginger family.⁴³ It is broadly cultivated in the Asian tropical regions. Turmeric is the plant's extract; it is known for its golden yellow color and widely used as a preservative, coloring agent, and a spice for food. India is the chief exporter of turmeric.⁴⁴ *Curcuma longa* has been also known for its therapeutic uses since the times of Ayurveda in 1900 BC, the science of long life.⁴⁵ Due to its antioxidant,⁴⁶ anti-inflammatory,⁴⁷ antimutagenic, antimicrobial,⁴⁸ and anticancer properties,⁴⁹⁻⁵⁰ turmeric has been acknowledged in Asian countries as a traditional medical herb.

Turmeric is constituted of a variety of phytochemicals; the three principal ones are: curcumin, demethoxycurcumin, and bisdemethoxycurcumin. The main phytochemical that is responsible for turmeric's therapeutic importance and counts around 2-5% of turmeric rhizome is curcumin. It is also the main natural polyphenol that gives turmeric the vibrant yellow color which is responsible for its usage as a dye.⁴⁵ Curcumin was first isolated in impure form in 1815 by Vogel and Pelletier.⁵¹ yet its chemical structure was not identified until 1910 by Milobedzka and Lampe.⁵²

2. Structure

Curcumin has a molecular weight of 368.37 g/mol, molecular formula $C_{21}H_{20}O_6$, and a melting point of 183 °C.⁵³ The chemical name of curcumin is 1,7-bis(4-hydroxy-3-methoxyphenyl)-1,6-heptadiene-3,5-dione. It is also called diferuloylmethane.⁵² Under physiological conditions, curcumin tautomerizes between two forms: an enolate and a bis-keto form. Structures of curcumin's tautomers are shown in figure I.3. The percentage of enol to keto form is highly dependent on the temperature and the properties of the solvent. Studies including X-ray diffraction patterns and DFT simulations indicate that the stability of the cis-enol form in vacuum and solution originates from the conjugation of the π -electron system where the enolisable hydrogen is evenly distributed between the two oxygens. It has been shown through NMR studies that curcumin exists as an enolic isomer in non-polar and aprotic solvents. However, in protic solvents, the keto-form predominates due to the rupturing of intramolecular hydrogen bonding.⁵⁴

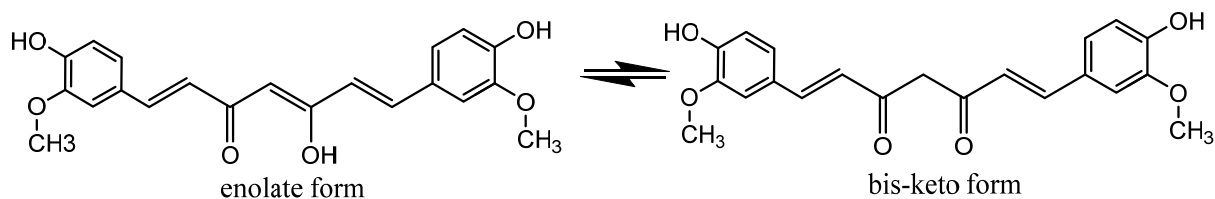


Figure I. 3 Chemical structures of curcumin tautomers

3. Photophysical properties of curcumin

The interesting fluorescence and absorption profile of curcumin has rendered it as a useful molecular probe for many sensing applications.⁵⁵ It has an absorption maximum in the range of 408-430 nm. Theoretical studies predicted that the broad absorption band between 410 and 300 nm is due to the π - π^* transition whereas the absorption maximum between 389 and 419 nm is for the keto and enol form, respectively.⁵⁶ Moreover, it emits between 540 and 600 nm depending on the solvent used and has a relatively low quantum yield and short lifetime.⁵⁷

Wang et al.⁵⁸ have studied curcumin's stability through studying its degradation in buffer solution, and it has been shown that it is more stable in acidic medium than in basic medium owing to the conjugated diene structure. In addition, photodegradation of curcumin into vanillin and p-hydroxybenzaldehyde as by-products has been widely reported.⁵⁹

4. Applications

Turmeric has been considered a major component of Asian cookery and traditional medicine for thousands of years. More recently, turmeric extracts have been extensively

used by the food industry as additives, flavorings, preservatives, and coloring agents (e.g. mustards and soft drinks). Indeed, curcumin is approved in the international numbering system for food additives with the code E100. Also, turmeric serves several nonmedical applications such as cosmetics, mostly in Hindu rituals and ceremonies.⁶⁰

a. Applications in bio-chemistry and medicine (therapeutic uses of curcumin)

Curcumin has been shown to exhibit a high therapeutic potential as an anti-inflammatory, antibacterial, anticancer, and antioxidant drug. Besides, curcumin has proven efficiency in wound healing and reducing cholesterol levels in the blood.⁶¹ Moreover, many studies have shown that curcumin can inhibit platelet aggregation,⁶² and suppress symptoms related to Alzheimer's disease.⁶³ All of these potential therapeutic uses for curcumin have established it as a crucial dietary supplement with a safety intake of up to 8g/day.⁶⁴

i. Anti-inflammatory and Antioxidant activities

In many chronic diseases which are known to display inflammation symptoms, curcumin has been shown to exhibit major therapeutic efficiency. Such diseases include Alzheimer's disease (AD), Parkinson's disease, multiple sclerosis, epilepsy, cerebral injury, cancer, allergy, asthma, bronchitis, colitis, rheumatoid arthritis, cardiovascular diseases, renal ischemia, psoriasis, diabetes, obesity, depression, fatigue, and AIDS. For example, in a study by Aggarwal et al., results have shown that curcumin can play a major role in the treatment of psoriasis. Treatment pathways of curcumin include inhibition of PhK activity, reducing the amount of keratinocyte transferrin receptor, and density of epidermal CD8⁺ T cells which are all associated with the appearance of psoriatic activity as assessed by

clinical, histologic, and immunohistochemical criteria.⁶⁵In 2003, Ram et al. focused their work on the anti-asthma property of curcumin. They have examined the effect of curcumin on the airway hyper-reactivity in a guinea pig model, and results have demonstrated that curcumin was very efficient in improving the impaired airway features in OVA-sensitized guinea pigs.⁶⁶

Oxidative stress and inflammation are quite related. They have similar pathological processes, and it is proven that both can induce one another. For instance, oxidative stress is caused by inflammatory cells that are known to release numerous reactive species at the inflammation site.⁶⁷ Several studies have established the proficiency of curcumin as an anti-inflammatory and antioxidant agent. For example, upon studying the scavenging activity of curcumin, Reddy and Lokesh have concluded that curcumin act as an effective scavenger of a number of reactive oxygen species (ROS) such as hydroxyl radicals and superoxide anions.⁶⁸

ii. Anticancer activity

Cancer is a complex disease that is characterized by abnormal cell proliferation and growth caused by accumulation of gene mutations. A common major factor of initiation and advancement of all types of cancer is inflammation. Because curcumin is a potential anticancer drug and anti-inflammatory agent, it is expected and has been proven to exhibit various therapeutic effects in several types of cancer. Curcumin is a well-established anticancer agent due to its ability to suppress the growth of various tumor cell lines by controlling the activity of several molecular aspects, which are implicated in

carcinogenesis.⁶⁹ Till now, the anticancer activity of curcumin has been the focus of more than 800 reports. Several *in vitro* and *in vivo* studies have established the potential of curcumin in preventing the growth of various cancer cells from different organs and body parts including blood,⁷⁰ colon,⁷¹ brain,⁶³ breast,⁷² pancreas,⁷³ prostate,⁷⁴ and skin cancers.⁷⁵ 14.1 million new cancer cases have been identified in 2012 according to Centers for Disease Control and Prevention. According to Ries et al., this number is expected to increase to 19.3 million by 2025.⁷⁶

b. Applications in Chemistry (Curcumin as a sensor and molecular probe)

Finding new fluorescence probes that can help in studying properties of liposomes or self-assembly aspects of micelles has been always a topic of great interest among spectroscopists. Due to its interesting fluorescence profile, curcumin is widely getting realized for its potential application as a molecular probe⁷⁷⁻⁷⁸ and sensor.⁷⁹⁻⁸⁰ The use of fluorescence technique in probing is widely favored over classical microscopy techniques because it offers detailed information reaching a single molecule sensitivity.⁸¹ For instance, a study conducted by Khoury et al. in 2016 revealed that curcumin can serve as an efficient, non-toxic, and easily accessible probe molecule to study the liposome properties. Furthermore, it was successfully proved in this study that curcumin can be used to observe the effect of cholesterol on liposomes and study ethanol induced interdigitation of liposomes.⁸² Another study proposed by Chebl et al. have shown that curcumin formulated with chitosan oligosaccharide and integrated with negatively charged silica nanoparticles to form nanocapsules can serve as a cost-effective and highly selective analytical technique

for cholesterol sensing without enzymatic reaction.⁸³ Moreover, Wu et al. reported curcumin as a chemosensor for fluoride anion in 2010.⁸⁴

5. Limitations of Curcumin

Despite the extensive research which has entrenched the therapeutic efficiency of curcumin against several health problems, curcumin alone is a poor therapeutic candidate due to its low oral bioavailability which is attributed to poor water-solubility, fast elimination from the body, and high rate of metabolism.⁸⁵ Yang et al. have shown that only $0.36 \pm 0.05 \mu\text{g/mL}$ was found in serum after intravenous administration of 10 mg/kg curcumin in rats. However, a maximum plasma concentration of $0.06 \pm 0.01 \mu\text{g/mL}$ was achieved for a 500 mg/kg of orally administered curcumin. This comparison specified that the oral bioavailability of curcumin was only 1%.⁸⁶ Multiple studies have surveyed the pharmacokinetics profile of curcumin in rodents and human and showed that the maximum plasma concentration reported till now is $0.051 \mu\text{g/mL}$ from 12g curcumin in human, $1.35 \mu\text{g/mL}$ from 2g/kg in rat, and $0.22 \mu\text{g/mL}$ from 1g/kg in mouse.⁸⁷

6. Means to overcome limitations of curcumin

To take advantage of all the therapeutic benefits offered by curcumin, multiple methods have been pursued to increase curcumin's solubility and oral bioavailability. Several strategies including phospholipid-curcumin complexes, liposomes, polymeric micelles, and curcumin nanoparticles have proved to be potential platforms in improving bioavailability of curcumin.

a. Phospholipid complexes

Liu et al. conducted a study on curcumin-phospholipid complexes which they have prepared and administered orally to Sprague-Dawley male rats at a dose of 100 mg/kg. They have shown that the maximum plasma curcumin concentration for curcumin-phospholipid complexes was 600 ng/mL while that of free curcumin was 267 ng/mL. This study has also found about a 1.5-fold increase in curcumin half-life in rats when it was formulated in a phospholipid complex.⁸⁸ Another study conducted by Maiti et al. showed that curcumin-phospholipid complex displayed a 5-fold enhancement in oral bioavailability in comparison with suspension of curcumin.⁸⁹

b. Delivery systems

i. Liposomes

Another approach which helps boosting the bioavailability of curcumin is the encapsulation of curcumin in delivery vehicles. Such systems act as a “cargo” space that carry water-insoluble drugs such as curcumin to its desired location for therapeutic applications. Examples of such systems are liposomes, polymeric micelles, and curcumin nanoparticles.

Liposomes are synthetic lipid-based drug delivery systems. They are described as vesicles having a phospholipid bilayer surrounding a hydrophilic core. In fact, studies to date have shown a significant enhancement of oral absorption of hydrophobic drugs when carried in liposomal drug delivery systems as compared to oral solid delivery or suspension techniques. Such systems are able to solubilize and stabilize both hydrophilic and lipophilic

drugs.⁹⁰ For example, an *in vivo* study revealed that curcumin's plasma concentration significantly improved from 64.6 ± 10.7 $\mu\text{g/L}$ in free curcumin to 319.2 ± 70.4 $\mu\text{g/L}$ in liposomal curcumin. This is estimated as a 4.96-fold enhancement in curcumin's bioavailability in comparison with orally administered free curcumin.⁹¹

ii. Polymeric Micelles

Polymeric micelles are self-assembled nanostructures whose size ranges between 20 and 100 nm.⁹² These structures are composed of amphiphilic macromolecules, such as block copolymers, which self-assemble in aqueous media to micelles having hydrophobic core and hydrophilic surface. In their core, they can accommodate many hydrophobic drugs.⁹³ Several lines of studies have proved that such structures are competent for solubilization of curcumin. In an attempt to increase the solubility of curcumin in aqueous media, Zhao et al. prepared a composite formulation of mixed micelles made up of P123 to F68 at a ratio of 2.05:1. The average size of these nanocapsules was found to be 68 nm. The encapsulation efficiency and drug-loading capacity were estimated to be 87% and 7% respectively. Curcumin showed a substantial increase in solubility from 11 ng/mL in the free state to 3.02 mg/mL when encapsulated in the micellar solution.⁹⁴

C. Fluorescence

Fluorescence is a simple and highly sensitive luminescence technique. It is based on photo-excitation of a molecule and collecting the emitted light in return. It is an interesting

method that is widely employed in various fields including DNA sequencing, biosensing, molecular interaction, biotechnology, etc.

In 1800's, several people have noticed and reported on how minerals transmitted and reflected colors; however, they failed to explain it when they attributed it to light scattering.

The term fluorescence was first used by Stokes between 1852 and 1853. He backed-up Becquerel observation ten years earlier when he concluded that the molecules emit at a longer wavelength than the incident light.⁹⁵

1. *Principal of fluorescence*

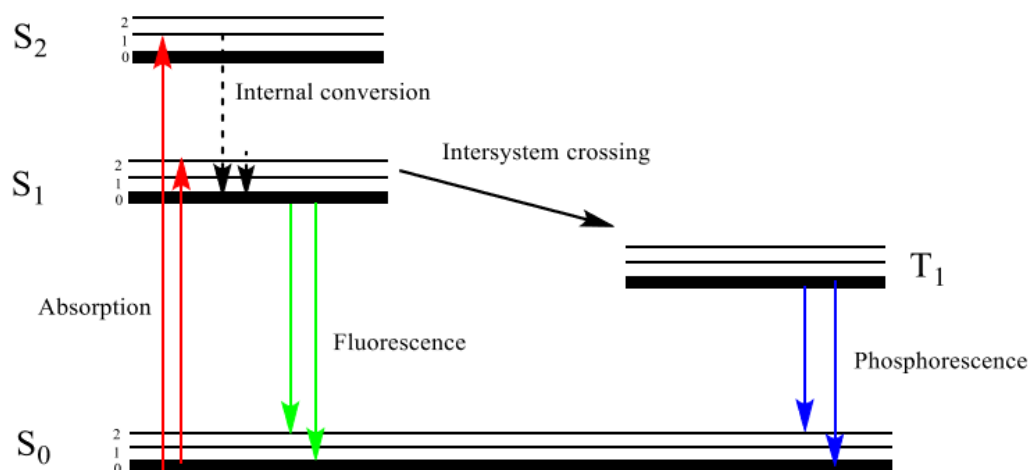


Figure I. 4 Jablonski diagram

A clear illustration of the fluorescence process can be given by Jablonski diagram as shown above in figure I.4. Right after light absorption (10^{-15} s), the molecule experiences various transition; some of them are light-emitting while others are not. The internal conversion process is when the molecule relaxes and returns to the lowest vibrational level

of the first excited state (10^{-12} s). The process in which energy of the system returns from the lowest vibrational level of the first excited state to ground state S_0 is called fluorescence (10^{-8} s). However, phosphorescence phenomenon is the result of the intersystem crossing (ISC) from the first excited S_1 state to a triplet state T_1 , followed by a forbidden transition to the ground state S_0 . Compared to fluorescence, phosphorescence is characterized by a delay in the emission which lead to a higher emission wavelength.⁹⁶

2. Quenching

Quenching is a fluorescence process described by a decrease in the fluorescence intensity. Two modes of quenching exist: collisional and static quenching.

a. Collisional quenching

Collisional quenching arises when the fluorophore in the excited state collides with the quencher. Stern-volmer plot represents collisional quenching, where F_0/F is plotted versus quencher concentration $[Q]$, and the result is a linear relation with a slope $k_q\tau_0$ where k_q is the bimolecular fluorescence quenching constant and τ_0 is the life-time of the fluorophore in the absence of the quencher.

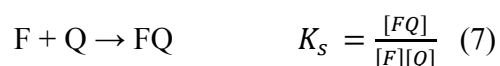
The dependence of the fluorophore lifetime on the quencher concentration is an important feature of collisional quenching, represented by the Stern-Volmer equation:

$$\frac{F_0}{F} = \frac{\tau_0}{\tau} = k_q \tau_0 [Q] + 1 \quad (6)$$

In addition, the rise in temperature will cause an enhancement in the diffusion rate. Hence, the collision rate will increase causing an increase in the quenching rate.

b. Static quenching

It occurs when the fluorophore bound to the quencher forms a stable and non-fluorescent complex in the ground state according to the equation:



So, the Stern-Volmer equation becomes as follows

$$\frac{F_0}{F} = K_s[Q] + 1 \quad (8)$$

This type of quenching, unlike collisional quenching, the lifetime of the uncomplexed fluorophore is unaffected by the quencher concentration and the raise in temperature causes the dissociation of the formed complex. Consequently, the quenching rate will decrease.⁹⁶

D. Aims

Self-assembly process attracts numerous interests for its applicability in drug delivery materials sciences and sensing application targeting specific systems. In chapter II of this work, our aim is to investigate self-assembly behavior of F108 copolymer in solution, which belongs to the class of block copolymers called pluronics. Therefore, using fluorescence probing technique, curcumin will be employed as an external probe to determine the CMC and CMT of F108. Secondly, this method will be apprehended to track changes in CMC and CMT with the addition of some modulators like sodium chloride and bile salts like sodium cholate and sodium deoxycholate. Finally, the position of curcumin inside the F108 micelles will be determined through fluorescence quenching, employing Cetylpyridinium bromide (CPB) and potassium iodide (KI) as quenchers.

Smart polymers with responsive properties have received much interest in the last few decades because of their crucial role in nanoscience and drug delivery applications. On the other hand, curcumin has proved efficiency as an anti-inflammatory, anti-oxidant, and anti-cancer agent. Nevertheless, its applicability is limited by its poor water-solubility and low oral bioavailability. Therefore, chapter III of this study will target enhancing the solubility and oral-bioavailability of curcumin through encapsulating it in F108 nanocapsules and characterizing these structures using X-ray diffraction (XRD), thermogravimetric analysis (TGA), scanning electron microscopy (SEM), and Fourier-transform infrared spectroscopy (FTIR). As an application, the anti-cancer activity of these nanocapsules will be assessed on two types of cancerous cells using photodynamic therapy.

Aside from its therapeutic efficiency, curcumin is well known for its analytical specificity as a fluorescence probe for targeted biomedical species. Hence, extensive research is being held on the sensing abilities of curcumin. Photophysical properties of curcumin can be tremendously boosted after being coated with a polymer. Therefore, in chapter IV of this work, we will encapsulate curcumin in F108 nanocapsules, but in a 1:40 curcumin to F108 ratio in order to check the effect of copolymer concentration on drug loading and emission spectrum of curcumin. A brief comparison on encapsulation of curcumin between the 1:1 and 1:40 nanocapsules will be done using X-ray diffraction, Scanning Electron Microscopy, and Thermogravimetric analysis. Using UV-visible and fluorescence spectroscopy, we will investigate whether increasing the copolymer concentration will successfully enhance the fluorescence signal of curcumin. Later, based on the functionality of curcumin as a fluorescent transducer, encapsulated curcumin will be used in biomedical application as DNA and RNA sensing.

CHAPTER II

UNDERSTANDING SELF-ASSEMBLY BEHAVIOR OF POLY(ETHYLENE OXIDE)-*BLOCK*-POLY(PROPYLENE OXIDE)-*BLOCK*-POLY(ETHYLENE OXIDE)

A. Introduction

Understanding self-assembly aspects of block copolymers was and is still of great importance to scientist because of their utility in a wide range of applications whether in chemistry, pharmacy, or medicine. Pluronic F108 belongs to this class of compounds; however, interestingly this pluronic, among other pluronics like F127 and P104, is known for its high hydrophilic percentage (around 80%).⁹⁷ F108 in solution behaves like surfactants; above critical micelle concentration and/or temperature, it aggregates into micelles of hydrophobic core and hydrophilic interface. Studying the CMC and CMT changes in block copolymers has been a subject of interest to many researchers. Different methods in literature were employed for this purpose. Such methods include surface tension measurements,²⁷⁻²⁸ FTIR technique,²⁹ DPH solubilization method,¹⁸ and fluorescence probing.³⁰ Fluorescence probes, mostly pyrene, proved to be a powerful technique for this aim. However, studying F108's behavior in solution using curcumin as a molecular probe is limited. Curcumin is a well-established ancient drug, existing as a β -diketo which tautomerizes between its enol and keto structures. Though interaction between curcumin and pluronics is strong as it is widely reported that curcumin gets buried in the hydrophobic cavity of pluronic micelles, studying F108 behavior in solution using curcumin as a

fluorescence probe is very limited. Interestingly, curcumin is becoming an established fluorescence probe for many systems like micelle,⁹⁸ liposomes,⁹⁹ and heterogeneous systems.⁹⁶ Thus, it is of great importance to comprehend the type of this interaction between curcumin and F108, taking advantage of curcumin's fluorescence properties and keeping its applicability in drug delivery, biomedical applications, and nanotechnology. In this manuscript, fluorescence techniques, using molecules like curcumin as an external fluorescence probe is proposed as a method to investigate the self-assembly behavior of F108 in water. The CMC and CMT are both determined at a fixed concentration and temperature, respectively. Results obtained are compared to those achieved using pyrene probing and DPH solubilization technique from literature. Effect of ionic strength and bile salt is also evaluated. Furthermore, the position of curcumin in the micelle is studied through quenching technique using CPB and KI as quenchers.

B. Materials and Methods

1. Materials

Pluronic F108, curcumin, Cetylpyridinium Bromide (CPB), sodium chloride (NaCl), potassium chloride (KI), sodium cholate (NaC), and sodium deoxycholate (NaDC) were obtained from Sigma-Aldrich and used as received. The solvents used were obtained from Sigma Aldrich and were of HPLC grade.

2. Sample preparation

Note: all the following experiments were carried out in duplicates

A stock solution of F108 (10 mg/mL) was prepared in double distilled water. Likewise, a stock solution of 1 mM curcumin was made in methanol. The stock solutions of CPB, KI, NaCl, sodium cholate, and sodium deoxycholate were distinctly prepared in double distilled water. Afterwards, dilutions were made as desired. All fluorescence measurements were performed at an excitation wavelength of 425 nm and emission spectra were collected over a wavelength range of 440-800 nm.

a. CMC study

For the CMC study, fluorescence measurements for samples of different F108 concentrations in this range (0, 2.28, 4.56, 6.85, 9.13, 13.7, 18.26, 27.4, 41.1, 54.8, 68.5, 82.2, 109.6, and 123.3 μ M) were conducted. To guarantee micelle formation, CMC study was performed at 45 °C which is higher than the literature value of CMT. Curcumin's concentration was maintained constant at 3.33 mM in all the samples. It is worthy to note that a sample without curcumin was prepared for each of the samples to check if F108 has any fluorescent properties, and it was shown that the error is within 10%, meaning that the fluorescence is solely due to curcumin's presence.

To study the effect of salt on CMC of F108, the different F108 samples were prepared at different salt concentration. The first salt tested was sodium chloride. 1, 10, 100, and 150 mM of NaCl was added to all the solutions. The same experiment was done by varying the concentration of sodium cholate and sodium deoxycholate as follows: 0.25, 0.5, and 5 mM for sodium cholate and 0.25, 0.5, and 1 mM for sodium deoxycholate.

b. CMT study

For the CMT study, a sample with 3.33 mM of curcumin and 82.2 μM (1.2 mg/mL) was prepared. The concentration of F108 was chosen to be higher than the literature value of CMC to ensure micellization. It is worthy to note that the amount of methanol present in the solution was less than 1 % (v/v) in order not affect our measurement. Fluorescence measurements of this sample were done at different temperatures (5, 10, 15, 20, 25, 30, 32, 34, 35, 36, 37, 38, 39, 40, 42, 46, 50, 55, 60, 65, and 70 °C).

c. Quenching study

For quenching experiments, F108 and curcumin concentrations were kept constant at 82.2 μM (1.2 mg/mL) and 3.33 mM respectively. The concentrations of the quenchers KI and CPB were varied as follows, respectively: 0, 0.2, 0.4 and 0.6 M for KI and 0, 45, 100, 200, 500 and 800 μM for CPB. Fluorescence measurements were also conducted at 45 °C. such low concentration range for CPB was selected because it can aggregate at low concentration, losing its quenching activity.

3. Instrumentation

Steady state fluorescence measurements were performed by a Jobin–Yvon–Horiba fluorimeter. Emission and excitation slits were both set at 5 nm. The fluorimeter is equipped with a 100 W Xenon lamp and an R-928 detector operating at 950 V. For temperature regulation, a thermostat was coupled to the fluorimeter sample holder. The temperature was read by an external thermometer.

Morphological characterizations of the aggregate were performed using a scanning electron microscope (SEM), Tescan, Vega 3 LMU with Oxford EDX detector (Inca XmaW20). Briefly, some drops of the desired solution of F108 and curcumin with the targeted salt was deposited on an aluminum stub, coated with carbon conductive adhesive tape.

C. Results and discussion

1. Self-assembly and critical micelle concentration

Although micellization is a spontaneous process, it only commences above a certain polymer concentration, the critical micellar concentration (CMC), at a fixed temperature. Detecting this concentration can be done by tracking the change in several physical properties as a function of the polymer concentration. Such properties include surface tension, electrical conductivity, or osmotic pressure. Other spectroscopic techniques like fluorescence can be employed to determine CMC. Probes like pyrene and *N*-phenyl-1-naphthylamine (NPN) are very well known for this target.¹⁰⁰ To investigate the CMC of F108 and reconfirm its value, curcumin was used as a fluorescence probe to examine the aggregation behavior of F108. Therefore, in the present study we followed the emission spectra of curcumin at different concentrations of F108 at 45 °C as it is shown in Figure II.1. The emission spectrum illustrated a maximum at ~512 nm after excitation at 420 nm. Afterwards, a blue shift to ~496 nm occurred at higher concentrations of F108 and remained constant at concentrations higher than 54.8 μM. The variation of fluorescence intensity at 512 nm with F108 concentration is shown in Figure II.2. As can be seen in this

figure, the fluorescence intensity of curcumin increased linearly until a particular concentration and continued to increase with a larger slope afterward. The break in fluorescence intensity vs F108 concentration must have arisen from the micellization/aggregation of F108. Therefore, it corresponds to CMC value and it is estimated to be $\sim 23.2 \mu\text{M}$ (Table II. 1). Our result is in excellent agreement with the CMC values reported in literature using pyrene probing are $22.0\text{-}22.6 \mu\text{M}^{101-102}$ at 37°C . The value obtained by simulation was lower and estimated to be around $17.1 \mu\text{M}^{102}$. Conflicting CMC values resulting from using different techniques is widely observed in previous studies.^{18, 103} The blue shift and the increase in the fluorescence intensity signify that curcumin experiences a more nonpolar environment in F108 micelles. This marks the incorporation of curcumin in the hydrophobic core of F108 micelles.¹⁰⁴

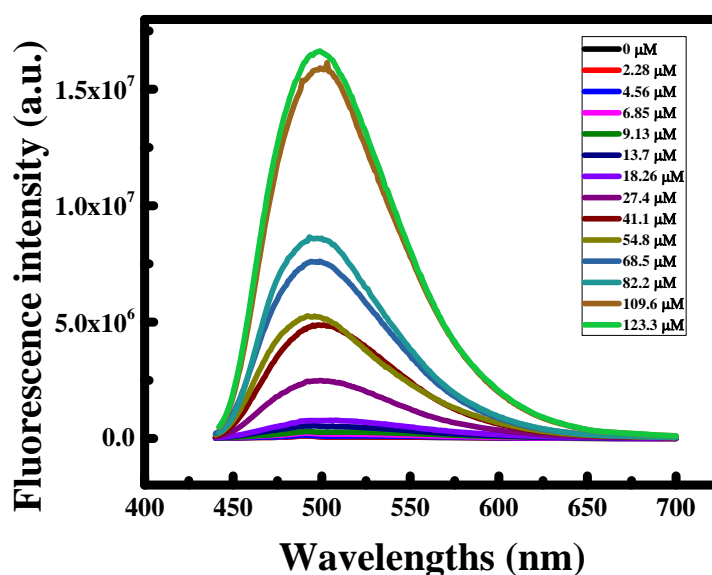


Figure II. 1 Fluorescence emission spectra of curcumin ($3.33 \mu\text{M}$) at different concentrations of F108

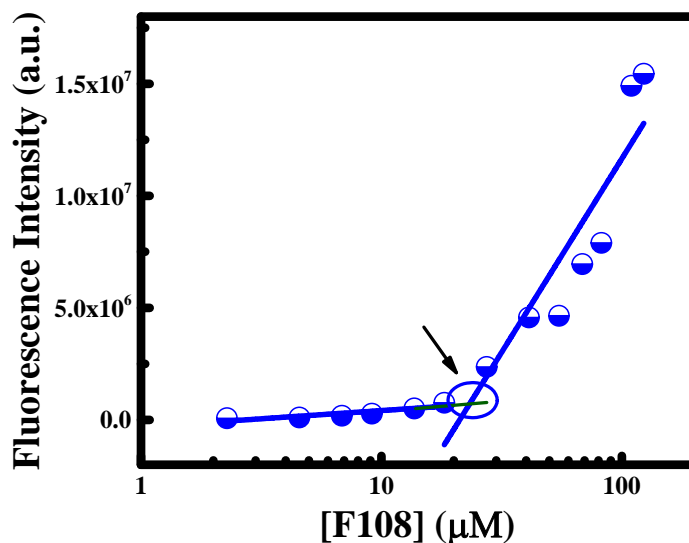


Figure II. 2 Fluorescence intensities of curcumin at 512 nm plotted versus concentration of F108

To examine the effect of ionic strength on the interaction of curcumin with F108, the fluorescence spectra of curcumin was tracked for the different concentrations of F108, where the concentration of NaCl was varied from 1 to 150 mM. The fluorescence intensity of curcumin was monitored at 512 nm for each NaCl concentration in the presence of different F108 concentrations (See Figure II. 4). It is evident from Table II.1 and Figure II.5 that the CMC value was significantly lowered from 23.2 to 7.94 μM as the NaCl concentration reaches 150 mM. This is estimated as a 3-fold decrease. Indeed, this observation is not surprising as it is widely conveyed in previous similar studies that NaCl reduces the CMC of micelle.⁹⁸ Previous studies utilizing SANS on pluronic F88 ($\text{E}_{103}\text{PO}_{39}\text{EO}_{103}$) have revealed that the PEO moiety got dehydrated with the addition of salt.¹⁰⁵ Reduction of CMC value i.e. enhancement of micellization in the presence of salt is quite expected as the NaCl salt introduces the salting-out effect.²⁸

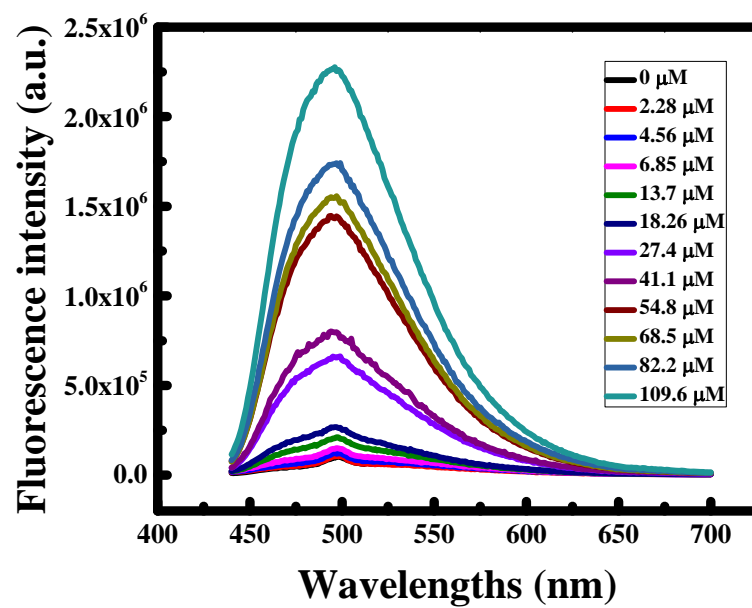


Figure II. 3 Fluorescence emission spectra of curcumin (3.33 μM) at different concentrations of F108 in the presence of 1 mM NaCl

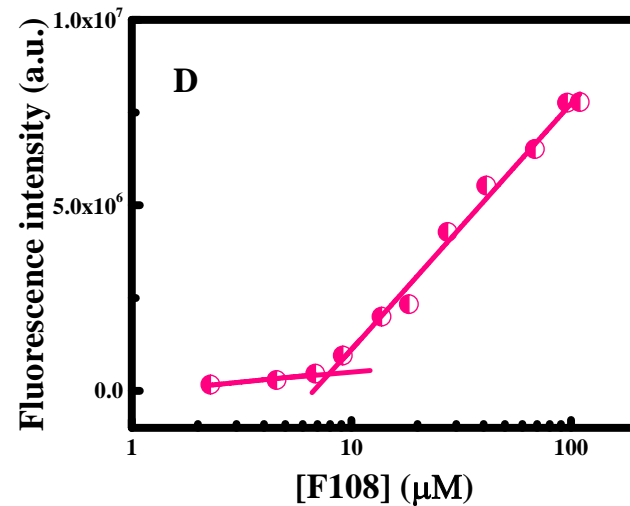
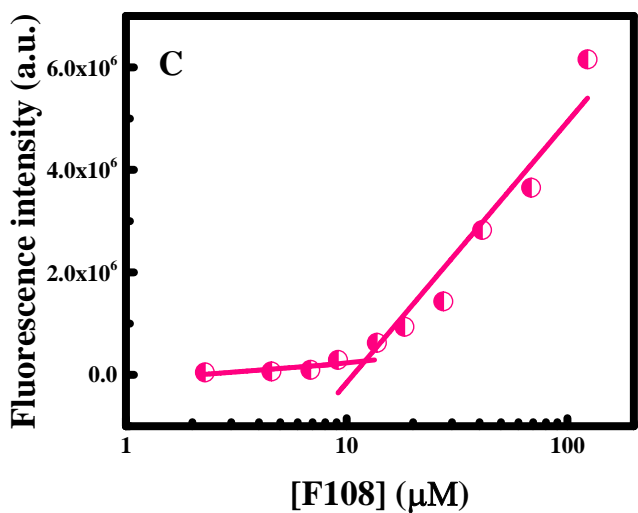
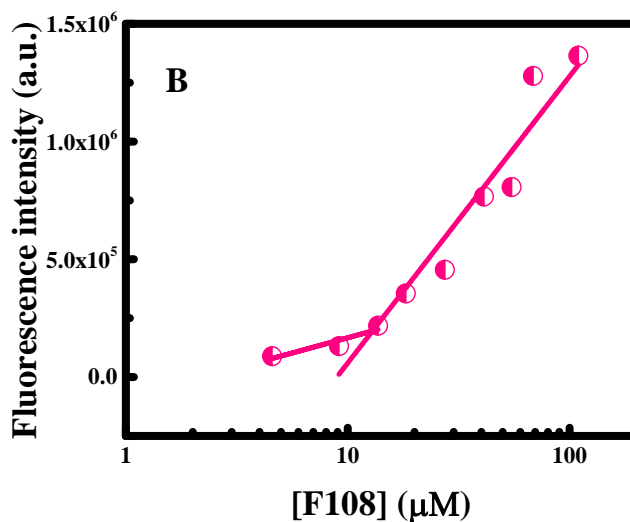
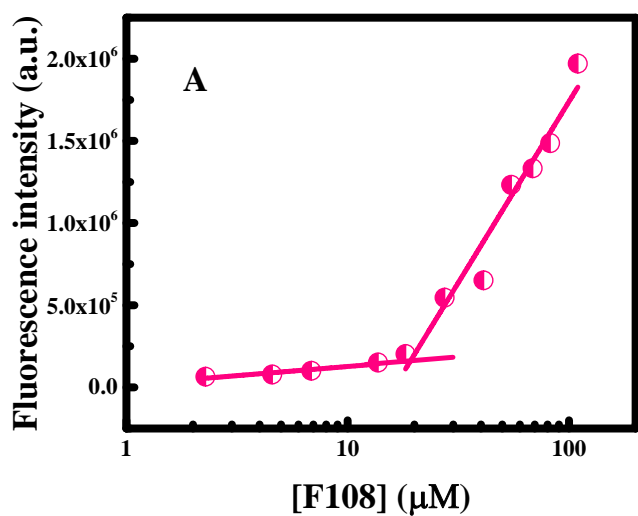


Figure II. 4 Fluorescence intensities of curcumin at 512 nm plotted versus concentration of F108 and 3.33 μM curcumin in the presence of A. 1 mM, B. 10 mM, C. 100 mM, and D. 150 mM NaCl

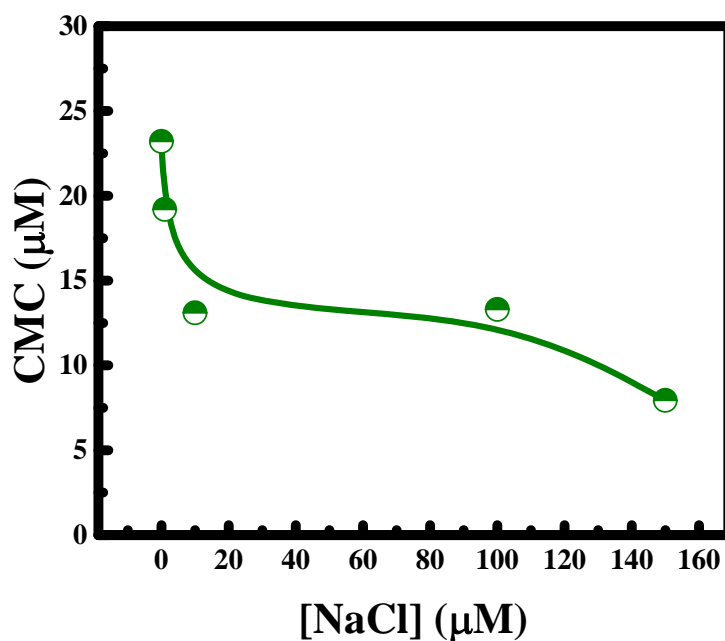


Figure II. 5 CMC variation with increasing concentration of sodium chloride

Bile salt contains a hydrophobic anion which gives it unique properties. In a heterogeneous environment where aggregation processes, micelles or membranes occur, bile salt interacts differently compared to ionic salt.⁹⁹ It can alter micelle/membrane properties through partitioning into these structures.⁹⁹ In this study, the effect of two bile salts, sodium cholate (NaC) (Figure II. 7) and sodium deoxycholate (NaDC) (Figure II. 7), on CMC of F108 was investigated. First, 0.25, 0.5. and 1 mM of NaC were added to solutions containing a range of F108 concentrations for which fluorescence measurements was conducted (See Figure II. 6). Rather than being quenched, an enhancement in the emission intensity of curcumin was observed (Figure II. 8). The increase in curcumin's fluorescence intensity in the presence of sodium cholate proposes a cooperation between the hydrophobic cholate anion and curcumin along with F108 that leads to stabilization of

the excited state of curcumin. However, the enhancement of intensity was more pronounced at higher concentrations of F108, and this is expected as curcumin's excited state gets more stabilized in the post-aggregation stage. A blue shift in the emission maximum of curcumin was noted as shown in (Figure II.6). The blueshift is a sign of aggregation of F108 in higher concentrations in which curcumin experiences a different microenvironment, namely a nonpolar one. CMC values in the presence of NaC presented in Table II.1 showed a 1-fold reduction compared to CMC of F108 then an increase was observed. In the presence of NaC, the aggregation/micelle formed is no more the same as we expect without NaC, because the hydrophobic cholate ions get integrated into the micelle/structure, largely locating around the Stern-layer of the micelle and exposing the charged anion towards the aqueous medium as presented in. Thus, hydrophobic cholate ion boosts to bring hydrophobic layers of polymer to come in contact with each other by reducing the CMC.

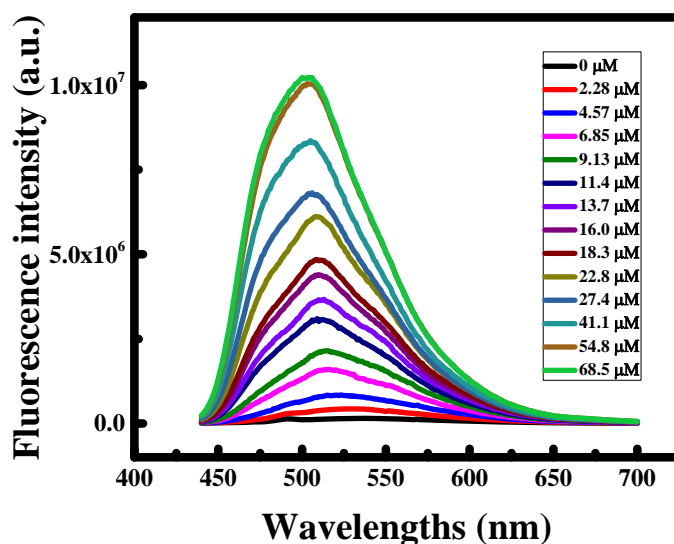


Figure II. 6 Fluorescence emission spectra of curcumin obtained at different concentrations of F108 and 3.33 μM curcumin in the presence of 0.25 mM NaC

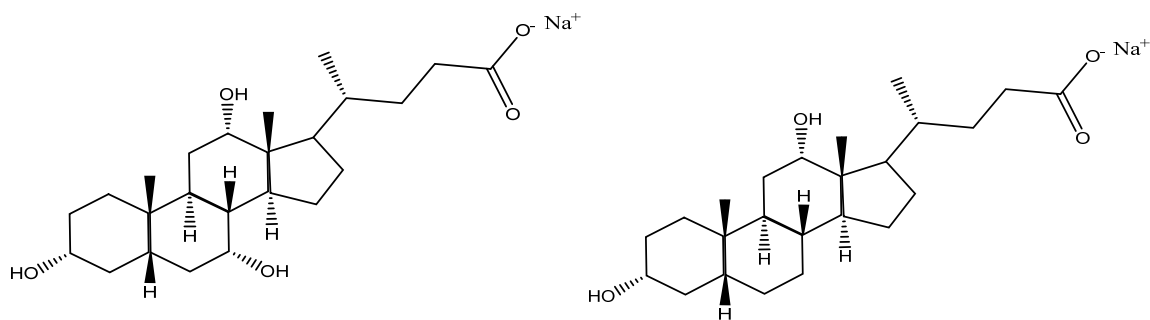


Figure II. 7 Structures of sodium cholate (left) and sodium deoxycholate (right)

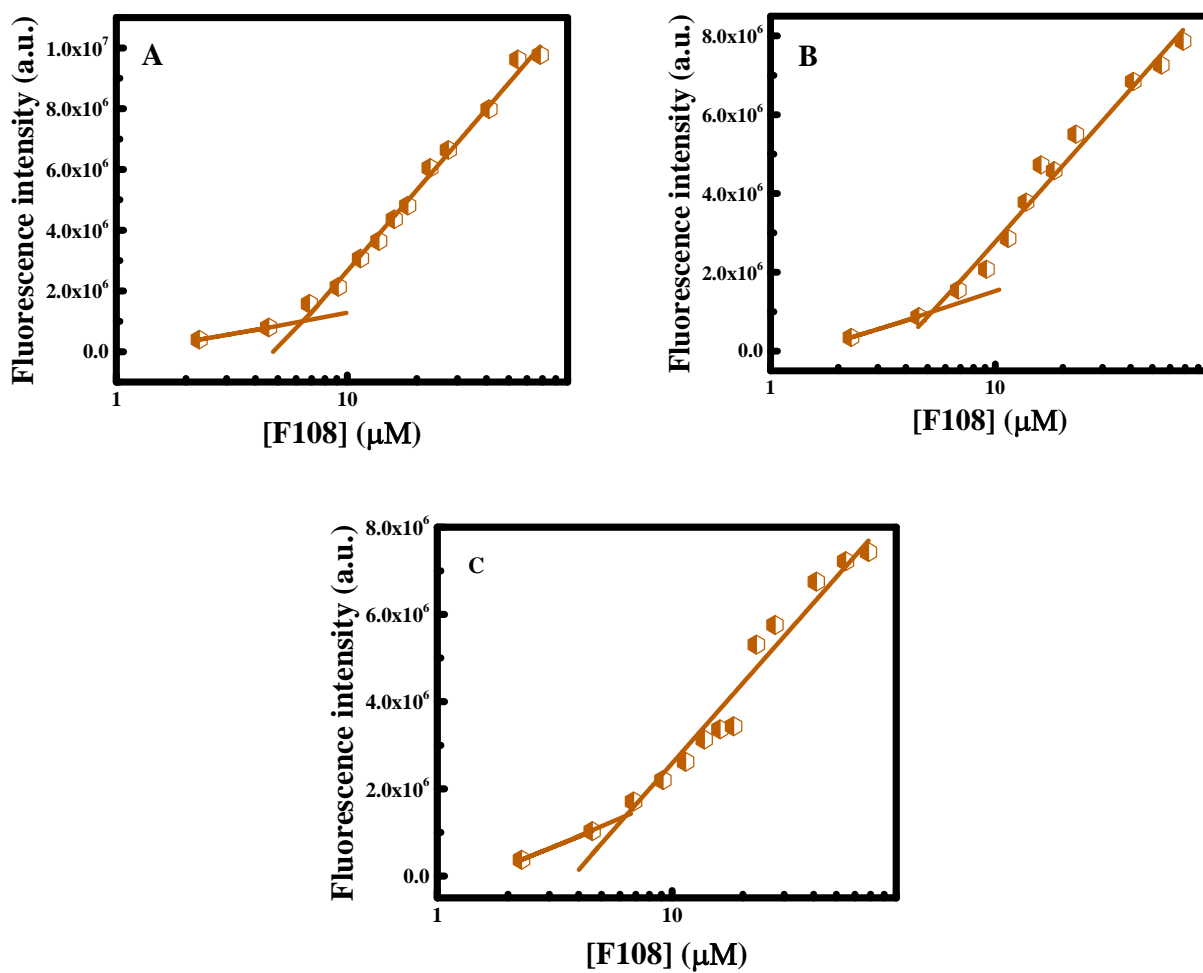


Figure II. 8 Fluorescence intensities of curcumin at 512 nm versus concentrations of F108 in the presence of 3.33 μM of curcumin and A. 0.25 mM, B. 0.5 mM, and C. 5 mM NaC

Another bile salt tested was sodium deoxycholate. Similar to NaC, an increase in the fluorescence intensity of curcumin and a blue shift were noticed at higher F108 concentrations, which is a sign of stabilizing curcumin's excited state (See Figure II.9). The CMC was estimated in the presence of 0.25, 0.5 and 1 mM of NaDC, and values are summarized in Table II.1. As mentioned earlier, CMC was estimated from the breaking point of the graphs which show the fluorescence intensity alteration as shown in Figure II.10. It was found that CMC decreased with the increase in NaDC concentration similar to what was observed for NaCl. However, the effect was more pronounced for NaDC compared to NaC (1-fold) and NaCl (9-fold for NaDC as compared to a 3-fold decrease for NaCl). This could be due to the hydrophobic nature of NaDC compared to NaC, as the polymeric aggregate may completely form a new kind of micelle in the presence of NaDC comparing with NaC due to lower CMC value. Note that at the highest concentration of NaDC (1 mM) there was no CMC detected due to its low value indicating fast micellization.

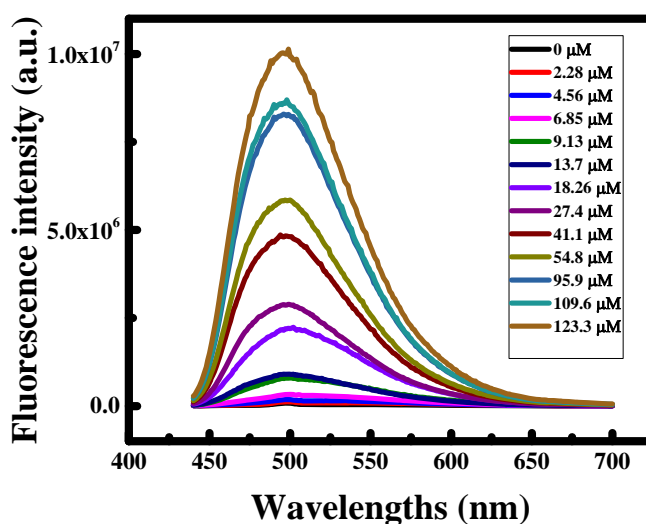


Figure II. 9 Fluorescence emission spectra of curcumin at different concentrations of F108 in the presence of 0.25 mM NaDC

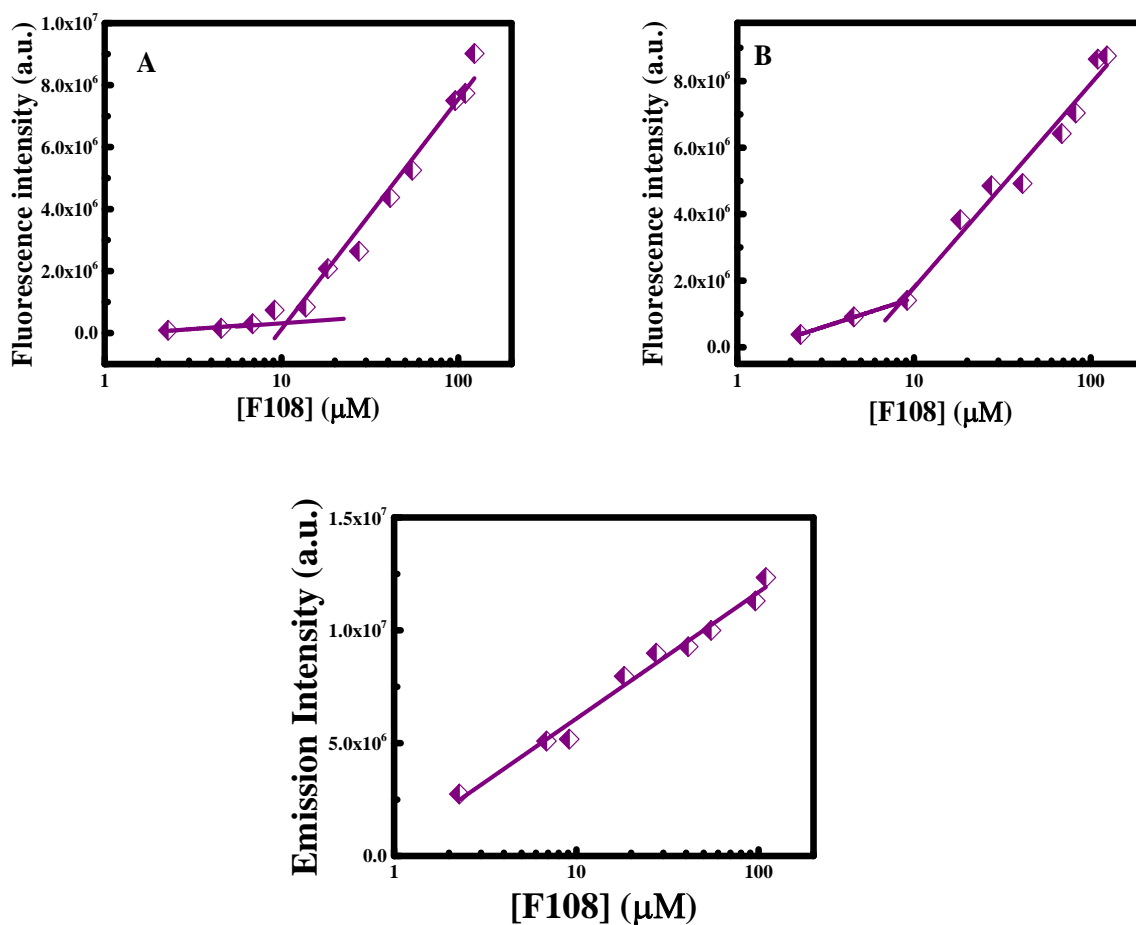


Figure II. 10 Fluorescence intensities of curcumin at 512 nm versus concentrations of F108 in the presence of A. 0.25 mM, B. 0.5 mM, and C. 1 mM NaDC

	Critical micellar concentration (CMC) (μM)							
	0 mM	0.25 mM	0.5 mM	1 mM	5.0 mM	10.0 mM	100.0 mM	150.0 mM
NaCl	23.2			19.2		13.1	12.1	7.94
NaC	23.2	6.36	5.23		6.25			
NaDC	23.2	12.5	9.05	Not detected				

Table II. 1 CMC values at different concentrations of sodium chloride, sodium cholate and deoxycholate

2. Self-assembly and critical micelle temperature

Micelle formation of pluronics is not only concentration-dependent, but also it is very sensitive to temperature.¹⁸ Pluronic polymers exist in the form of unimers at low temperatures and start to form micellar aggregates at temperatures higher than CMT.¹⁰⁶⁻¹⁰⁷ Because temperature has a direct crucial effect on the micellization process, we decided to evaluate the CMT of F108 at a concentration (82.2 μM) that exceeded the CMC of F108 (23.2 μM) observed in our previous results. Fluorescence spectra of aqueous solution with 82.2 μM F108 (named solution X) and 3.02 μM curcumin were monitored at 2-5 $^{\circ}\text{C}$ temperature intervals over the range 5-70 $^{\circ}\text{C}$ as shown in Figure II. 11. Emission intensity of curcumin remained almost constant between 5 and 35 $^{\circ}\text{C}$ (Figure II. 12). This is expected because at low temperature, F108 does not aggregate in aqueous solution. Thus, a hydrophobic pocket in which curcumin can be solubilized and stabilized was not formed yet, and, as a result, the fluorescence intensity of curcumin was very low. When temperature reached 35 $^{\circ}\text{C}$, an abrupt increase in the intensity occurred. This sudden enhancement indicates the formation of micelles with hydrophobic interior in which curcumin can be solubilized, giving a characteristic spectrum.¹⁰⁸ Increasing the temperature of copolymer aqueous solution ruptures the hydrogen bonds between the PPO block and water molecules. This leads to the dehydration of the PPO groups, permitting the hydrophobic interactions between the hydrophobic segments to take place.¹⁰⁹ Therefore, we can say that there is a distinct temperature at which fluorescence intensity enhances dramatically indicating the aggregation of unimers into micelles. This break point can

therefore be designated out as CMT. In our case, it was obtained at 35 °C. This is in good agreement with literature values obtained by Alexandridis et al.¹⁸ using DPH solubilization technique; CMT obtained at 68 μM F108 was 36 °C which is quite comparable to our value (35 °C) obtained at 82.2 μM, keeping in mind that CMT decreases as the concentration of the pluronic increases. At ~55 °C, an unexpected sudden decrease in the intensity was observed. This can be attributed to the decrease in the micelles' viscosity at very high temperatures, which will push curcumin away from the hydrophobic interior to the aqueous exterior, and, thus, making it insoluble again. Therefore, there are two factors that interplay in this process: aggregation and viscosity of micelles. The first factor dominates starting from the CMT up to a certain high temperature after which the viscosity factor takes over.

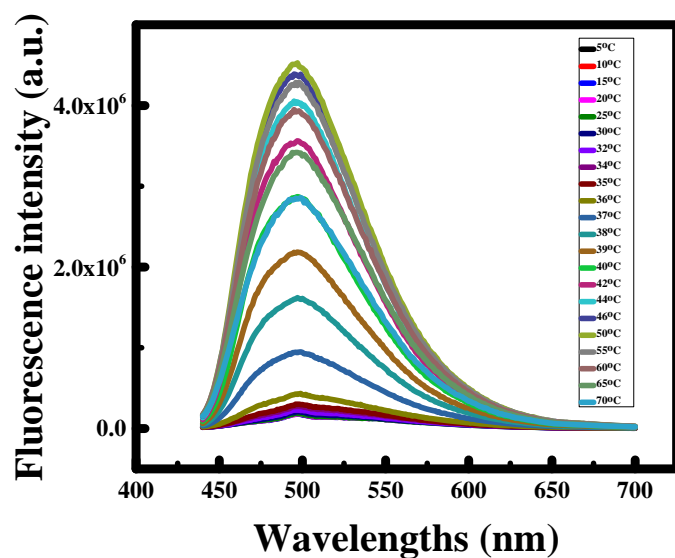


Figure II. 11 Fluorescence emission spectra of 3.33 μM curcumin obtained at a fixed concentration of F108 and different temperatures

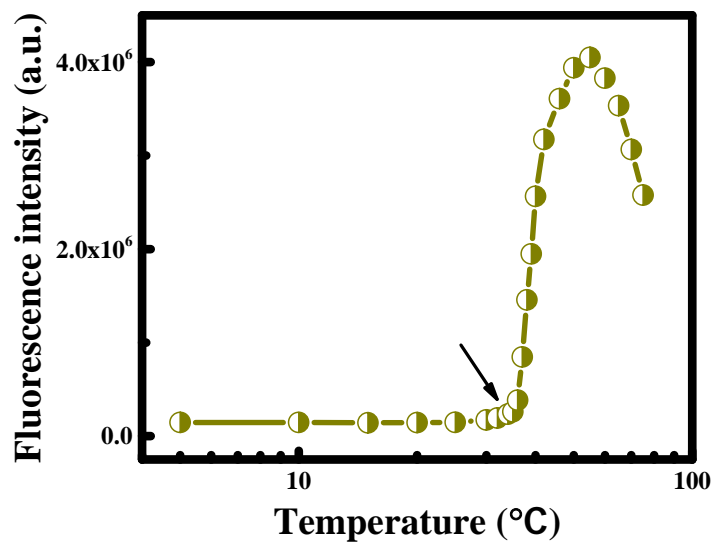


Figure II. 12 Fluorescence emission spectra of 3.33 μM curcumin obtained at a fixed concentration of F108 and different temperatures
Fluorescence intensities of curcumin at 512 nm versus temperature

Similar to the previous part, we tried to figure out the effect of NaCl on the CMT value of F108. So, we added 1, 10, 100, and 150 mM NaCl to the solution X for which the fluorescence intensity of curcumin was monitored (Figure II. 14). Results of CMT are shown in Table II. 2. Interestingly, the trend obtained shows decreasing values of CMT but the effect was not very pronounced (only 3 °C decrease). Hence, salts have a more pronounced and direct effect on CMC than CMT. This is in accordance with literature studies where it is manifested that all ionic liquids or salts causes the reduction of CMT whenever their concentration increases.¹⁰⁹

0.25, 0.5, 1 and 5 mM of NaC were also added to solution X to check the interaction of hydrophobic bile salt on the CMT of micellization (Figure II. 16, 18). Results show a negligible effect for this salt on the CMT of F108. However, adding NaDC progressively decreased the CMT from 35 °C to around 31.7 °C, which means that NaDC has a higher influence on the micellization of F108 compared to NaC. NaDC and NaCl both were able to reduce the CMT, endorsing the micellization process.

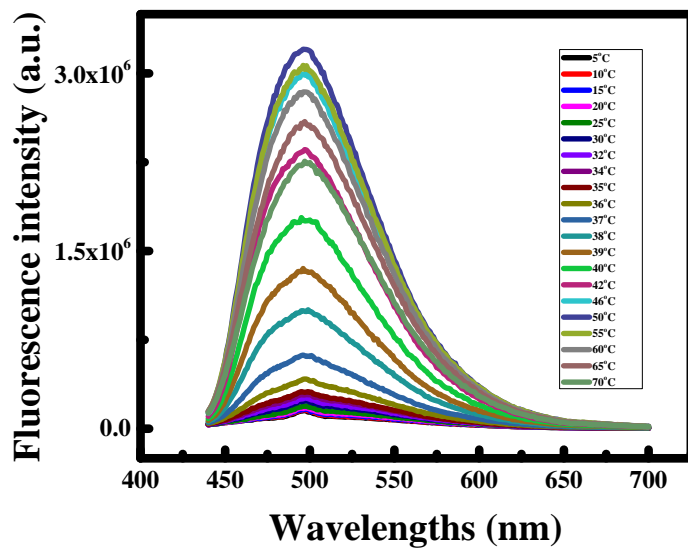


Figure II. 13 Fluorescence emission spectra of 3.33 μM curcumin obtained at a fixed concentration of F108 and different temperatures

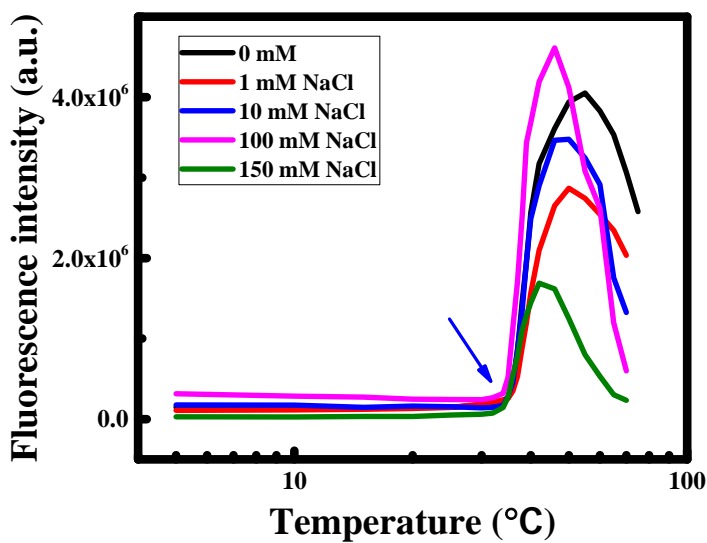


Figure II. 14 Fluorescence emission spectra of 3.33 μM curcumin obtained at a fixed concentration of F108 and different temperatures

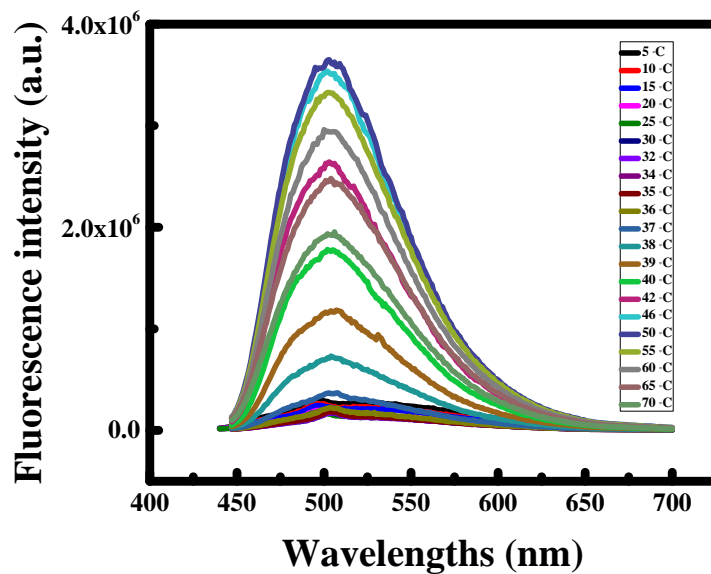


Figure II. 15 Fluorescence emission spectra of 3.33 μM curcumin obtained at a fixed concentration of F108 and different temperatures

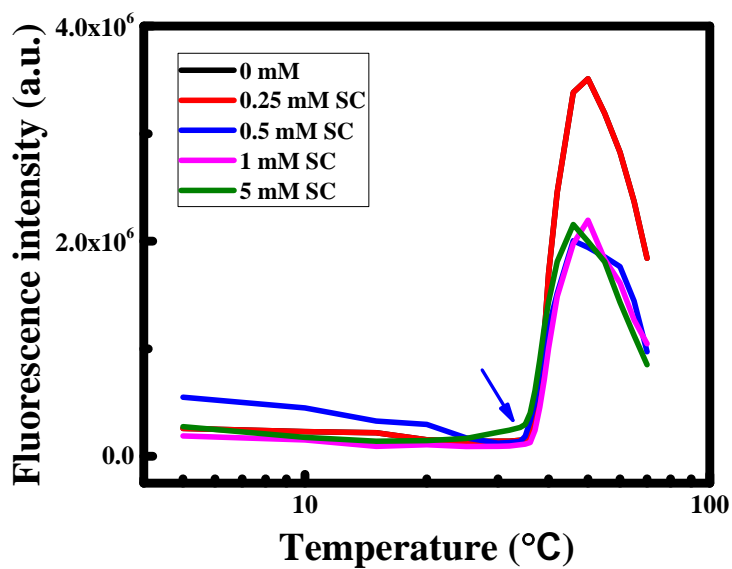


Figure II. 16 Fluorescence intensities of curcumin at 512 nm versus temperatures at different concentrations of sodium cholate

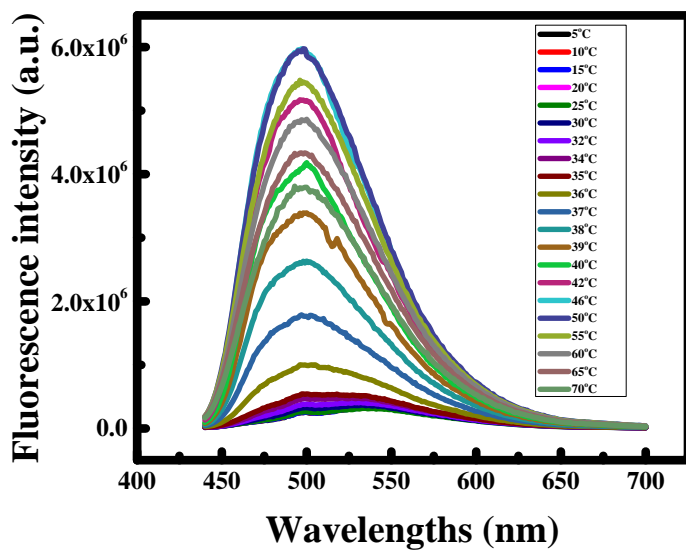


Figure II. 17 Fluorescence emission spectra of curcumin at different temperatures in the presence of 0.25 mM sodium deoxycholate

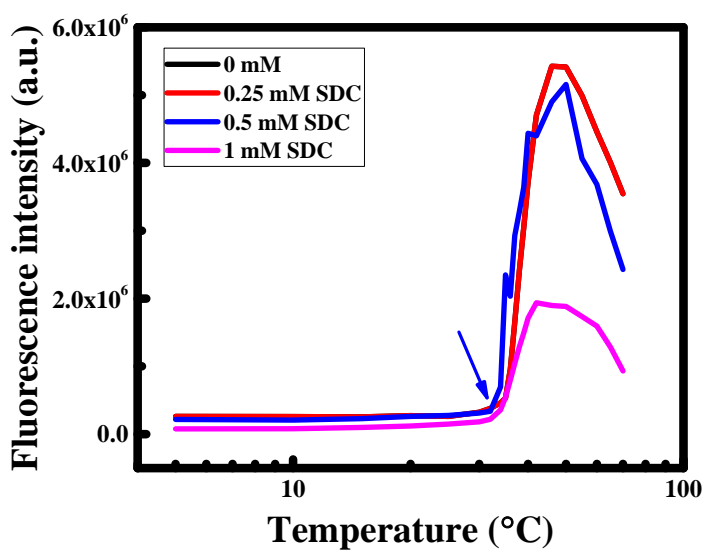


Figure II. 18 Fluorescence intensities of curcumin at 512 nm versus temperature at different concentrations of sodium deoxycholate

Critical micellar temperature (CMT) (°C)								
	0 mM	0.25 mM	0.5 mM	1 mM	5.0 mM	10.0 mM	100.0 mM	150.0 mM
NaCl	35.0			35.0		33.8	33.5	32.1
NaC	35.0	36.0	33.7	35.7	35.0			
NaDC	35.0	34.1	32.0	31.7				

Table II. 2 CMT values at different concentrations of sodium chloride, sodium cholate and deoxycholate

3. Location of probe molecule, curcumin

Any process which diminishes the fluorescence intensity of a molecule can be referred to as a fluorescence quenching. Crucial information about the distribution and microenvironment of a drug can be obtained by fluorescence quenching studies on polymer bound fluorescence probe by external quencher molecule. In our study, two established quenchers were used: a hydrophilic quencher, KI¹¹⁰ and another hydrophobic one, CPB. It is well-known in the literature that Γ has a preference to stay in the aqueous phase because of its negatively charged surface. However, CPB's long 16 carbon unit hydrocarbon chain can get easily fused in the hydrophobic region whereas the positive pyridinium moiety of CPB stays in vicinity to water molecules.¹¹¹ In this study, the fluorescence quenching of curcumin by KI and CPB was measured using the Stern-Volmer plot:¹¹⁰

$$\ln \frac{I_0}{I} = 1 + K_{SV}[KI] \quad (9)$$

Where I_0 and I are the intensities of curcumin in the absence and presence of the quencher molecule, respectively, and K_{SV} is the Stern-Volmer quenching rate constant.

Results shown in Figure II. 20 shows that the fluorescence intensity of curcumin decreases as the concentration of CPB increases indicated in the trend of fluorescence emission spectra in Figure II. 19. CPB quenches the fluorescence intensity of curcumin by electron transfer process.¹¹² Curcumin acts as a donor where electron in the excited state is transferred from the aromatic ring of curcumin to electron deficient N-atom of CPB.¹¹³ The CPB tail intercalates into the hydrophobic part of F108 micelles and stays at the Stern layer with its charged moiety exposed at the surface. Therefore, interaction between curcumin and pyridinium ion will only be favored if F108 micelles allow curcumin to align parallel to the hydrophobic tail of CPB similar to what is reported for curcumin in liposomes.¹¹⁴⁻¹¹⁵ So, the reduced intensity of curcumin is logical as it interacts with CPB at the Stern layer, donating an electron to the N^+ -atom of CPB, after which it escapes the hydrophobic pocket to the aqueous medium. This suggests that curcumin is also located within the hydrophobic domain of micelle near the Stern layer. The Stern-Volmer plot for fluorescence quenching of curcumin by CPB is shown in Figure II. 21, and it shows a linear increasing trend having K_{SV} equal to 0.00201 M^{-1} . The quenching rate constant (K_{sv}) of curcumin by CPB in liposomes was found to be 0.00187 M^{-1} , and this is in good agreement with our value. On the other hand, quenching by KI gave us almost no change in the fluorescence intensity of curcumin as shown in Figure II. 22. This suggests the absence of interaction between curcumin and I^- ; this conclusion is quite expected as it is known that I^- prefers to stay in the aqueous domain where it is so distant from curcumin located at the interface of the micelle.

Therefore, this further assures our observation from CPB quenching where it is clearly demonstrated that curcumin enters the hydrophobic pocket of the micelle successfully but stays at the Stern layer.

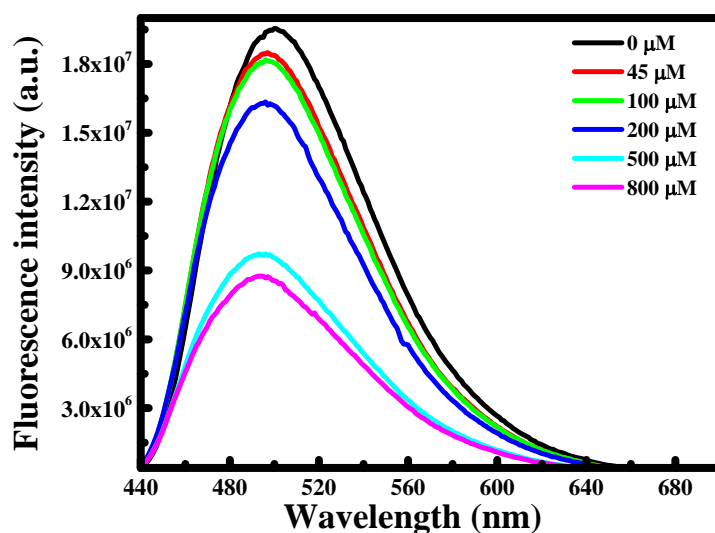


Figure II. 19 Fluorescence emission spectra of curcumin obtained at different concentrations of CPB

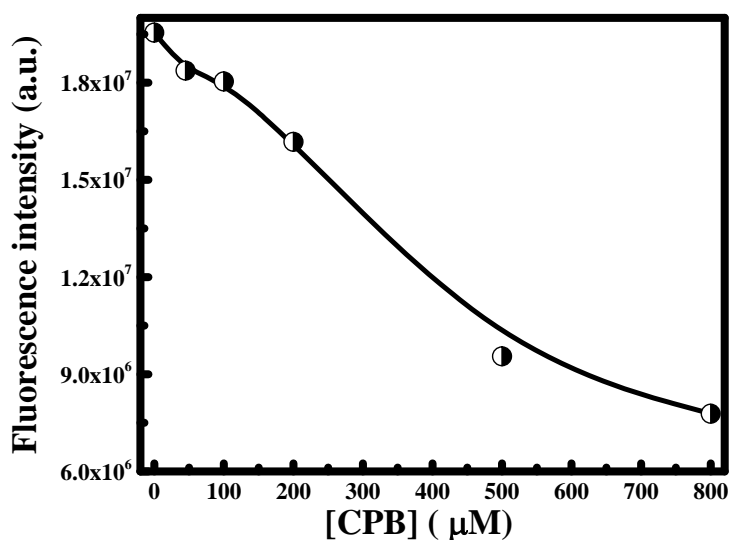


Figure II. 20 Emission intensity of curcumin at 512 nm versus concentration of CPB

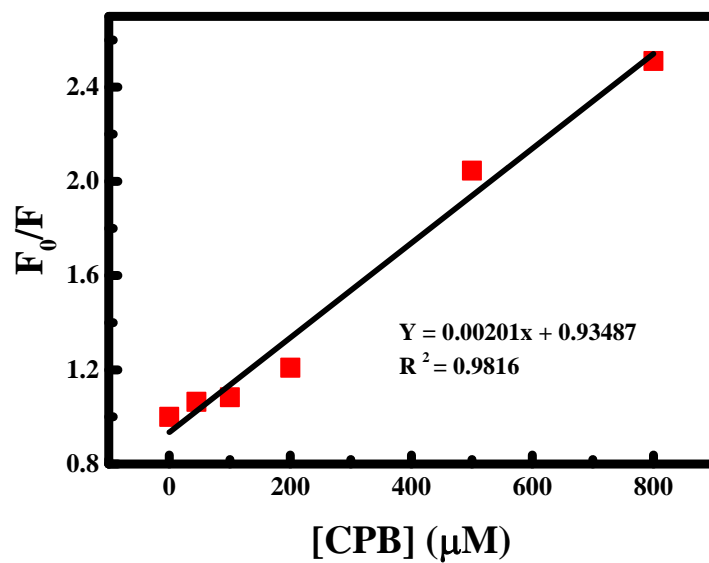


Figure II. 21 F_0/F versus concentration of CPB (Stern volmer plot)

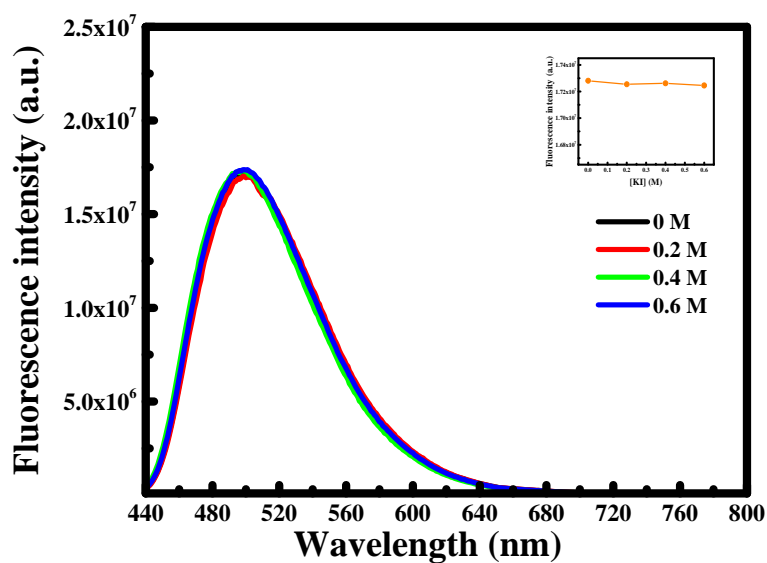


Figure II. 22 Fluorescence emission spectra of curcumin at different concentrations of KI. Inset is the emission intensity plotted at 512 nm versus KI concentrations

4. Formation of F108 micelles in solution

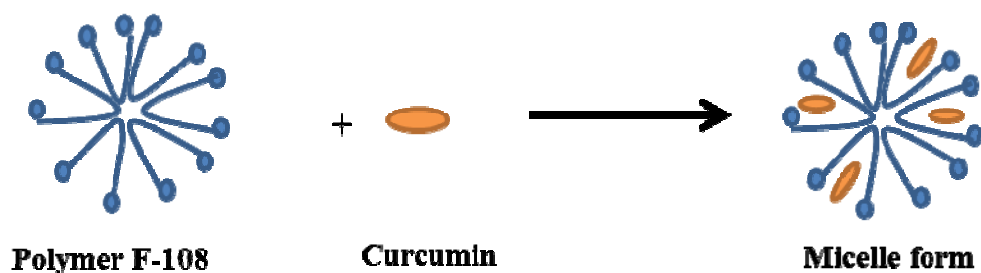


Figure II. 23 Schematic illustration of curcumin-F108 micelle formation

D. Conclusion:

To study the micellization behavior of f108 in solution, curcumin was used as a fluorescence probe to determine the CMC and CMT of f108, which were found to be 23.2 μM and 35 $^{\circ}\text{C}$, respectively. Curcumin was also used to track changes in CMC and CMT with the addition of different salts. It was found that NaCl reduced the CMC and CMT respectively owing to the salting out effect. However, NaC and NaDC decreased the CMC but did not affect the CMT much. Fluorescence quenching using KI and CPB was performed to locate curcumin in the micelle. It was found that curcumin is positioned at the stern layer of the F108 micelle.

CHAPTER III

NANOCAPSULE FORMATION OF POLY(ETHYLENE OXIDE)- *BLOCK*-POLY (PROPYLENE OXIDE)-*BLOCK*- POLY(ETHYLENE OXIDE) FOR CURCUMIN DELIVERY

A. Introduction

Smart polymers with responsive properties have received much interest in the last few decades because of their crucial role in nanoscience and drug delivery applications.¹¹⁶⁻¹¹⁷ Water-soluble polymers, specifically, are of great importance in stabilizing nanoparticles, drug delivery, tissue engineering, bioelectronics, and biosensing applications.¹¹⁸ Properties like non-toxicity, biological compatibility, chemical diversity and high commercial availability increase interest in such polymers for a wide range of formulations and health-care or medicinal applications.¹¹⁹ The chemical dissimilarity between the two blocks of pluronics renders them as amphiphilic molecules with surface-active properties. The segregation in the polarity of the two blocks in aqueous media, PEO solubility and PPO insolubility, give rise to useful nanostructures, called micelles, formed in solution by the process of self-assembly. Because of their nano-size, structure diversity, and adsorption properties¹²⁰⁻¹²¹ such structures proved importance in many applications like: drug-delivery,¹²² nanoparticle synthesis,¹²³ effective dispersants for inks/pigments,¹²⁴ and various emulsion applications.¹²⁵ F108 belong to this class of block copolymers. It has a high hydrophilic character, 80 % PEO, an average molecular weight of 14600 g/mol, and can self-assemble into micelles in aqueous solution or can form nanoparticles under specific

conditions. Such structures are constituted of a swollen hydrophobic core with all the PPO blocks aggregated and a hydrophilic surface where the PEO terminal chains are exposed to the polar solvent molecules, such as water.³¹ The hydrophobic domain offers a cargo space for delivering various hydrophobic drugs, which is at the core of the utility of these structures in drug delivery applications.³⁸⁻³⁹ Curcumin, or 1,7-bis(4-hydroxy-3-methoxyphenyl)-1,6-heptadiene-3,5-dione, is a β -diketo structure which tautomerizes between an enol and keto structures. It is a major constituent of turmeric extract which has illustrated many therapeutic uses, including anti-inflammatory, anti-oxidant,⁶⁵ and anti-cancer activities.¹²⁶ However, curcumin is limited by its low oral bioavailability which is attributed to poor water-solubility, fast elimination from the body, and high rate of metabolism.⁸⁵ Therefore, different methods have been employed to overcome limitations. Such methods include developing different formulations, like liposomes, phospholipid complexes, or polymeric micelles. In this work, our aim is to enhance the solubility and oral-bioavailability of curcumin through encapsulating it in F108 nanocapsules and characterizing these structures using X-ray diffraction (XRD), thermogravimetric analysis (TGA), scanning electron microscopy (SEM), and Fourier-transform infrared spectroscopy (FTIR). In previous studies, there were attempts to encapsulate curcumin in F68 and F127 micelles¹²⁷ and other pluronics. However, limited research demonstrated encapsulation of curcumin in F108 nanocapsules, having a 1:1 ratio of curcumin to F108. Moreover, using photodynamic therapy, this study aims at testing the therapeutic activity of these nanocapsules in two types of cancer cells, A-549 and A-537 cells.

B. Materials and Methods

Note: Experiments were made in duplicates and nanocapsules were prepared in triplicates

1. Materials

Curcumin and pluronic F108 were purchased from Sigma-Aldrich. To increase its solubility, acetone of HPLC grade was obtained from ALPHA Chimie and used to dissolve curcumin. Deoxyribonucleic acid from Aldrich and ribonucleic acid from Toscat.

Cell cultures

The cell cultures consisted of human lung adenocarcinoma (A549) and human malignant melanoma (A375) purchased from ATCC cell collection, USA. The cells were handled under sterile conditions as previously described.¹²⁸⁻¹³¹

2. 1:1 Nanocapsules preparation

Nanocapsules were prepared by adding 10 mg of curcumin to 10 mg of pluronic F108 and dissolving in 2.5 mL acetone. The solution was kept under stirring for 40 minutes. In the meantime, 2.5 mL of double distilled water was being added dropwise while the solution was under continuous sonication. After that, acetone was evaporated, and the solution was diluted to 10 mL using double distilled water. The formed nanocapsules were left for two overnights to precipitate. The supernatant solution was discarded, and the nanocapsules were allowed to freeze dry for two consecutive days. Finally, a lyophilized formulation was obtained and characterized to be used later on for application.

3. *Sample preparation*

a. Cytotoxicity assays

The cytotoxicity assessment was undertaken by seeding and incubating the respective cells 24 h pre-exposure (in a CO₂ incubator) on 96 well plates at a density of 25,000 cells per well. The tested substances original stock solution was dissolved in DMSO prior to dilution in culture medium. The dilution consisted of a serial dilution (3-fold) for cell survival assessment (Figure III. 6). The percentage of DMSO did not exceed 1%, a concentration not toxic under our experimental conditions. The cytotoxicity was measured 24 hours post-exposures using the MTS assay as previously reported in the literature.^{128-129, 132-133} Briefly, the assay was based on a color reaction with healthy cells converting the yellow Formazan into red color mainly through mitochondrial dehydrogenase activity. Color was measured at 492 nm wavelength in a Multiskan Ascent 96 well Plate Reader. Statistical analysis was undertaken in GraphPad Prism 7 software. All experiments were conducted in triplicates and each point on the presented graphs represented the average of three independent experiments undertaken under identical conditions.

b. The comet assay

The comet assay kit was purchased from Trevigen and consisted of 25 slides. Exposed and control cells (positive using KMnO₄ and negative control using HBSS) were immediately processed for DNA single and double strand damages as per kit manufacturer instruction. Briefly cells were lifted from the 96 well plates, assessed for viability using the countess cell counter. This was followed by mixing the cells at a density of 1×10^5 with

low melting agarose prior to spreading on the comet slide. The slides were allowed to set then subjected to various treatments to unwind and denature DNA. The final step consisted of electrophoresis to allow DNA of damaged cells to migrate as a comet. The various comet parameters were measured using the CASP software.^{129, 131}

4. Instrumentation

The size of nanocapsules was measured using scanning electron microscopy (SEM). This analysis was done using Tescan, Vega 3 LMU with Oxford Edx detector (Inca XmaW20) SEM, where 1 mg of the nanocapsules were dissolved in 20 mL of double distilled water, and few drops of the nanocapsules suspension were placed on an aluminium stub, coated with carbon adhesive. The SEM analysis of this sample was done after being dried.

XRD characterization was achieved using a Bruker D8 advance X-ray diffractometer (Bruker AXS GmbH, Karlsruhe, Germany) at 40 kV, 40 mA (1,600 W) using Cu K α radiation ($\lambda = 1.5418 \text{ \AA}$), with a 1.2 mm primary beam slit and 2.0 mm detector slit. The X-ray scans were carried out for 2θ between 3 and 80 degrees at 0.02° increments.

Thermogravimetric Analysis (TGA) was performed using a Netzsch TGA 209 in the temperature range of 100 to 1000 °C with an increase of $10 \text{ }^\circ\text{C min}^{-1}$ under an N₂ atmosphere.

5. Spectroscopic method

FT-IR spectra were recorded using a Thermo Scientific Nicolet iS5 FT-IR Spectrophotometer using KBr pellets.

C. Results and Discussion

1. Formation of nanocapsules

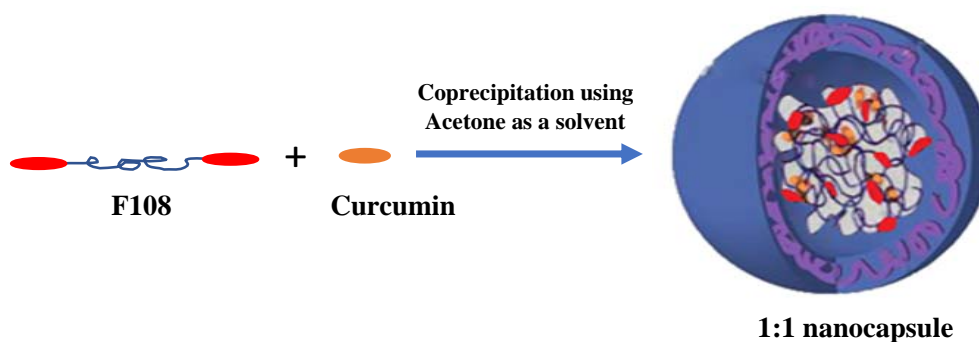


Figure III. 1 Schematic illustration showing the formation of 1:1 nanocapsules

The SEM image of the prepared 1:1 nanocapsules is shown in Figure III. 2. The figure depicts the shape of these particles is spherical and their sizes vary from 270 to 310 nm.

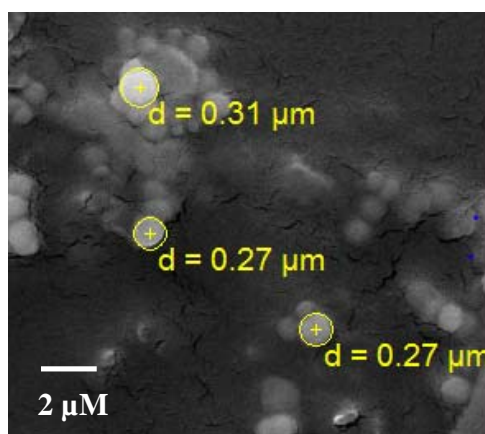


Figure III. 2 SEM images of 1:1 nanocapsules

2. Interaction between curcumin and F108 within the Nanocapsules

The X-ray diffraction pattern was used to characterize the encapsulation interaction between curcumin and F108 in the 1:1 nanocapsules. The diffractograms of F-108, curcumin and the 1:1 nanocapsules are illustrated in Figure III. 3. The characteristic peaks of F-108 were obtained at 19.4° and 23.6° . This crystal line structure is resulting from the formation of PEO crystallites.¹³⁴ As for the curcumin, the main characteristic peaks appeared at diffraction angles of 2Θ equal to 8.06° , 9.20° , 12.46° , 14.95° and 17.75° signifying that curcumin is present in the crystalline form. Yet, it is found that all the relative peaks of curcumin except 14.95° are absent in the spectrum of 1:1 nanocapsules, and the peak at 14.95° was shifted to 14.01° . Hence, this indicates the loss of packing in curcumin structure upon interaction in the nanocapsules.

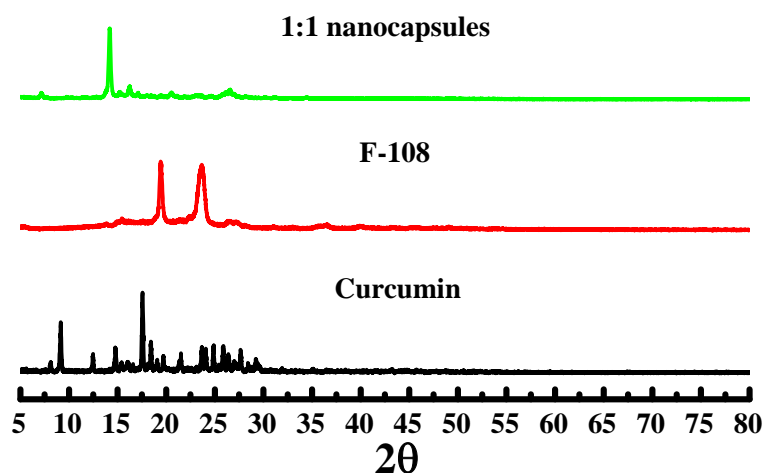


Figure III. 3 XRD patterns

Fourier transform infrared spectroscopy was employed to characterize the 1:1 nanocapsules and depict the type of interaction between curcumin and F108 in the 1:1 nanocapsules (Figure III. 4). In the FTIR spectrum of curcumin, the peak at 3508 cm^{-1} represents the phenolic O-H stretching vibration whereas the peak at 1626 cm^{-1} is due to mixed C=C stretching. Another two bands at 1602 cm^{-1} and 1508 cm^{-1} are attributed to the symmetric aromatic ring stretching vibrations $\nu(\text{C C}_{\text{ring}})$ and (C=O) stretch, respectively. The peak at 1424 cm^{-1} corresponds to the C-H asymmetric stretching whereas C-O stretch appears in the 1280 , 1207 and 1150 cm^{-1} bands. In addition, C-O-C stretch corresponds to the band at 1026 cm^{-1} . The 960 cm^{-1} band corresponds to the trans -CH vibration and finally the peak at 856 cm^{-1} corresponds to C-C skeleton vibration.¹³⁵ In the FT-IR spectrum for the F-108 polymer, the peaks at 2890 cm^{-1} , 1476 cm^{-1} and 1110 cm^{-1} , represent the asymmetric stretching vibrations of -O-H, -C-H, C-C and C=O respectively.¹³⁶

Hence, the band at 3508 cm^{-1} and 1150 cm^{-1} present in the curcumin FT-IR, were shifted to 3409 cm^{-1} and 1130 cm^{-1} respectively in the 1:1 nanocapsules. The shift in these bands verifies the interaction of the curcumin with the polymer at these sites.

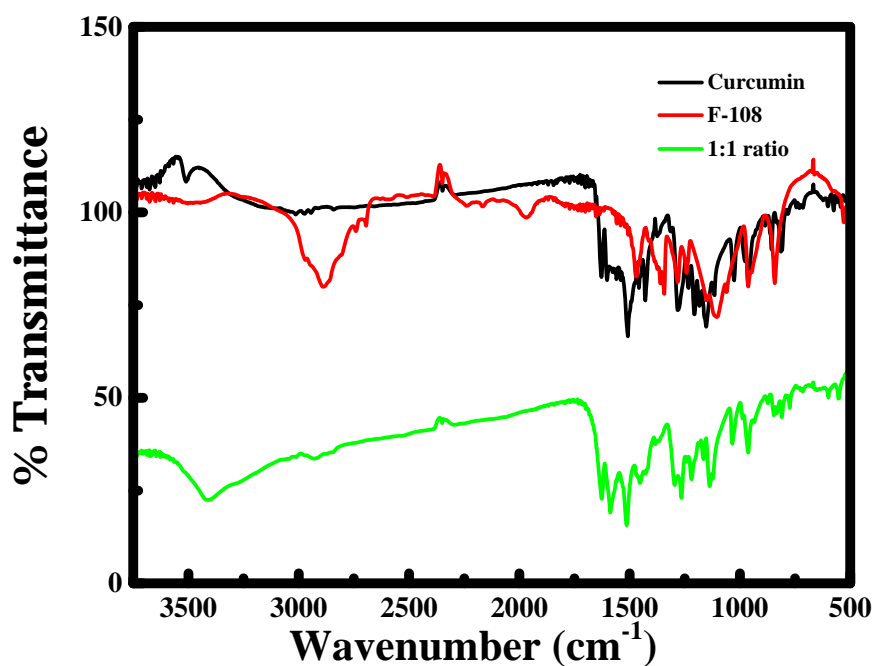


Figure III. 4 FTIR spectra of free curcumin, F108 and 1:1 nanocapsules

Thermogravimetric analysis was used to assess the stability of our prepared 1:1 nanocapsules. Interestingly, no loss of water around 100 °C in any of the three samples was observed which means our samples are dehydrated, and our formed nanocapsules are stable. F-108 illustrated a sharp weight loss between ~350 °C and 400 °C. However, both curcumin and 1:1 nanocapsules illustrated similar degradation pattern which started earlier at ~250 °C. The similarity between curcumin and nanocapsules degradation pattern and the earlier degradation of the nanocapsules compared to F108 suggests that curcumin is incorporated inside the F108 nanocapsules.

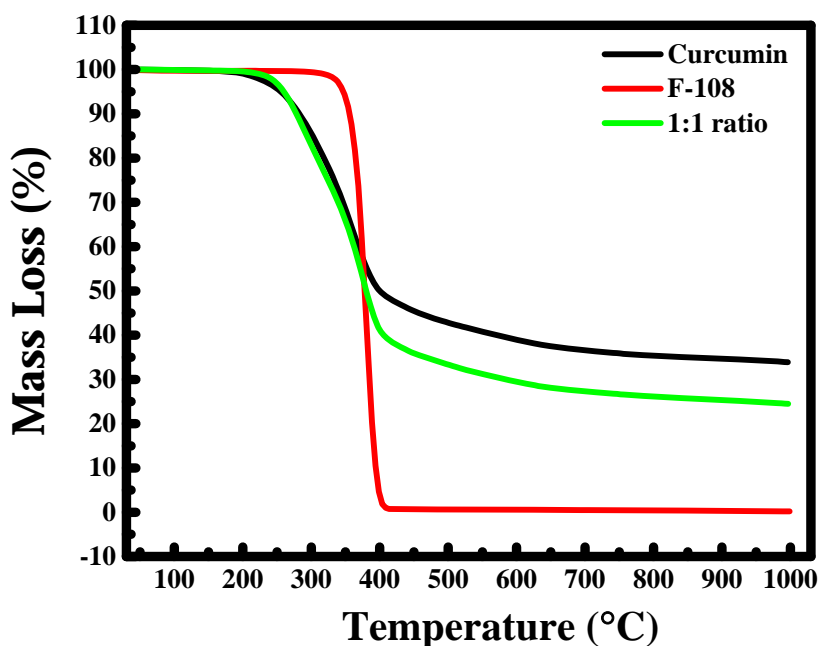


Figure III. 5 TGA patterns for F108, curcumin and 1:1 nanocapsules

3. Photodynamic therapy

In this study, we assessed the toxicity of three compounds; curcumin, nanocapsules, and a polymer F-108 control using two established cancerous human cell lines: A549 human lung adenocarcinoma cells and A375 human malignant melanoma. The various compounds were assessed for toxicity (with or without controlled light irradiation) using the MTS cytotoxicity assay *in vitro*. The irradiated wells were exposed to 30 min blue light irradiation post 6 hours incubation with the drug and the drug was left for a total of 24 h. The IC_{50} on MDA-MB-468 human breast cancer cell lines in the dark was previously reported in the dark ($IC_{50} \sim 1-5 \mu\text{M}$ after 72 h-96 h incubation) and was shown to be time-dependent with negligible activity at 24 h that significantly increase with incubation time

ranging until 96 h.¹³⁷ The IC₅₀ on A549 was found to be 11.2 μM after 72 h incubation.¹³⁸ It was found that curcumin induced apoptosis in upper aerodigestive tract cancer cells through the activation of tumor suppressor p73 and inhibition of p-AKT and Bcl-2.¹³⁸ In this study,¹³⁸ it was also shown that the apoptotic activity of curcumin was increased with the concentration of curcumin and incubation time. In our experiments, we have set the incubation time to 24 h to probe the potential effect of encapsulating the curcumin in nanocapsules as delivery mechanism. The respective IC₅₀ calculated by Graphpad were reported in Table III. 1. The IC₅₀ of curcumin after 24 h exposure in the dark was 148.7 ± 1.0 μM on A549 and 125.4 ± 1.2 μM on A375 cells. After light exposure, curcumin displayed an IC₅₀ of 48.9 ± 0.1 μM on A549 and 47.6 ± 1.1 μM on A375 cells. The phototoxicity indices (IC₅₀ Dark / IC₅₀ Light) of curcumin were 3.0 on A549 and 2.6 on A375. The nanocapsules displayed IC₅₀ in the dark of 4.4 ± 0.1 μM on A549 and 3.9 ± 0.1 μM on A375 cells. Upon light exposure using similar experimental conditions to ones used for curcumin, the IC₅₀ of nanocapsules were 1.8 ± 0.1 μM on A549 and 1.8 ± 0.1 μM on A375 cells. The phototoxicity indices were 2.4 and 2.2 on A549 and A375 respectively. The IC₅₀ of the plain polymer F-108 could not be determined since the cell survival was above 50% even at the highest soluble concentration of the polymer in cell culture media. There was a 34-fold and 32-fold decrease in IC₅₀ on A549 and A375 respectively attributed to the encapsulation of curcumin.

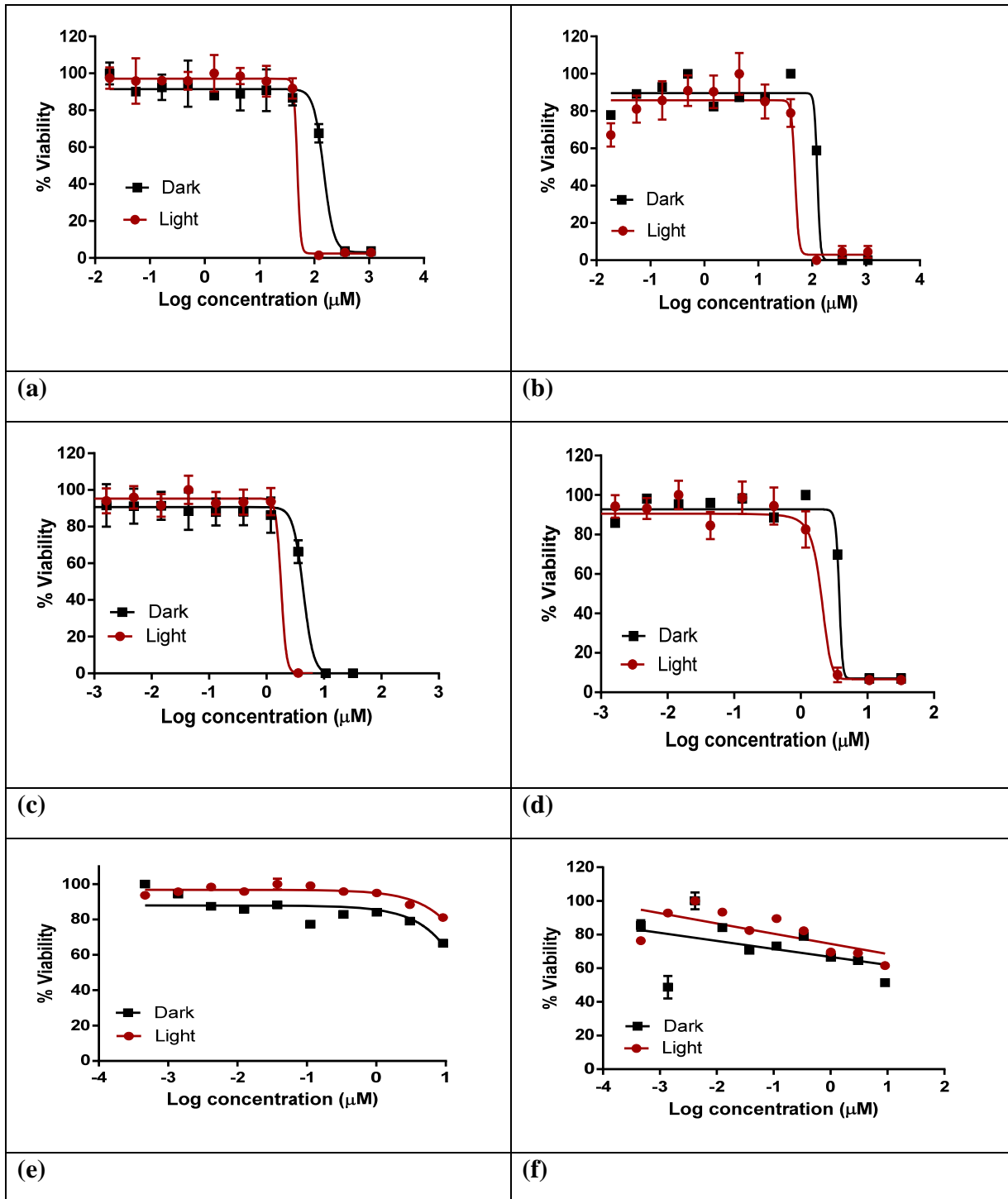


Figure III. 6 Effects of light on compound activity as measured on A549 and A375 cells. (a) Curcumin using A549 cells, (b) curcumin using A375 cells, (c) nanocapsules using A549 cells, (d) nanocapsules using A375 cells, (e) polymer F-108 using A549 cells, (f) polymer

Compounds	IC ₅₀			
	A549		A375	
	Light	Dark	Light	Dark
Curcumin	48.9 ± 0.1	148.7 ± 1.0	47.6 ± 1.1	125.4 ± 1.2
Nanocapsules	1.8 ± 0.1	4.4 ± 0.1	1.8 ± 0.1	3.9 ± 0.1
Polymer F-108	N/A		N/A	

Table III. 1 Calculated IC₅₀ of curcumin, nanocapsules and the polymer F-108 on A549 and A375 cell lines. Each value represents the average of three independent experiments performed on the same day and using the same batch of cells.

Single cell gel electrophoresis, commonly known as comet assay was undertaken on exposed and control A375 cells to elucidate the potential genotoxic mechanism of action of each compound. The comet assay detected single-strand and double-strand breaks and typically indicated DNA damages. The Tail Moment Index (TMI) was calculated from the data generated by the CASP Software using the comet photos and consisted of tail DNA content of cells multiplied by the tail length and divided by 1000. The data displayed in Figure III. 7 shows a significant increase in DNA damage upon light activation in both the nanocapsules and the curcumin compound when compared to the dark conditions. In addition, the extent of DNA damage measured around the IC₅₀ concentration in the nanocapsules was less than the curcumin compound which could be due to the fact that curcumin contain > 200 times more the concentration of curcumin molecules than the nanocapsules at the concentrations used. Upon light exposure, the DNA damage is significantly increased in both the nanocapsules and curcumin indicating efficient

photodynamic therapy in the tested cell line. The increase of DNA damage upon irradiation is likely caused by the production of reactive oxygen species (ROS) which was previously shown to increase when using curcumin for *in vitro* photodynamic therapy of cancer.¹³⁹

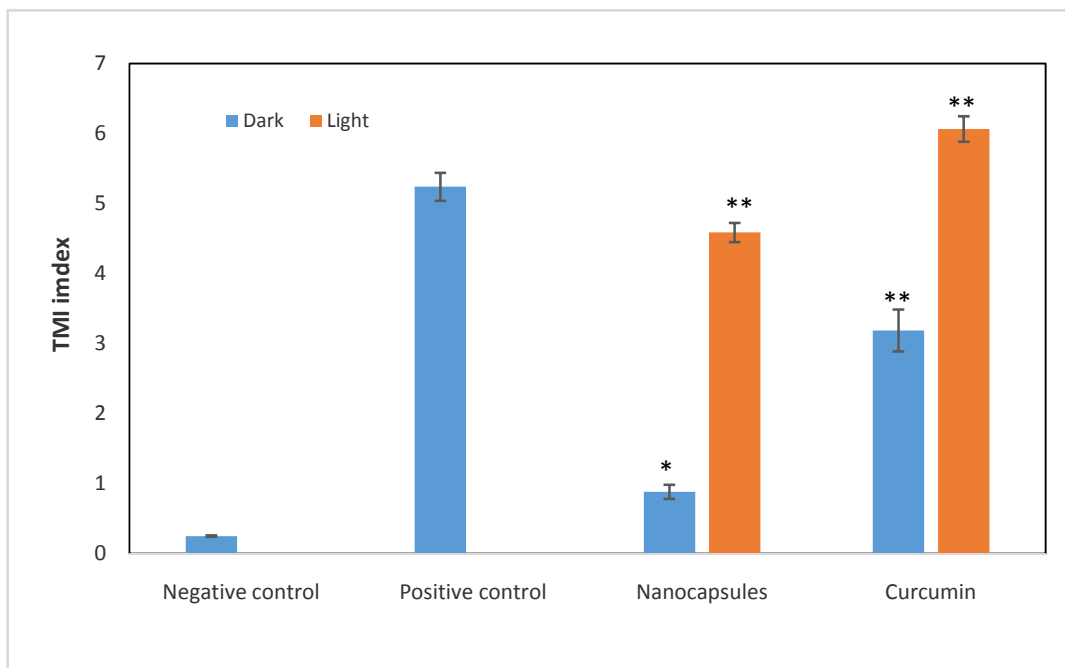


Figure III. 7 DNA damage assessment using the comet assay on negative control (pure cells), positive control (KMnO_4 solution), nanocapsules and curcumin in the dark (blue) and upon light irradiation (red). The concentration of nanocapsules and curcumin were at the IC_{50} in the dark. Statistical significance was reported versus the negative control as follow: * $P \leq 0.05$ and ** $P \leq 0.01$.

D. Conclusion

Curcumin is a well-established therapeutic agent; however, it is limited due to its low water solubility. Therefore, various methods in previous research studies aimed at enhancing curcumin's solubility in water, including encapsulating curcumin in polymeric micelles, liposomes, gold nanoparticles, etc. In this chapter, our aim was to boost the solubility of curcumin in water through encapsulating it in F108 nanocapsules in 1:1 drug to copolymer ratio. This was done using coprecipitation method with acetone as a solvent. Later, nanocapsules were characterized using SEM, XRD, TGA, and FTIR spectroscopy. SEM imaging revealed our prepared nanocapsules as spherical particles whose size was between 270 nm and 310 nm. The XRD spectra of the 1:1 nanocapsules compared to free curcumin clearly illustrated the vanishing of some peaks with a shift in some peaks, indicating successful interaction between curcumin and F108. Besides, the IR spectra further assured this interaction took place at the hydroxyl and carbonyl site of curcumin and F108. TGA patterns showed that nanocapsules are dehydrated and stable till ~250 °C. The cytotoxicity of nanocapsules, curcumin, and F108 control was assessed using two types of human cancerous cells (with or without controlled light irradiation): A549 human lung adenocarcinoma cells and A375 human malignant melanoma. For A549 and A375 respectively, results indicated a 34-fold and 32-fold decrease in the IC₅₀, suggesting enhanced anticancer activity of curcumin when encapsulated. IC₅₀ also decreased in the presence of irradiated light, indicating an efficient photodynamic therapy. The mechanism of action of curcumin was assessed using comet assay on A375 cells. Results showed an increase in the DNA damage for both curcumin and nanocapsules upon exposure to light,

indicating successful photodynamic therapy. The increase in DNA damage was most likely to happen because of the generation of more reactive oxygen species (ROS) in the presence of light.

CHAPTER IV

NANOCAPSULE FORMATION OF POLY(ETHYLENE OXIDE)-*BLOCK*-POLY (PROPYLENE OXIDE)-*BLOCK*-POLY(ETHYLENE OXIDE) FOR FLUORESCENCE SENSING

A. Introduction

Multifunctional nanocapsules present great importance for their potential as probes to label and detect specific targets of interest in biological systems, because they can be detected/imaged using multiple modalities, such as fluorescence. The polymer plays an indispensable role in the process of design, preparation, and development of multifunctional nanoparticles in virtue of excellent biocompatibility and easy surface functionalization. Physicochemical properties of fluorophores can be extremely improved after being coated with a polymer. When the fluorophores are incorporated inside giant polymers, higher fluorescence signal intensity, better biostability (owe to the exclusion of oxygen by the polymer encapsulation), compared to original modality, can be obtained.¹⁴⁰ In this work, curcumin is encapsulated inside of F108 copolymer in 1:40 drug to copolymer ratio to check the effect of copolymer concentration on encapsulation and drug loading. These 1:40 nanocapsules are later characterized by X-ray diffraction, Thermogravimetric Analysis, Scanning Electron Microscopy, UV-visible and fluorescence spectroscopy. A brief comparison between the 1:1 and 1:40 nanocapsules is illustrated based on the characterization. Based on the functionality of curcumin as a fluorescent transducer, encapsulated curcumin is used in biomedical application as DNA and RNA sensing.¹⁴¹ In the field of nanoparticles research and analytical chemistry, emission spectra are recently

being utilized. When the analyte interacts with the probe, the emission intensity is greatly increased.¹⁴²

B. Materials and Methods

Note: Experiments were conducted in duplicates and nanocapsules were repeated in triplicates

1. 1:40 Nanocapsules preparation

Nanocapsules were prepared by adding 10 mg of curcumin to 400 mg of pluronic F108 and dissolving in 2.5 mL acetone. The solution was kept under stirring for 40 minutes. In the meantime, 2.5 mL of double distilled water was being added dropwise while the solution was under continuous sonication. After that, acetone was evaporated, and the solution was diluted to 10 mL using double distilled water. The formed nanocapsules were left for two overnights to precipitate. The supernatant solution was discarded, and the nanocapsules were allowed to dry for two consecutive days. Finally, a lyophilized formulation was obtained and characterized to be used later on for sensing application.

2. Sample preparation

a. UV and fluorescence measurements

For the fluorescence and UV-visible spectroscopic measurement, 1 mg of the nanocapsules were added to 10 mL of double distilled water. For the curcumin sample, 1 mg of curcumin was dissolved in 3 mL of methanol. 50 μ L of this sample was dissolved afterwards in 2990 μ L of double distilled water. Drug loading of the two types of nanocapsules was measured using UV-Vis spectroscopic technique.

b. Drug loading

For establishing the curcumin calibration curve (Figure IV. 1), a stock solution of 1 mM of curcumin was prepared in 3 mL of methanol. Out of this stock, 8 different standards with the following concentrations were prepared: 1, 3, 5, 7, 10, 15, 17, and 20 μM . The solutions of nanocapsules were prepared by dissolving 1 mg in 3 mL methanol and diluting 100 times. UV-visible spectroscopic measurements were performed at a range of 200-800 nm.

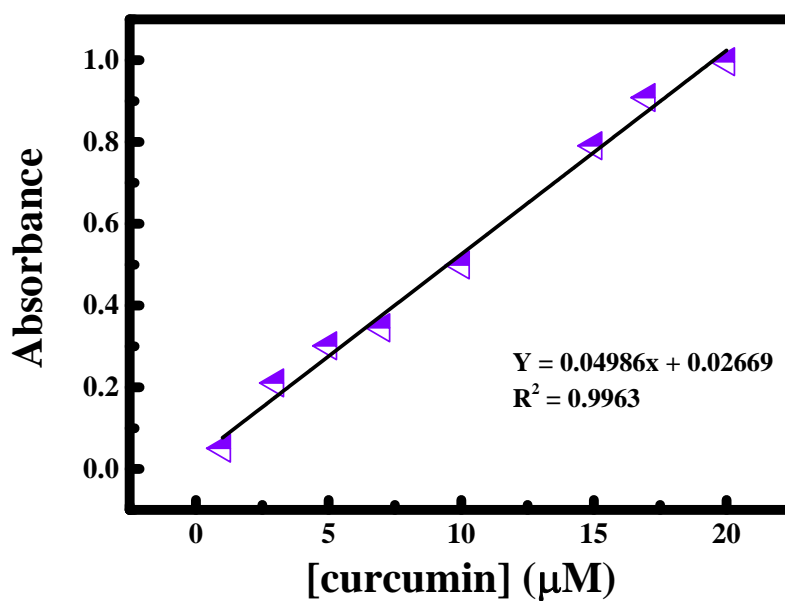


Figure IV. 1 Calibration curve of curcumin

Drug loading was calculated according to the following formulas¹⁴³⁻¹⁴⁴

$$\text{Drug loading (\%)} = \frac{\text{weight of curcumin in NHPs}}{\text{weight of NHPs}} \times 100$$

c. DNA and RNA sensing

For sensing study, stock solutions of 300 μM in DDW of DNA and RNA were prepared in order to make up several solutions with known concentration in the range 0 to 100 μM . All the experiments were done by keeping the concentration of the nanocapsules constant in a total volume of 3 mL.

3. Instrumentation

The size of nanocapsules was measured using scanning electron microscopy (SEM). This analysis was done using Tescan, Vega 3 LMU with Oxford Edx detector (Inca XmaW20) SEM, where 2 mg of the nanocapsules were dissolved in 15 mL of double distilled water, and few drops of the nanocapsules suspension were placed on an aluminium stub, coated with carbon adhesive. The SEM analysis of this sample was done after being dried.

XRD characterization was achieved using a Bruker D8 advance X-ray diffractometer (Bruker AXS GmbH, Karlsruhe, Germany) at 40 kV, 40 mA (1,600 W) using Cu $K\alpha$ radiation ($\lambda = 1.5418 \text{ \AA}$), with a 1.2 mm primary beam slit and 2.0 mm detector slit. The X-ray scans were carried out for 2θ between 3 and 80 degrees at 0.02° increments.

Thermogravimetric Analysis (TGA) was performed using a Netzsch TGA 209 in the temperature range of 100 to 1000 $^\circ\text{C}$ with an increase of $10 \text{ }^\circ\text{C min}^{-1}$ under an N_2 atmosphere.

4. Spectroscopic method

The absorption spectra were recorded using a JASCOV-570 UV-VIS-NIR Spectrophotometer at room temperature.

FT-IR spectra were recorded using a Thermo Scientific Nicolet iS5 FT-IR Spectrophotometer using KBr pellets.

The steady-state fluorescence spectra (excitation and emission) were recorded at room temperature using Jobin-Yvon-Horiba Fluorolog III fluorometer and the Fluor Essence program where the excitation and emission slits width were 5 nm. A 100 W Xenon lamp was used the source of excitation. The detector used wad R-928 operating at a voltage of 950 V.

C. Results and discussion

1. Formation of nanocapsules

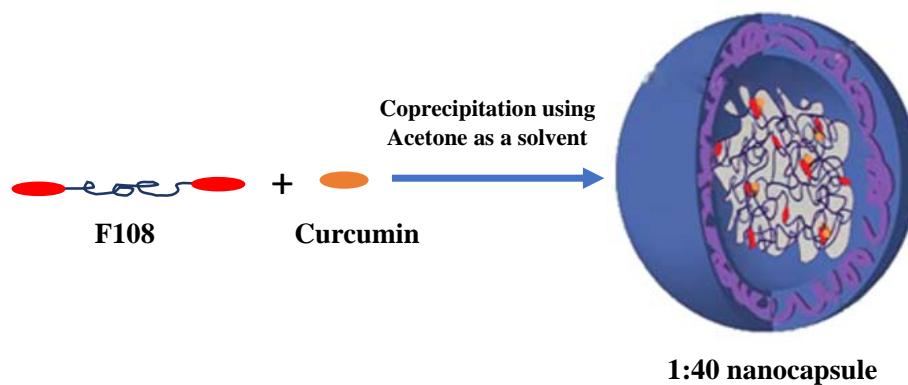


Figure IV. 2 Schematic illustration showing the formation of 1:40 nanocapsules

Figure IV. 3 shows the shape and size of the prepared 1:40 nanocapsules. The size of the nanocapsules range from 240 to 380 nm which is slightly larger than the 1:1 nanocapsules. On the other hand, the shape of the nanocapsules is also spherical as depicted for the 1:1 nanocapsules.

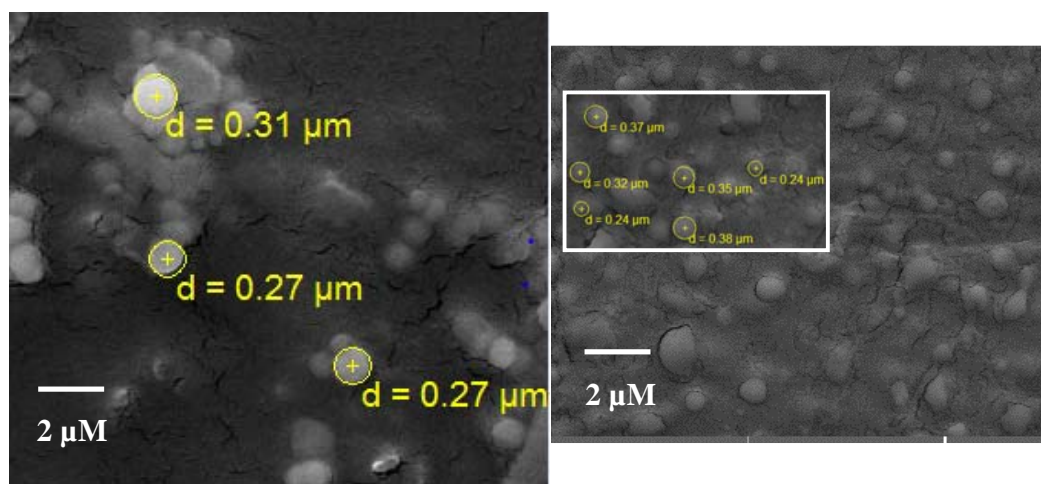


Figure IV. 3 SEM images of 1:1 nanocapsules (left) and 1:40 nanocapsules (right) with inset showing magnification of particles

2. *Interaction within Nanocapsules*

The X-ray diffraction pattern was used to analyze the effect of the polymer concentration in the encapsulation phenomena. The diffractograms of F108, curcumin and the prepared nanocapsules with different ratio of polymer are depicted in Figure IV. 4. The characteristic peaks of F108 were obtained at 19.4° and 23.6° . Hence, it showed a crystal line structure resulting from the formation of PEO crystallites.¹³⁴ As for the curcumin, the main characteristic peaks appeared at diffraction angles of 2θ equal to 8.06° , 9.20° , 12.46° , 14.95° and 17.75° indicating that curcumin is present in the crystalline form. Yet, it is found that all the relative peaks of curcumin except 14.95° are absent in the spectrum of 1:1

and 1:40 capsule and the peak at 14.95° was shifted to 14.01° in both nanocapsules. Hence, the relative peaks of polymer were absent in the 1:1 nanocapsule and present in the 1:40 nanocapsule, which suggests that curcumin peaks are too broadened and the XRD pattern is dominated by the structure of F108. The degree of crystallinity was calculated for the curcumin, 1:1 nanocapsules and 1:40 nanocapsules. The percentage crystallinity of curcumin was 77.1% which was altered when encapsulated, where the percentage crystallinity of the 1:1 and 1:40 nanocapsules was found to be 66.2% and 55.1 % respectively. The decrease in the degree of crystallinity suggests that curcumin may have lost its packed structure upon formation of nanocapsules especially in the 1:40 which viewed lower crystallinity.

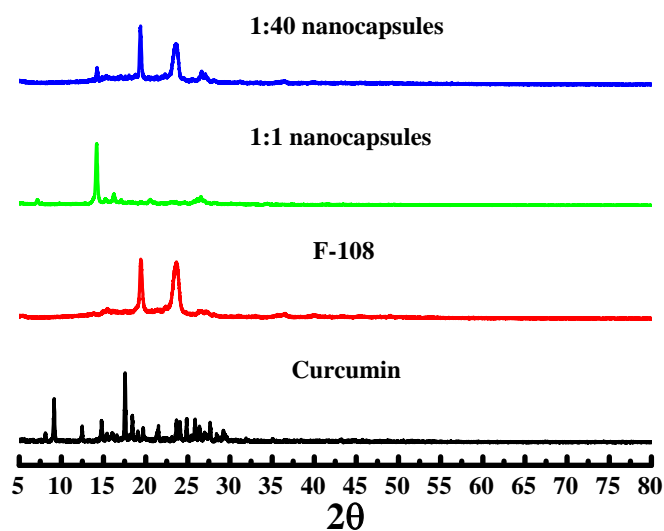


Figure IV. 4 XRD comparing the 1:1 to 1:40 nanocapsules along with curcumin and F108

In the FT-IR spectrum of curcumin, the peak presents at 3508 cm^{-1} correspond to the phenolic O-H stretching vibration, the peak at 1626 cm^{-1} has a predominantly mixed $\nu(\text{C}=\text{C})$ stretch. Another band at 1602 cm^{-1} is attributed to the symmetric aromatic ring stretching vibrations $\nu(\text{C C}_{\text{ring}})$. The 1508 cm^{-1} peak is assigned to $(\text{C}=\text{O})$ stretch. A C-H asymmetric stretch is attributed to 1424 cm^{-1} . C-O stretch is presented at 1280 , 1207 and 1150 cm^{-1} bands. In addition, C-O-C stretch corresponds to the band at 1026 cm^{-1} . The band at 960 cm^{-1} correspondsto the trans-CH vibration and finally the peak at 856 corresponds to C-C skeleton vibration.¹³⁵

As for the FT-IR spectrum for the F108 polymer, the peaks at 2890 cm^{-1} , 1476 cm^{-1} and 1110 cm^{-1} , correspond to asymmetric stretching vibrations of $-\text{O}-\text{H}$, $-\text{C}-\text{H}$, C-C and C-O respectively.¹³⁶Hence, the band at 3508 cm^{-1} and 1150 cm^{-1} present in the curcumin FT-IR, were shifted to 3409 cm^{-1} and 1130 cm^{-1} respectively in both nanocapsules. The shift in these bands verifies the interaction of the curcumin with the polymer at the hydroxyl and carbonyl sites, revealing the incorporation of the curcumin in the F108 nanocapsules. This is in a good agreement with a previous study conducted by Mata et al. in 2005, which also demonstrated a shift in the C-O-C band of L64.²⁹ Note that the band peaks at 1150 and 1026 cm^{-1} were absent in the 1:40 nanocapsules but present in the 1:1 nanocapsules verifying more incorporation of curcumin in the 1:40 nanocapsules.¹³⁵

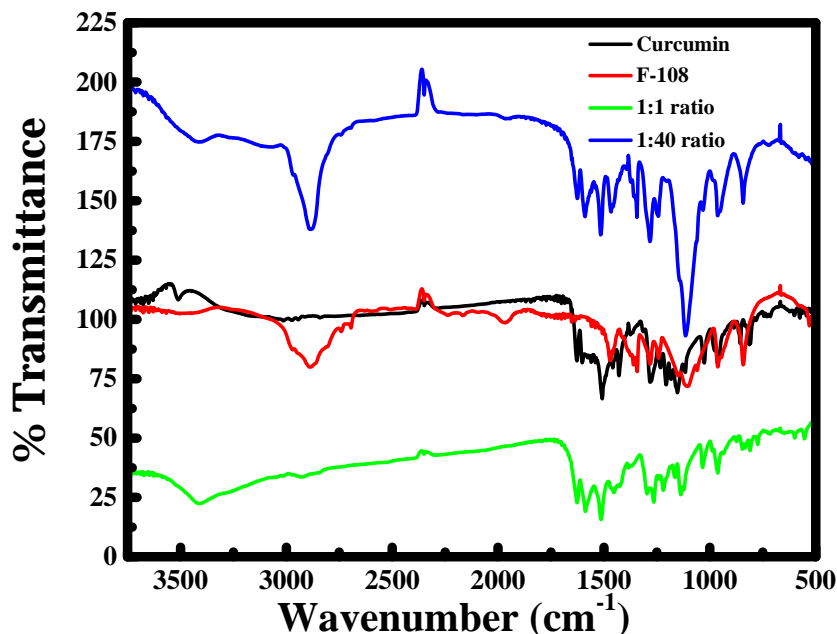


Figure IV. 5 FTIR spectra of 1:1 and 1:40 nanocapsules, curcumin, and F108

Thermogravimetric analysis was used to assess the stability of our prepared 1:1 and 1:40 nanocapsules. Interestingly, no weight loss was observed around 100 °C in any of the four samples, meaning our samples are dehydrated, and our formed nanocapsules are stable. Thermogravimetric analysis of F108 shows that it is stable until ~350 °C after which it illustrates a sharp weight loss that stops at ~400 °C. For the 1:1 nanocapsules, as illustrated in chapter III, there is loss of curcumin between ~250 °C and ~400 °C. However, this loss is not present in the 1:40 nanocapsules where we have more degradation and higher weight loss, similar to F108, due to the presence of higher amount of F108. Hence, the 1:40 nanocapsules are more stable since no degradation of curcumin was observed, meaning that curcumin is protected by the F108 copolymer in the nanocapsule.

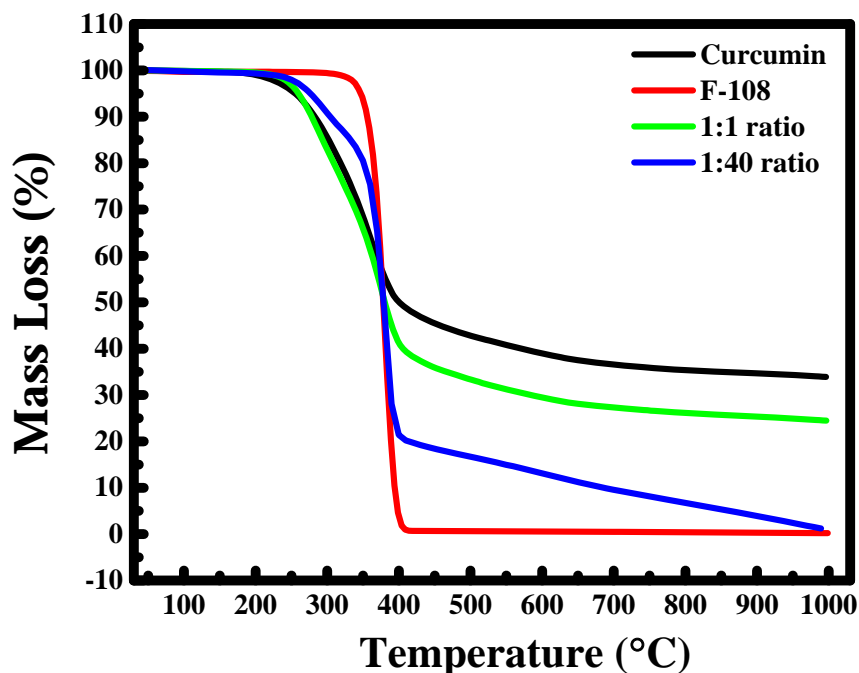


Figure IV. 6 TGA patterns of 1:1 and 1:40 nanocapsules, curcumin, and F108

3. Drug loading

The drug loading of both nanocapsules (1:1 and 1:40) was found in 1 mg of nanocapsules. Drug loading content of 1:1 nanocapsules was found to be lower than that of 1:40 (14.6% and 79.1% for 1:1 and 1:40 nanocapsules, respectively). This is expected as the drug loading percentage must increase with the increase in drug to copolymer ratio.¹²⁷ This is in a good agreement with previous findings where it was clearly demonstrated that the drug loading and encapsulation efficiency of oxcarbazepine increased sharply with the increase in P84 concentration.¹⁴⁵ Other examples found in literature illustrate this finding also.¹⁴⁶

4. Optical properties of curcumin within Nanocapsules

For free curcumin, 1:1 nanocapsules, and 1:40 nanocapsules, the absorption spectra are shown first in Figure IV.7 followed by the fluorescence spectra at excitation wavelength of 425 nm (Figure IV.8) then the fluorescence yield graphs (Figure IV.9).

In the emission spectrum, free curcumin has a maximum at ~551 nm. A red shift to 574 nm occurred in 1:1 nanocapsules followed by a blue shift to 560 nm in 1:40 nanocapsules. In the 1:1 nanocapsules, curcumin molecules are in close vicinity which may result in their dimerization at very high concentration along with association of these molecules with F108 polymer chains. This aggregation causes a decrease in the π - π^* gap of the curcumin molecule which is the reason behind the red shift.¹⁴⁷ However, this aggregation is lost in 1:40 nanocapsules due to the high concentration of F108. Thus, the 1:40 nanocapsules and curcumin molecules are exposed to F108 polymer chain as well as towards the solvent molecules. This resulted in a blue shift to 560 nm compared to 1:1 nanocapsules.

The higher fluorescence intensity and absorbance in 1:40 suggests that the higher concentration of the curcumin, which causes dimerization, saturates the absorbance and reduces the fluorescence due to self-quenching of many curcumin molecules present in proximity in the 1:1 nanocapsules compared to 1:40 nanocapsules. Therefore, 1:40 nanocapsules gives higher fluorescence intensity and higher absorbance.

The relative fluorescence yield was calculated for free curcumin, 1:1, and 1:40 nanocapsules by measuring the absorbance at 425 nm and dividing the fluorescence

spectrum at 425 nm excitation by this absorbance value. It was found that the relative fluorescence yield increase about 1.33-fold in 1:1 Nanocapsules compared to free curcumin in double distilled water whereas this fluorescence yield is further enhanced to 7.81 in 1:40 nanocapsules. This is estimated as 6-fold enhancement. Therefore, using 1:40 nanocapsules can potentially give higher sensitivity during fluorescence sensing compared to free curcumin and 1:1 nanocapsules. This is the reason behind using 1:40 nanocapsules for sensing study.

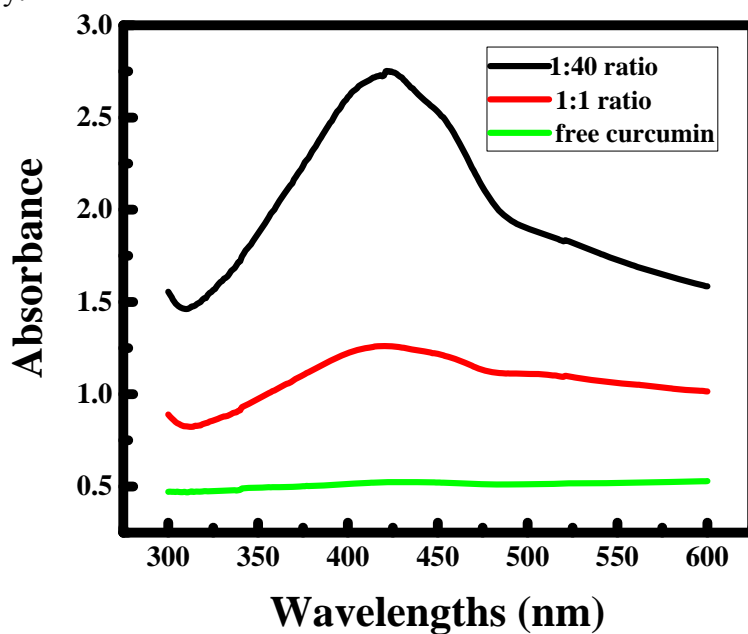


Figure IV. 7 Absorption spectra

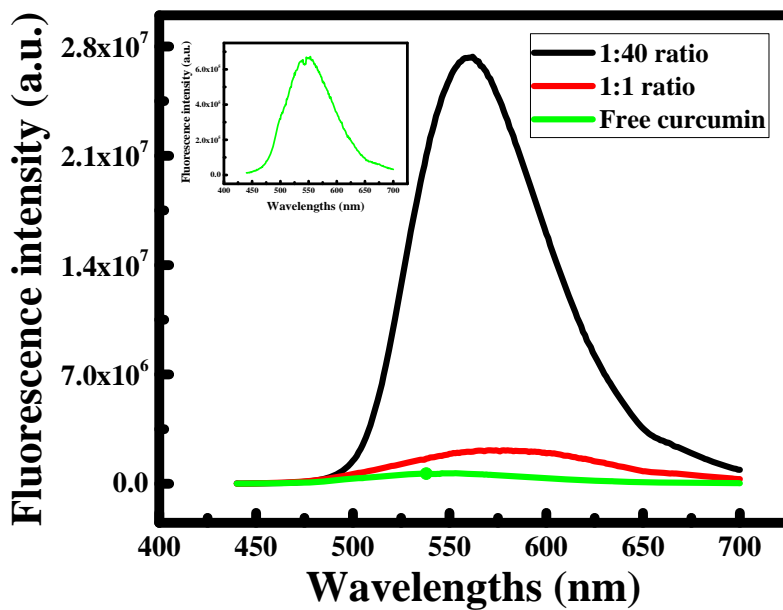


Figure IV. 8 Fluorescence emission spectra at excitation wavelengths 425 nm

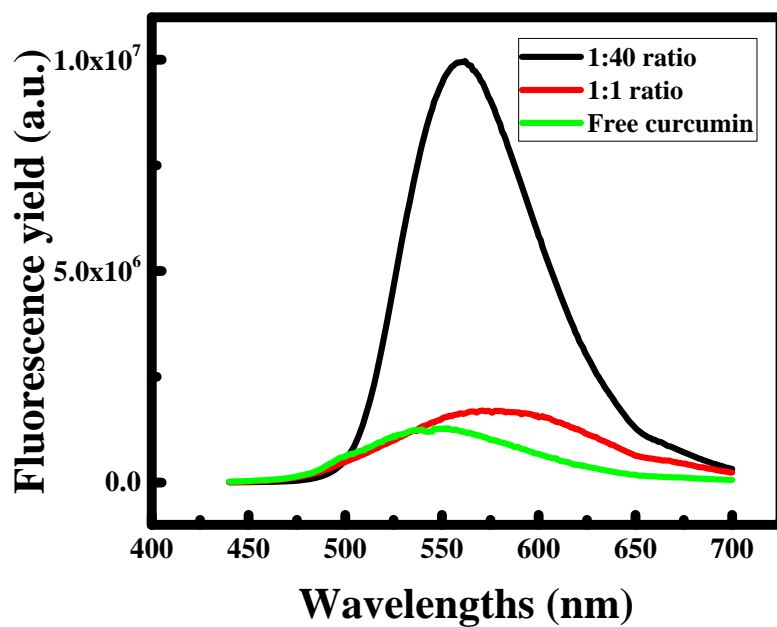


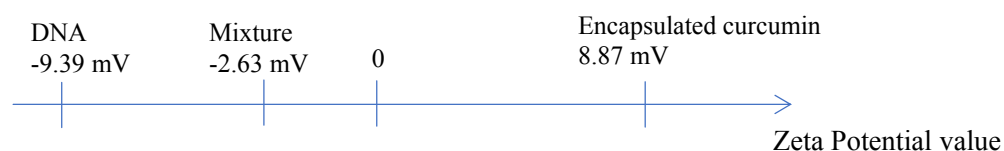
Figure IV. 9 Relative fluorescence yields of the prepared nanocapsules compared to free curcumin

5. *DNA and RNA sensing*

The encapsulated curcumin in F108 polymer prepared in 1:40 ratio, were used to detect DNA and RNA in aqueous solution. Interestingly, addition of DNA had a remarkable effect on emission spectrum of the nanocapsules, about 5-fold increase in emission intensity was observed, as shown in Figure IV.10. with a blue shift from 550 nm to 535 nm upon the increasing of the concentration of DNA in the mixture. However, this could be due to the large surface area and the high surface free energy of the nanocapsules, which leaves the DNA molecule inevitably adsorbed on the surface of nanocapsules and thus takes the place of curcumin. This phenomenon could be the consequence of the multivalent binding with the polymer, which forms the larger aggregates. Emission intensity is sensitive to the aggregation particle, thus, presence of DNA in the solution helps in creating aggregates and boosts emission intensity. The linear correlation of emission signal alteration of encapsulated curcumin vs. DNA concentration is plotted in Figure IV.10. As can be seen in the plot, in a range of concentration between 0 - 1000 μM , the curve showed linear change with a limit of detection equal to 50 μM . This linear increase was very well fitted with a linear equation, $Y = 5442.50x + 16843.55$ with $R^2=0.994$. Such a good correlation justifies the applicability of the present method for the determination of DNA in the given concentration range.

The interaction between the nanocapsules and the DNA molecules was also verified by zeta potential analysis (Figure IV.11). The nanocapsules had a positively charged surface, the DNA were negatively charged due to the phosphate group inducing in

aggregate molecules with negatively charged surface with a zeta value between that of the nanocapsules and the DNA.



As for RNA, a boost in the emission intensity was obtained while increasing the concentration of the RNA in the solution (Figure IV.12), regarding the aggregation formation. The zeta potential analysis was also established to verify the interaction between the RNA and the nanocapsules. The zeta value of the RNA in the solution was relatively between the value of encapsulated curcumin and RNA alone.



The linear correlation of emission signal alteration of encapsulated curcumin vs. RNA concentration is plotted in Figure IV.12. It is clear that in a range of concentration between 0 - 1000 μM , the curve showed linear change with a limit of detection equal to 60 μM . This linear increase was very well fitted with a linear equation, $Y = 30044.63x + 15546.74$ with $R^2 = 0.994$.

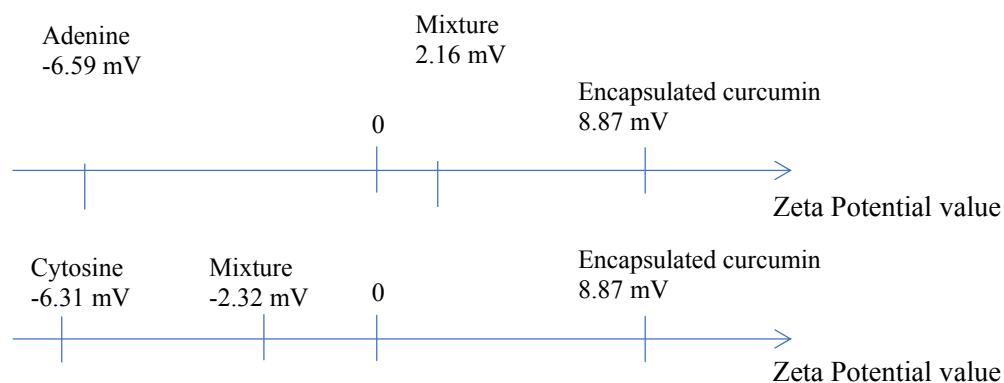
Although available methods can detect DNA molecules in lower concentration range (Table IV. 1). none of them work in the higher concentration range of the present method.

As nanocapsules were able to detect DNA and RNA molecules that have similar properties, it was necessary to comprehend the interaction between these two molecules and the nanocapsules.

The DNA molecule consists of two long polynucleotide chains made of four types of nucleotide subunits. Each nucleotide contains a phosphate group, a sugar group and a nitrogen base. The four types of nitrogen bases are adenine which has an amino group (-NH₂), thymine (T), guanine (G), and cytosine (C) belonging to pyrimidine bases. Thymine contains a methyl group and cytosine contains a hydrogen atom with an amino group, in addition to the guanine. Furthermore, the sugar is deoxyribose, attached to a single phosphate group (hence the name deoxyribonucleic acid). Each of these chains is known as a *DNA chain*, or a *DNA strand*. *Hydrogen bonds* between the base portions of the nucleotides hold the two chains together. Similarly, RNA molecule contains also adenine, guanine and cytosine bases but instead of thymine they have another base called uracil.¹⁴⁸

The specific placement of hydrogen bond donor and acceptor groups provides unique structural identity. The hydrogen atoms of amino groups provide hydrogen bond donors, and the carbonyl oxygen and ring nitrogens provide hydrogen bond acceptors. When bases become ionized, their hydrogen bonding properties are changed. This can lead to many non-Watson-Crick base pairs. Adenine is prone to protonation at low pH, which can lead to the formation of an A+C wobble base pair. Cytosine is also very prone to

protonation which can lead to a C⁺ Hoogsteen base pair. The ionized form of thymidine can form a T-G base pair.¹⁴⁹ In order to verify the above hypothesis and explain the real interaction in the solution, the fluorescence synchronous of encapsulated curcumin with Adenine, Cytosine, Guanine, Thymine and Uracil was established. As it is noticed in Figure IV. 13, 100 μ M of Guanine, Thymine and Uracil did not alter the emission intensity of encapsulated curcumin unlike ~5-fold increase observed for same concentration of Adenine and cytosine indicating the formation of A⁺ and C⁺ in aqueous solution. The zeta potential was established in Figure IV.14 and Figure IV.15. The zeta potential value of adenine and cytosine in the presence of encapsulated curcumin was found to be between the value of encapsulated curcumin alone and adenine/cytosine alone. Thus, the real interaction of DNA with the encapsulated curcumin is well verified by the interaction of the adenine and cytosine nucleotides.



The analytical recovery using the proposed method was estimated by testing 3 different unknown concentration using the last calibration curve obtained. The results

obtained are summarized in Table IV. 2 and Table IV. 3. The percent of recovery DNA and RNA of our method was found to be between 96-101%.

Finally, the photo-stability of polymer encapsulating curcumin was verified, which is illustrated in Figure IV.16. When the fluorescence emission signal of encapsulated curcumin was recorded in the absence and presence of DNA and RNA for one hour, the signal was found to be remarkably stable indicating the current sensor is quite stable during measurement time.

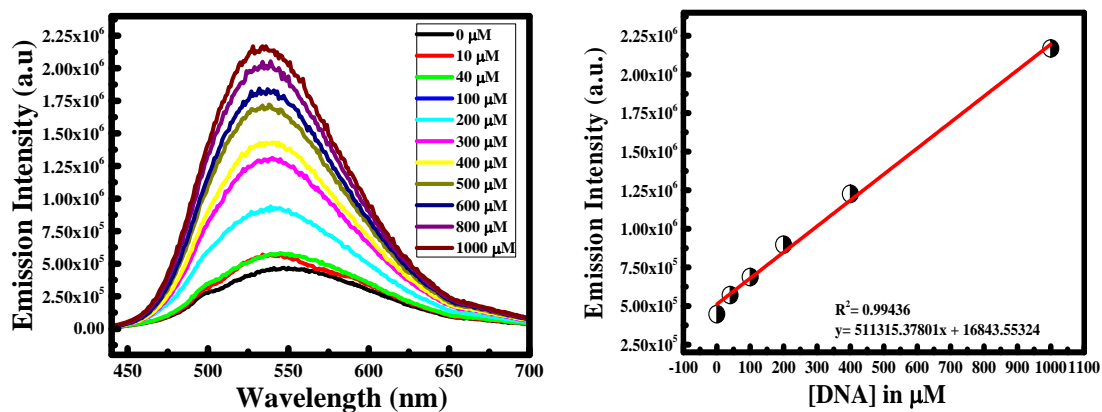


Figure IV. 10 Fluorescence emission spectra of 1:40 nanocapsules at different DNA concentrations (left) and linear correlation of the intensities at 540 nm versus DNA concentration

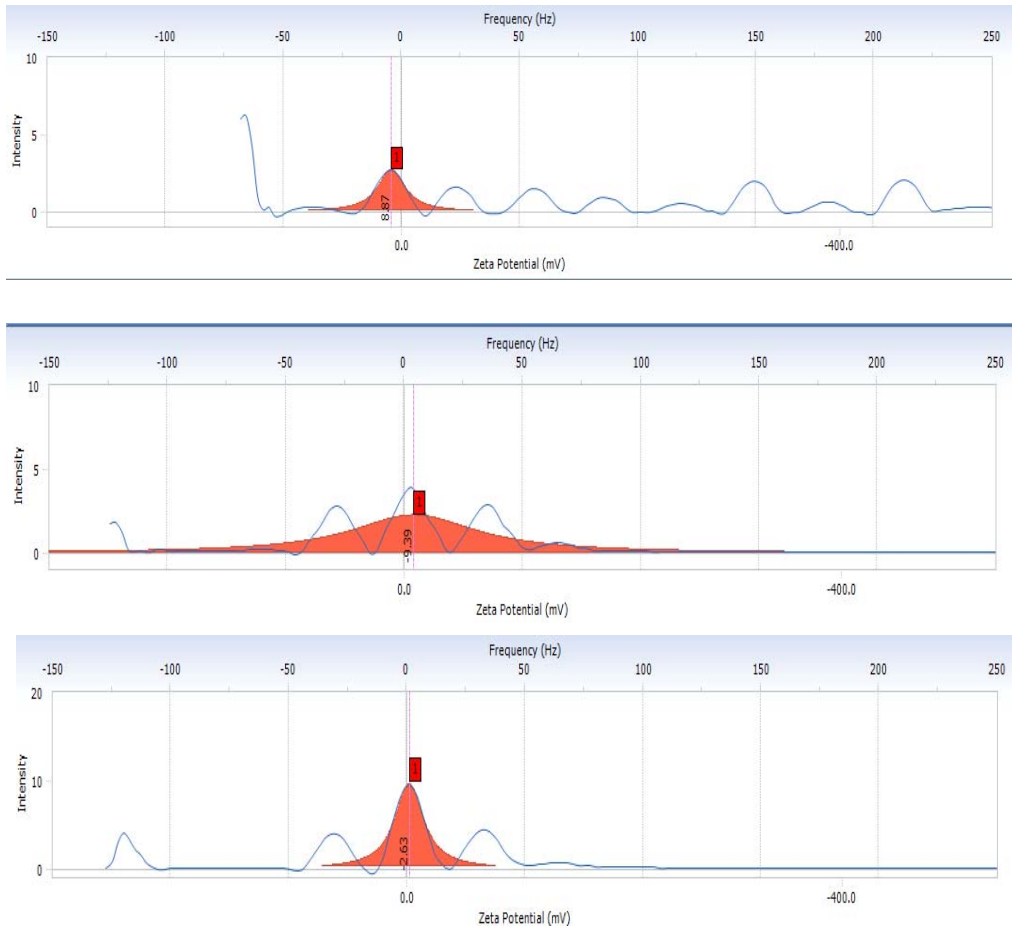


Figure IV. 11 Zeta potential curves for 1:40 nanocapsules (top), DNA (middle), and mixture of nanocapsules and DNA (bottom)

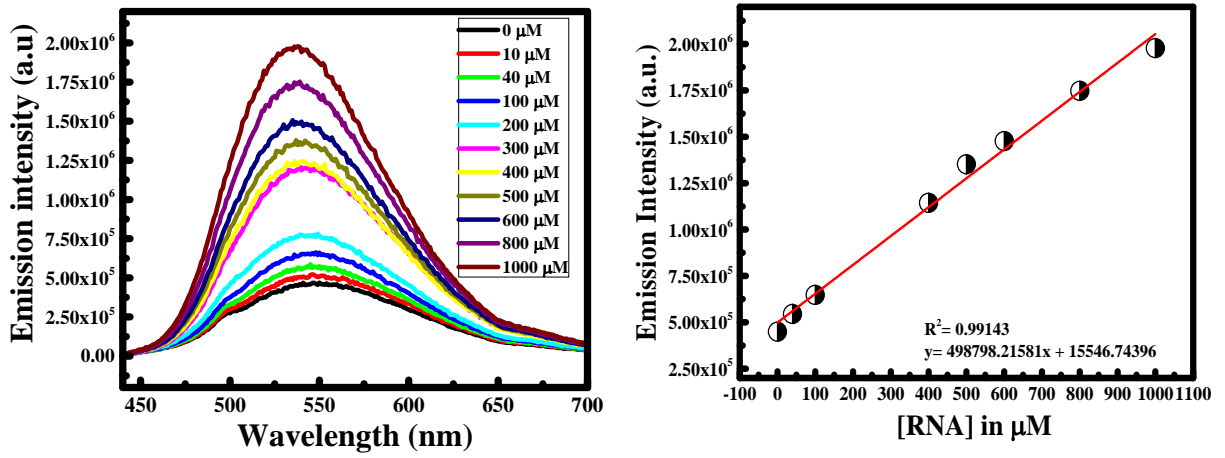


Figure IV. 12 Fluorescence emission spectra of 1:40 nanocapsules at different RNA concentrations (left) and linear correlation of the intensities at 540 nm versus RNA concentration

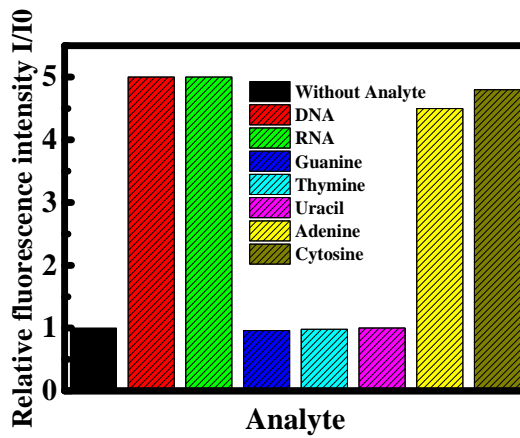


Figure IV. 13 Nucleotide analysis

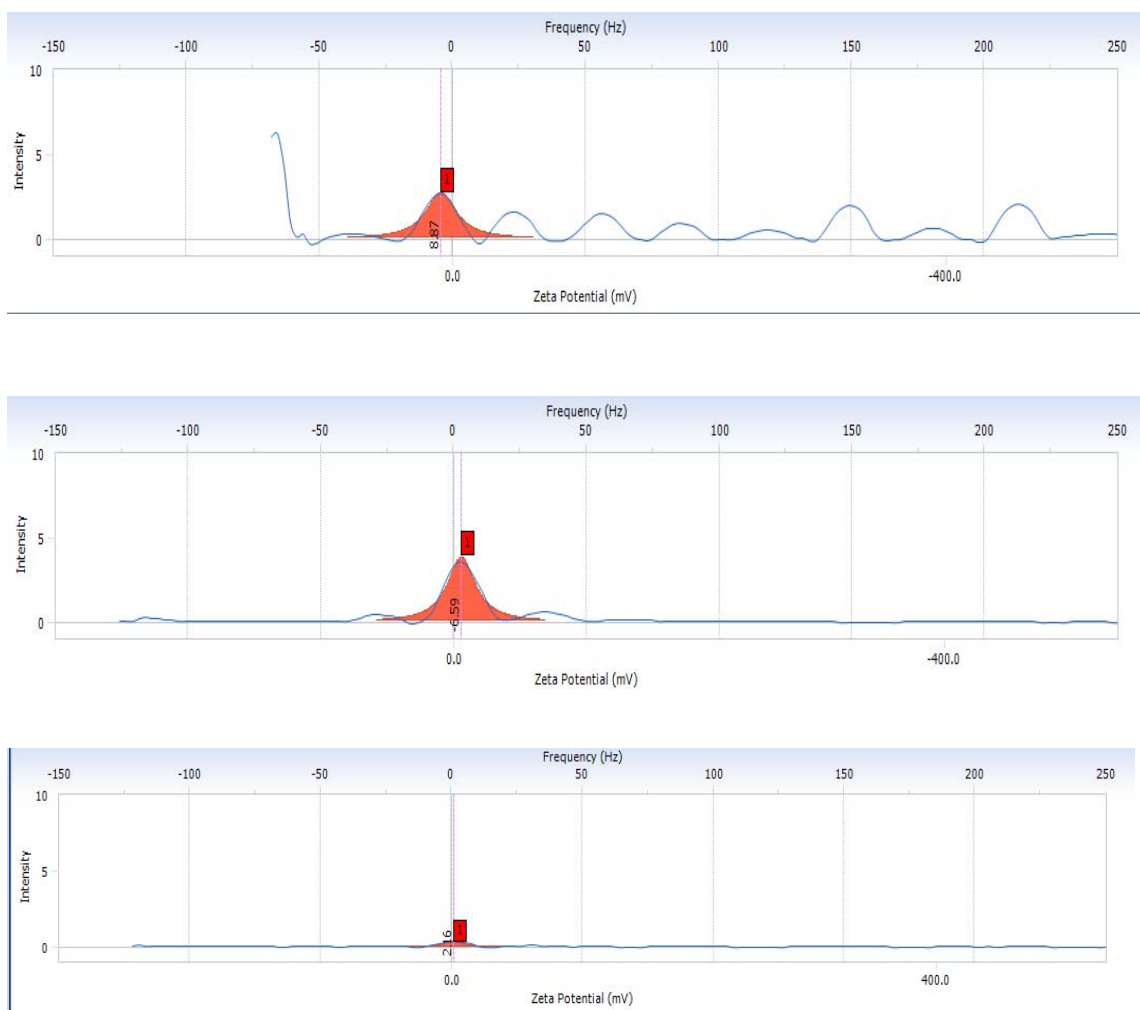


Figure IV. 14 zeta potential curves of 1:40 nanocapsules (top), adenine (middle) and their mixture (bottom)

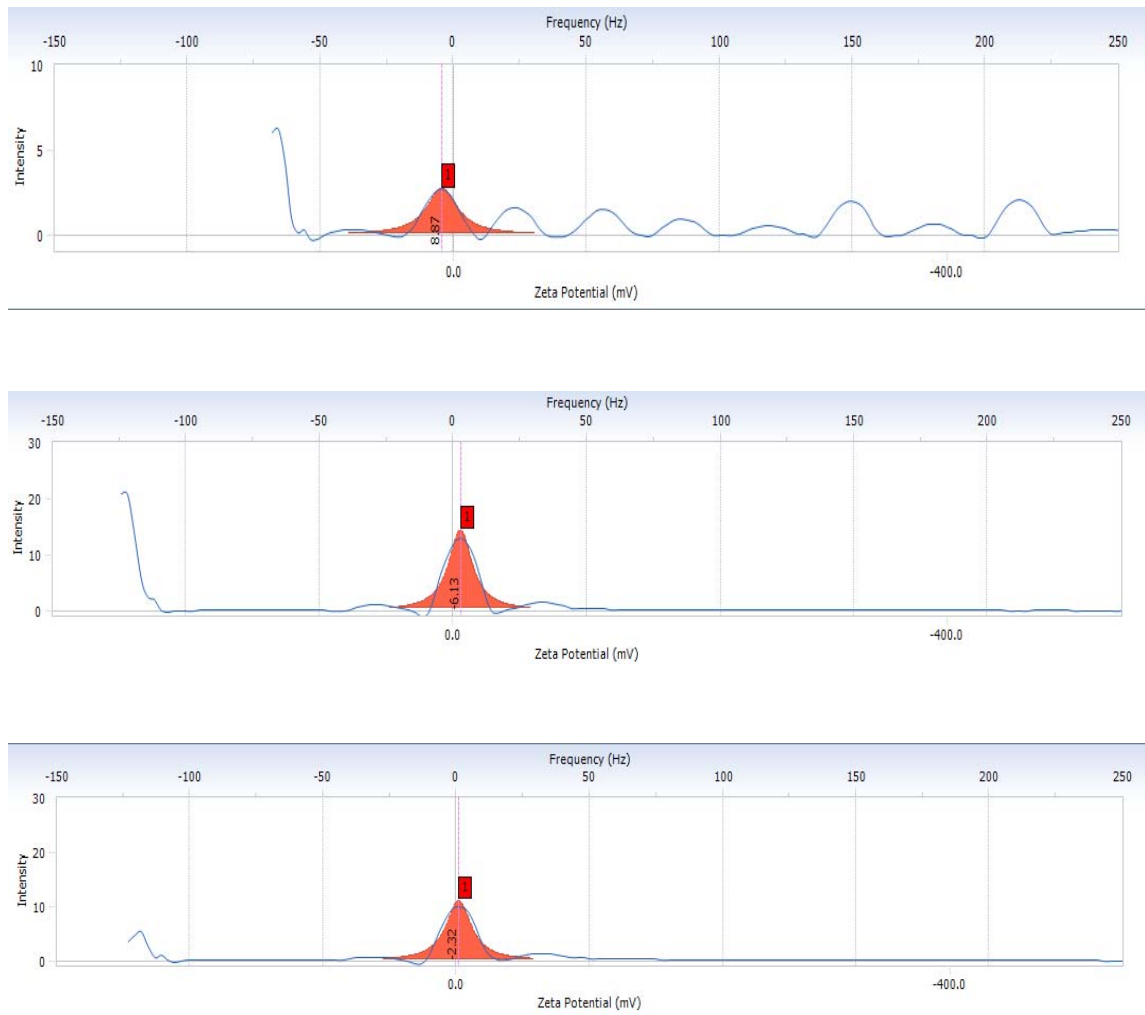


Figure IV. 15 zeta potential curves of 1:40 nanocapsules (top), cytosine (middle), and their mixture (bottom)

Methods	Concentration Range	References
Fluorescence change of Ethidium Bromide after binding with DNA	0.1-10 $\mu\text{g.mL}^{-1}$	¹⁵⁰
Fluorescence change of Hoechst33258 dye after binding with DNA	0.01-15 $\mu\text{g.mL}^{-1}$	¹⁵¹
Fluorescence change of PicoGreen dye after binding with DNA	25-1000 pg.mL^{-1}	¹⁵²
Fluorescence change of SYBR Green I dye after binding with DNA	0.002-2 $\mu\text{g.mL}^{-1}$	¹⁵³
Fluorescence change of polymer encapsulated curcumin after binding with DNA	6.5-650 $\mu\text{g.mL}^{-1}$	This work

Table IV. 1 DNA sensing in literature

	Theoretical Concentration (ppm)	Experimental Concentration (ppm)	Recovery (%)
Unknown 1	1	1.01	101
Unknown 2	10	9.87	98.7
Unknown 3	45	45.05	100.1

Table IV. 2 DNA recovery table

	Theoretical Concentration (ppm)	Experimental Concentration (ppm)	Recovery (%)
Unknown 1	0.5	0.48	96
Unknown 2	12	12.01	100.08
Unknown 3	50	49.5	99

Table IV. 3 RNA recovery table

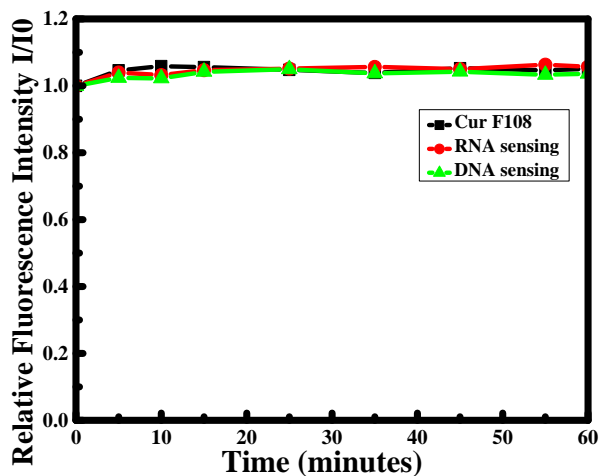


Figure IV. 16 Photostability measurements

D. Conclusion

Physicochemical properties of fluorophores can be tremendously enhanced after being coated with a polymer in the form of multifunctional nanocapsules. These formulations have been a subject of interest for their utility in probing specific targets of interest. Encapsulation of fluorophores inside copolymers can result in higher fluorescence signal intensity, better biostability (owe to the exclusion of oxygen by the polymer encapsulation), compared to original modality. In this work, curcumin was encapsulated inside the F108 copolymer in 1:40 drug to copolymer ratio. SEM imaging showed spherical particles whose size was enlarged from 190-310 nm in the 1:1 nanocapsules to 240 -380 nm in the 1:40 nanocapsules. X-ray analysis, FTIR, and TGA characterization clearly revealed the higher stability of 1:40 nanocapsules. Moreover, it was shown that these nanocapsules present higher encapsulation of curcumin, which was further confirmed by the drug loading study (15 and 80% for the 1:1 and 1:40 nanocapsules, respectively).

The UV-visible and fluorescence characterization further showed higher fluorescence and absorbance for the 1:40 nanocapsules due to absence of dimerization. The relative fluorescence yield of the 1:40 nanocapsules compared to 1:1 nanocapsules showed a 6-fold enhancement, which renders them as more sensitive probes to be used later on in our sensing study.

In addition, results of DNA and RNA sensing have demonstrated the applicability of the 1:40 nanocapsules as a robust sensor for these molecules. A boost in the emission intensity and blue shift are two observations which established our 1:40 nanocapsules as an efficient sensor for the DNA and RNA concentration with 50 μM and 60 μM detection limits for DNA and RNA, respectively. Zeta potential values further confirmed the interaction between the nanocapsules and our targeted molecules. Furthermore, zeta values demonstrated that the real interaction of DNA with the encapsulated curcumin is well verified by the interaction of the adenine and cytosine nucleotides. Moreover, our prepared nanocapsules presented a high percentage recovery of DNA and RNA (96-101%). Finally, stability results illustrated a high photostability of encapsulated curcumin, indicating that our nanocapsules can be considered as a stable sensor during measurement time.

CHAPTER V

CONCLUSION

In the present work, self-assembly properties of F108 copolymer was studied in solution using fluorescence-based technique, employing curcumin as an external probe. The aggregation behavior of F108 was studied through investigating changes in critical micelle concentration (CMC) and temperature (CMT) in solution. These were determined by tracking emission intensities for solutions with different concentrations of F108 where all of them contain a fixed concentration of the probe, curcumin. Results have shown that CMC and CMT value were equal to 23.2 μM and 35°C , respectively. Values determined were in a good agreement with literature values obtained through simulation studies and pyrene probing. Therefore, our employed method based on curcumin probing, which is not often employed as pyrene probing, can be considered a reliable method to study aggregation behavior of copolymers in solution. In addition, changes in CMC and CMT values were investigated in the presence of ionic salt, such as NaCl, and bile salts, such as sodium cholate (NaC) and sodium deoxycholate (NaDC). Fluorescence results illustrated a clear decrease in the CMC with the increase in concentration of all three salts except for NaC. However, the effect was the most noticeable for NaDC, around 9-fold decrease, compared to 3 and 1-fold decrease for NaCl and NaC, respectively. Accordingly, it can be concluded that the effect of deoxycholate outweighed the salting out activity of NaCl in pushing more curcumin into the hydrophobic domain. On the other hand, the effect of the three salts on the CMT of F108 was less remarkable, with a 1-fold decrease for NaCl and NaDC and almost no change for NaC. Lastly, fluorescence quenching experiment, using

both CPB and KI as quenchers. Results have established CPB a more suitable quencher for the curcumin-F108 micellar system. Since CPB tail is known to be located at the stern layer of the micelle, curcumin position was also established to be around the same region.

Aside from its fluorescent properties, curcumin is a well-established therapeutic agent that is yet limited by its poor solubility in water and low oral bioavailability. To overcome these limitations, using coprecipitation method, curcumin was encapsulated inside F108 in the form of nanocapsules having a 1:1 curcumin to F108 ratio. Nanocapsules were characterized by Scanning Electron Microscopy (SEM), thermogravimetric analysis (TGA), X-ray diffraction (XRD), and Fourier Transform Infrared Spectroscopy (FTIR). SEM imaging revealed nanocapsules as spherical particles with a size ranging from 270 to 310 nm. Besides, the interaction between curcumin and F108 was evaluated by comparing the XRD of the 1:1 nanocapsules to free curcumin and F108. XRD spectra demonstrated change in packing structure of curcumin upon encapsulation. This was signified by the disappearance of some peaks and the shift in some other peaks of curcumin in the 1:1 nanocapsules. Moreover, FTIR suggested a hydrogen bonding between curcumin and F108. This was illustrated by the shift of the bands at 3508 cm^{-1} and 1150 cm^{-1} in the FTIR spectrum of curcumin to 3409 cm^{-1} and 1130 cm^{-1} in the 1:1 nanocapsules. In addition, the degradation pattern of 1:1 nanocapsules indicated their stability up till $\sim 250\text{ }^{\circ}\text{C}$. Anticancer activity of curcumin was assessed through testing toxicity assays on two types of cancerous cells: A549 and A375 cells, in the presence and absence of light. Data have displayed a 34-fold and 32-fold decrease in the IC_{50} value of A549 and A375 cells, respectively ascribed to encapsulation of curcumin. This finding demonstrated an enhancement in the anticancer activity of curcumin in

the nanocapsules. Furthermore, comet assays illustrated a higher DNA damage for both curcumin and nanocapsules upon exposure to light, indicating efficient photodynamic therapy.

Furthermore, photophysical properties of a fluorophore can be greatly enhanced when it is encapsulated in polymeric formulations. Such properties include the boost of fluorescence signal and higher biostability. Therefore, using coprecipitation method, a different formulation of the previous nanocapsules was synthesized where the curcumin to F108 ratio was 1:40. SEM imaging displayed 1:40 nanocapsules as spherical particles ranging from 240 to 380 nm. Change in structural packing of curcumin was verified in both nanocapsules through XRD results which illustrated a shift of all the relative peaks of curcumin and the shift of the band at 14.95° to 14.01° . Nevertheless, a more intense decrease in the degree of crystallinity in the 1:40 nanocapsules has clearly proved an enhanced interaction of curcumin with F108 (66.2 % and 55.1 % in 1:1 and 1:40 nanocapsules respectively as compared to 77.1 % for free curcumin). Moreover, the band peaks at 1150 and 1026 cm^{-1} in the FTIR spectra of free curcumin were absent in 1:40 nanocapsules but present in the 1:1 nanocapsules confirming the higher interaction of curcumin and F108 in the 1:40 nanocapsules. In addition, higher stability of the 1:40 nanocapsules was assured by TGA. Drug loading results demonstrated an enhancement in curcumin loading from 14.9 % to 79.1 % in the 1:40 nanocapsules. Furthermore, in the UV-Vis spectroscopic characterization of both nanocapsules, the blue shift and the increase in the fluorescence intensity and absorbance in the 1:40 nanocapsules accounts for the fact that curcumin is in a more nonpolar environment. This has supported the fact that photophysical properties can be greatly enhanced by encapsulation in polymeric formulations. Calculations of the relative fluorescence yield showed a 6-fold enhancement in the 1:40 nanocapsules, which

rendered them as more sensitive probes to be used later on in our sensing study. Therefore, based on the functionality of curcumin as a fluorescent transducer, encapsulated curcumin was used in biomedical application as DNA and RNA sensing. After conducting sensing experiments, we noticed an enhancement in the emission intensity of curcumin with increasing DNA and RNA concentrations and a blue shift. These were motives which established our 1:40 nanocapsules as a robust sensor for DNA and RNA concentrations in solution. Detection limits were found to be 50 μ M and 60 μ M for DNA and RNA respectively. Zeta potential studies further assured the interaction between the nanocapsules and our targeted molecules because values of DNA/RNA and nanocapsules mixture mediated zeta potential values of each of the nanocapsules and DNA/RNA alone. Furthermore, zeta potential measurements further verified the real interaction of DNA through the interaction of the adenine and cytosine nucleotides between two DNA/RNA chains. Moreover, our prepared nanocapsules presented a high percentage recovery of DNA and RNA (96-101%). Finally, curcumin showed a stable fluorescence signal in the presence and absence of DNA and RNA. This suggests the photostability of encapsulated curcumin and established it as a stable sensor during measurement time.

In chapter II of this work, we have established curcumin as an efficient molecular probe for studying the properties of F108 self-assembly in aqueous solution. Therefore, in the future, we will try to investigate self-assembly properties of other polymers and systems as well as studying the influence of other modulators on these systems using curcumin as a fluorescence probe. Furthermore, our insight is to synthesize various formulations of the nanocapsules with different drug to copolymer ratio (1:10, 1:60, 1:100, etc). Besides, we will attempt to study the

cytotoxicity assays of the 1:40 nanocapsules using photodynamic therapy. Finally, sensing new analytes like ascorbic acid, melamine, antioxidants, or other analytes will be a good step towards establishing our nanocapsules containing curcumin as a multifunctional sensor.

REFERENCES

1. Israelachvili, J., Thermodynamic and Geometric Aspects of Amphiphile Aggregation into Micelles, Vesicles and Bilayers, and the Interactions between them. *Proc. Int. School Phys. Enrico Fermi Course XC* **1985**.
2. Glotzer, S. C.; Solomon, M. J., Anisotropy of building blocks and their assembly into complex structures. *Nature materials* **2007**,*6* (8), 557.
3. Lombardo, D.; Kiselev, M. A.; Magazù, S.; Calandra, P., Amphiphiles self-assembly: basic concepts and future perspectives of supramolecular approaches. *Advances in Condensed Matter Physics* **2015**,*2015*.
4. Dynamics of surfactant self assemblies. In *Micelles, Microemulsions, Vesicles and Lyotropic Phases* [Online] 1st edition ed.; Zana, R., Ed. CRC Press: Boca Raton, 2005.
5. Holmberg, K.; Jönsson, B.; Kronberg, B.; Lindman, B., Surfactants and Polymers in Aqueous Solution. John Wiley & Sons Ltd. : Chichester, 2003.
6. Sekhon, B. S., Surfactants: pharmaceutical and medicinal aspects. **2014**.
7. Tehrani-Bagha, A.; Holmberg, K., Solubilization of hydrophobic dyes in surfactant solutions. *Materials* **2013**,*6* (2), 580-608.
8. Bouchemal, K.; Briançon, S.; Perrier, E.; Fessi, H., Nano-emulsion formulation using spontaneous emulsification: solvent, oil and surfactant optimisation. *International journal of pharmaceutics* **2004**,*280* (1-2), 241-251.
9. Binks, B. P., Particles as surfactants—similarities and differences. *Current opinion in colloid & interface science* **2002**,*7* (1-2), 21-41.
10. Lourith, N.; Kanlayavattanukul, M., Natural surfactants used in cosmetics: glycolipids. *International journal of cosmetic science* **2009**,*31* (4), 255-261.
11. Yokoyama, M. In *Polymeric micelle drug carriers for tumor targeting*, ACS symposium series, Oxford University Press: 2006; pp 27-39.
12. Lee, Y.; Chung, H. J.; Yeo, S.; Ahn, C.-H.; Lee, H.; Messersmith, P. B.; Park, T. G., Thermo-sensitive, injectable, and tissue adhesive sol-gel transition hyaluronic acid/pluronic composite hydrogels prepared from bio-inspired catechol-thiol reaction. *Soft Matter* **2010**,*6* (5), 977-983.
13. Khullar, P.; Singh, V.; Mahal, A.; Kaur, H.; Singh, V.; Banipal, T. S.; Kaur, G.; Bakshi, M. S., Tuning the shape and size of gold nanoparticles with triblock polymer micelle structure transitions and environments. *The Journal of Physical Chemistry C* **2011**,*115* (21), 10442-10454.
14. Yang, P.; Zhao, D.; Margolese, D. I.; Chmelka, B. F.; Stucky, G. D., Block copolymer templating syntheses of mesoporous metal oxides with large ordering lengths and semicrystalline framework. *Chemistry of Materials* **1999**,*11* (10), 2813-2826.
15. Riess, G., Micellization of block copolymers. *Progress in polymer science* **2003**,*28* (7), 1107-1170.
16. Alexandridis, P.; Hatton, T. A., Poly (ethylene oxide)-poly (propylene oxide)-poly (ethylene oxide) block copolymer surfactants in aqueous solutions and at interfaces: thermodynamics, structure, dynamics, and modeling. *Colloids and Surfaces A: Physicochemical and Engineering Aspects* **1995**,*96* (1-2), 1-46.
17. Robertson, J. D.; Patikarnmonthon, N.; Joseph, A. S.; Battaglia, G., Block copolymer micelles and vesicles for drug delivery. *Engineering polymer systems for improved drug delivery* **2013**, 163-188.
18. Alexandridis, P.; Holzwarth, J. F.; Hatton, T. A., Micellization of poly (ethylene oxide)-poly (propylene oxide)-poly (ethylene oxide) triblock copolymers in aqueous solutions: thermodynamics of copolymer association. *Macromolecules* **1994**,*27* (9), 2414-2425.

19. Tanford, C., *The hydrophobic effect: formation of micelles and biological membranes 2d ed.* J. Wiley.: 1980.
20. Alexandridis, P.; Holzwarth, J. F., Differential scanning calorimetry investigation of the effect of salts on aqueous solution properties of an amphiphilic block copolymer (Ploxamer). *Langmuir* **1997**,*13* (23), 6074-6082.
21. Alexandridis, P.; Athanassiou, V.; Fukuda, S.; Hatton, T. A., Surface activity of poly (ethylene oxide)-block-poly (propylene oxide)-block-poly (ethylene oxide) copolymers. *Langmuir* **1994**,*10* (8), 2604-2612.
22. Price, C., Micelle formation by block copolymers in organic solvents. *Pure and Applied Chemistry* **1983**,*55* (10), 1563-1572.
23. Morigaki, K.; Walde, P.; Misran, M.; Robinson, B. H., Thermodynamic and kinetic stability. Properties of micelles and vesicles formed by the decanoic acid/decanoate system. *Colloids and Surfaces A: Physicochemical and Engineering Aspects* **2003**,*213* (1), 37-44.
24. Schott, H., Surfactant systems: Their chemistry, pharmacy and biology. By D. Attwood and AT Florence. Chapman & Hall, London EC4P 4EE, United Kingdom. 1983. 794 pp. *Journal of Pharmaceutical Sciences* **1985**,*74* (10), 1140-1141.
25. Yu, G.-E.; Deng, Y.; Dalton, S.; Wang, Q.-G.; Attwood, D.; Price, C.; Booth, C., Micellisation and gelation of triblock copoly (oxyethylene/oxypropylene/oxyethylene), F127. *Journal of the Chemical Society, Faraday Transactions* **1992**,*88* (17), 2537-2544.
26. Mai, Y.; Eisenberg, A., Self-assembly of block copolymers. *Chemical Society Reviews* **2012**,*41* (18), 5969-5985.
27. Desai, M.; Jain, N. J.; Sharma, R.; Bahadur, P., Temperature and salt-induced micellization of some block copolymers in aqueous solution. *Journal of Surfactants and Detergents* **2000**,*3* (2), 193-199.
28. Jain, N.; George, A.; Bahadur, P., Effect of salt on the micellization of pluronic P65 in aqueous solution. *Colloids and Surfaces A: Physicochemical and Engineering Aspects* **1999**,*157* (1-3), 275-283.
29. Zheng, L.; Guo, C.; Wang, J.; Liang, X.; Bahadur, P.; Chen, S.; Ma, J.; Liu, H., Micellization of Pluronic L64 in salt solution by FTIR spectroscopy. *Vibrational spectroscopy* **2005**,*39* (2), 157-162.
30. Patel, K.; Bahadur, P.; Guo, C.; Ma, J.; Liu, H.; Nakashima, K., Salt-Induced Micellization of Pluronic F88 in Water. *Journal of Dispersion Science and Technology* **2008**,*29* (5), 748-755.
31. Bodratti, A. M.; Alexandridis, P., Formulation of Ploxamers for Drug Delivery. *functional biomaterials* **2018**.
32. Nagarajan, R.; Ganesh, K., Comparison of solubilization of hydrocarbons in (PEO-PPO) diblock versus (PEO-PPO-PEO) triblock copolymer micelles. *Journal of colloid and interface science* **1996**,*184* (2), 489-499.
33. Mitchell, A.; Broadhead, J., Hydrolysis of solubilized aspirin. *Journal of pharmaceutical sciences* **1967**,*56* (10), 1261-1266.
34. Valle, J. W.; Armstrong, A.; Newman, C.; Alakhov, V.; Pietrzynski, G.; Brewer, J.; Campbell, S.; Corrie, P.; Rowinsky, E. K.; Ranson, M., A phase 2 study of SP1049C, doxorubicin in P-glycoprotein-targeting pluronics, in patients with advanced adenocarcinoma of the esophagus and gastroesophageal junction. *Investigational new drugs* **2011**,*29* (5), 1029-1037.
35. Saettone, M. F.; Giannaccini, B.; Delmonte, G.; Campigli, V.; Tota, G.; La Marca, F., Solubilization of tropicamide by ploxamers: physicochemical data and activity data in rabbits and humans. *International journal of pharmaceuticals* **1988**,*43* (1-2), 67-76.
36. Kabanov, A. V.; Chekhonin, V.; Alakhov, V. Y.; Batrakova, E.; Lebedev, A.; Melik-Nubarov, N.; Arzhakov, S.; Levashov, A.; Morozov, G.; Severin, E., The neuroleptic activity of

- haloperidol increases after its solubilization in surfactant micelles. *FEBS letters* **1989**,258 (2), 343-345.
37. SAITO, Y.; KONDO, Y.; ABE, M.; SATO, T., Solubilization behavior of estriol in an aqueous solution of pluronic L-64 as a function of concentration and temperature. *Chemical and pharmaceutical bulletin* **1994**,42 (6), 1348-1350.
 38. Sezgin, Z.; Yüksel, N.; Baykara, T., Preparation and characterization of polymeric micelles for solubilization of poorly soluble anticancer drugs. *European Journal of Pharmaceutics and Biopharmaceutics* **2006**,64 (3), 261-268.
 39. Kwon, G. S.; Kataoka, K., Block copolymer micelles as long-circulating drug vehicles. *Advanced drug delivery reviews* **1995**,16 (2-3), 295-309.
 40. Kadam, Y.; Yerramilli, U.; Bahadur, A., Solubilization of poorly water-soluble drug carbamezapine in Pluronic® micelles: Effect of molecular characteristics, temperature and added salt on the solubilizing capacity. *Colloids and Surfaces B: Biointerfaces* **2009**,72 (1), 141-147.
 41. Saito, Y.; Sato, T., Effects of inorganic salts on solubilization of estriol in an aqueous solution of poly (ethylene oxide)/poly (propylene oxide)/poly (ethylene oxide) triblock copolymer. *Drug development and industrial pharmacy* **1998**,24 (4), 385-388.
 42. Fioritto, A. F.; Bhattachar, S. N.; Wesley, J. A., Solubility measurement of polymorphic compounds via the pH-metric titration technique. *International journal of pharmaceutics* **2007**,330 (1-2), 105-113.
 43. Priyadarsini, K., The chemistry of curcumin: from extraction to therapeutic agent. *Molecules* **2014**,19 (12), 20091-20112.
 44. Nisar, T.; Iqbal, M.; Raza, A.; Safdar, M.; Iftikhar, F.; Waheed, M., Turmeric: A promising spice for phytochemical and antimicrobial activities. *Am Eur J Agric Environ Sci* **2015**,15 (7), 1278-1288.
 45. Aggarwal, B. B.; Sundaram, C.; Malani, N.; Ichikawa, H., Curcumin: the Indian solid gold. In *The molecular targets and therapeutic uses of curcumin in health and disease*, Springer: 2007; pp 1-75.
 46. Ak, T.; Gülçin, İ., Antioxidant and radical scavenging properties of curcumin. *Chemico-biological interactions* **2008**,174 (1), 27-37.
 47. Srimal, R.; Dhawan, B., Pharmacology of diferuloyl methane (curcumin), a non-steroidal anti-inflammatory agent. *Journal of pharmacy and pharmacology* **1973**,25 (6), 447-452.
 48. Reddy, R. C.; Vatsala, P. G.; Keshamouni, V. G.; Padmanaban, G.; Rangarajan, P. N., Curcumin for malaria therapy. *Biochemical and biophysical research communications* **2005**,326 (2), 472-474.
 49. Vera-Ramirez, L.; Pérez-Lopez, P.; Varela-Lopez, A.; Ramirez-Tortosa, M.; Battino, M.; Quiles, J. L., Curcumin and liver disease. *Biofactors* **2013**,39 (1), 88-100.
 50. E Wright, L.; B Frye, J.; Gorti, B.; N Timmermann, B.; L Funk, J., Bioactivity of turmeric-derived curcuminoids and related metabolites in breast cancer. *Current pharmaceutical design* **2013**,19 (34), 6218-6225.
 51. Vogel, A.; Pelletier, J., Examen chimique de la racine de Curcuma. *J Pharm* **1815**,1, 289-300.
 52. Miłobadzka, J.; v. Kostanecki, S.; Lampe, V., Zur Kenntnis des curcumins. *Berichte der deutschen chemischen Gesellschaft* **1910**,43 (2), 2163-2170.
 53. Aggarwal, B. B.; Kumar, A.; Bharti, A. C., Anticancer potential of curcumin: preclinical and clinical studies. *Anticancer research* **2003**,23 (1/A), 363-398.
 54. Priyadarsini, K. I., Photophysics, photochemistry and photobiology of curcumin: Studies from organic solutions, bio-mimetics and living cells. *Journal of Photochemistry and Photobiology C: Photochemistry Reviews* **2009**,10 (2), 81-95.

55. Ponnuel, K.; Santhiya, K.; Padmini, V., Curcumin based chemosensor for selective detection of fluoride and cyanide anions in aqueous media. *Photochemical & Photobiological Sciences* **2016**,*15* (12), 1536-1543.
56. Khopde, S. M.; Indira Priyadarsini, K.; Palit*, D. K.; Mukherjee, T., Effect of Solvent on the Excited state Photophysical Properties of Curcumin. *Photochemistry and photobiology* **2000**,*72* (5), 625-631.
57. Chignell, C. F.; Bilskj, P.; Reszka, K. J.; Motten, A. G.; Sik, R. H.; Dahl, T. A., Spectral and photochemical properties of curcumin. *Photochemistry and photobiology* **1994**,*59* (3), 295-302.
58. Wang, Y.-J.; Pan, M.-H.; Cheng, A.-L.; Lin, L.-I.; Ho, Y.-S.; Hsieh, C.-Y.; Lin, J.-K., Stability of curcumin in buffer solutions and characterization of its degradation products. *Journal of pharmaceutical and biomedical analysis* **1997**,*15* (12), 1867-1876.
59. Khurana, A.; Ho, C.-T., High performance liquid chromatographic analysis of curcuminoids and their photo-oxidative decomposition compounds in *Curcuma longa* L. *Journal of liquid chromatography* **1988**,*11* (11), 2295-2304.
60. Strimpakos, A. S.; Sharma, R. A., Curcumin: preventive and therapeutic properties in laboratory studies and clinical trials. *Antioxidants & redox signaling* **2008**,*10* (3), 511-546.
61. Yuan, H.-y.; Kuang, S.-y.; Zheng, X.; Ling, H.-y.; Yang, Y.-B.; Yan, P.-K.; Li, K.; Liao, D.-F., Curcumin inhibits cellular cholesterol accumulation by regulating SREBP-1/caveolin-1 signaling pathway in vascular smooth muscle cells. *Acta Pharmacologica Sinica* **2008**,*29* (5), 555.
62. Kolodziejczyk, J.; Olas, B.; Saluk-Juszczak, J.; Wachowicz, B., Antioxidative properties of curcumin in the protection of blood platelets against oxidative stress *in vitro*. *Platelets* **2011**,*22* (4), 270-276.
63. Garcia-Alloza, M.; Borrelli, L.; Rozkalne, A.; Hyman, B.; Bacskai, B., Curcumin labels amyloid pathology *in vivo*, disrupts existing plaques, and partially restores distorted neurites in an Alzheimer mouse model. *Journal of neurochemistry* **2007**,*102* (4), 1095-1104.
64. Chainani-Wu, N., Safety and anti-inflammatory activity of curcumin: a component of tumeric (*Curcuma longa*). *The Journal of Alternative & Complementary Medicine* **2003**,*9* (1), 161-168.
65. Aggarwal, B. B.; Harikumar, K. B., Potential therapeutic effects of curcumin, the anti-inflammatory agent, against neurodegenerative, cardiovascular, pulmonary, metabolic, autoimmune and neoplastic diseases. *The international journal of biochemistry & cell biology* **2009**,*41* (1), 40-59.
66. Ram, A.; Das, M.; Ghosh, B., Curcumin attenuates allergen-induced airway hyperresponsiveness in sensitized guinea pigs. *Biological and Pharmaceutical Bulletin* **2003**,*26* (7), 1021-1024.
67. Cotran, R., Acute and chronic inflammation. *Robbins Pathological Basis of Disease* **1999**, 50-88.
68. Reddy, A. C. P.; Lokesh, B. R., Studies on the inhibitory effects of curcumin and eugenol on the formation of reactive oxygen species and the oxidation of ferrous iron. *Molecular and cellular biochemistry* **1994**,*137* (1), 1-8.
69. Shishodia, S.; Chaturvedi, M. M.; Aggarwal, B. B., Role of curcumin in cancer therapy. *Current problems in cancer* **2007**,*31* (4), 243-305.
70. Pae, H.-O.; Jeong, S.-O.; Jeong, G.-S.; Kim, K. M.; Kim, H. S.; Kim, S.-A.; Kim, Y.-C.; Kang, S.-D.; Kim, B.-N.; Chung, H.-T., Curcumin induces pro-apoptotic endoplasmic reticulum stress in human leukemia HL-60 cells. *Biochemical and biophysical research communications* **2007**,*353* (4), 1040-1045.
71. Patel, B. B.; Sengupta, R.; Qazi, S.; Vachhani, H.; Yu, Y.; Rishi, A. K.; Majumdar, A. P., Curcumin enhances the effects of 5-fluorouracil and oxaliplatin in mediating growth inhibition of

- colon cancer cells by modulating EGFR and IGF-1R. *International journal of cancer* **2008**,*122* (2), 267-273.
72. Aggarwal, B. B.; Bhatt, I. D.; Ichikawa, H.; Ahn, K. S.; Sethi, G.; Sandur, S. K.; Natarajan, C.; Seeram, N.; Shishodia, S., 10 Curcumin—Biological and Medicinal Properties. **2006**.
73. Wang, Z.; Zhang, Y.; Banerjee, S.; Li, Y.; Sarkar, F. H., Retracted: Notch-1 down-regulation by curcumin is associated with the inhibition of cell growth and the induction of apoptosis in pancreatic cancer cells. *Cancer* **2006**,*106* (11), 2503-2513.
74. Shenouda, N. S.; Zhou, C.; Browning, J. D.; Ansell, P. J.; Sakla, M. S.; Lubahn, D. B.; MacDonald, R. S., Phytoestrogens in common herbs regulate prostate cancer cell growth *in vitro*. *Nutrition and cancer* **2004**,*49* (2), 200-208.
75. Sun, A.; Shoji, M.; Lu, Y. J.; Liotta, D. C.; Snyder, J. P., Synthesis of EF24- tripeptide chloromethyl ketone: a novel curcumin-related anticancer drug delivery system. *Journal of medicinal chemistry* **2006**,*49* (11), 3153-3158.
76. Ries, L. A.; Harkins, D.; Krapcho, M.; Mariotto, A.; Miller, B.; Feuer, E. J.; Clegg, L. X.; Eisner, M.; Horner, M.-J.; Howlader, N., SEER cancer statistics review, 1975-2003. **2006**.
77. Patra, D.; El Khoury, E.; Ahmadi, D.; Darwish, S.; Tafech, R. M., Effect of Curcumin on Liposome: Curcumin as a Molecular Probe for Monitoring Interaction of Ionic Liquids with 1, 2-Dipalmitoyl-sn-Glycero-3-Phosphocholine Liposome. *Photochemistry and photobiology* **2012**,*88* (2), 317-327.
78. Patra, D.; Barakat, C., Unique role of ionic liquid [bmin][BF₄] during curcumin-surfactant association and micellization of cationic, anionic and non-ionic surfactant solutions. *Spectrochimica Acta Part A: Molecular and Biomolecular Spectroscopy* **2011**,*79* (5), 1823-1828.
79. Mouslmani, M.; Bouhadir, K. H.; Patra, D., Poly (9-(2-diallylaminoethyl) adenine HCl-co-sulfur dioxide) deposited on silica nanoparticles constructs hierarchically ordered nanocapsules: curcumin conjugated nanocapsules as a novel strategy to amplify guanine selectivity among nucleobases. *Biosensors and Bioelectronics* **2015**,*68*, 181-188.
80. Patra, D.; Aridi, R.; Bouhadir, K., Fluorometric sensing of DNA using curcumin encapsulated in nanoparticle-assembled microcapsules prepared from poly (diallylammonium chloride-co-sulfur dioxide). *Microchimica Acta* **2013**,*180* (1-2), 59-64.
81. Sezgin, E.; Schwille, P., Fluorescence techniques to study lipid dynamics. *Cold Spring Harbor perspectives in biology* **2011**, a009803.
82. El Khoury, E.; Patra, D., Length of hydrocarbon chain influences location of curcumin in liposomes: Curcumin as a molecular probe to study ethanol induced interdigitation of liposomes. *Journal of Photochemistry and Photobiology B: Biology* **2016**,*158*, 49-54.
83. Chebl, M.; Moussa, Z.; Peurla, M.; Patra, D., Polyelectrolyte mediated nano hybrid particle as a nano-sensor with outstandingly amplified specificity and sensitivity for enzyme free estimation of cholesterol. *Talanta* **2017**,*169*, 104-114.
84. Wu, F.-Y.; Sun, M.-Z.; Xiang, Y.-L.; Wu, Y.-M.; Tong, D.-Q., Curcumin as a colorimetric and fluorescent chemosensor for selective recognition of fluoride ion. *Journal of Luminescence* **2010**,*130* (2), 304-308.
85. Anand, P.; Sundaram, C.; Jhurani, S.; Kunnumakkara, A. B.; Aggarwal, B. B., Curcumin and cancer: an “old-age” disease with an “age-old” solution. *Cancer letters* **2008**,*267* (1), 133-164.
86. Yang, K.-Y.; Lin, L.-C.; Tseng, T.-Y.; Wang, S.-C.; Tsai, T.-H., Oral bioavailability of curcumin in rat and the herbal analysis from *Curcuma longa* by LC-MS/MS. *Journal of chromatography B* **2007**,*853* (1-2), 183-189.
87. Lao, C. D.; Ruffin, M. T.; Normolle, D.; Heath, D. D.; Murray, S. I.; Bailey, J. M.; Boggs, M. E.; Crowell, J.; Rock, C. L.; Brenner, D. E., Dose escalation of a curcuminoid formulation. *BMC complementary and alternative medicine* **2006**,*6* (1), 10.

88. Liu, A.; Lou, H.; Zhao, L.; Fan, P., Validated LC/MS/MS assay for curcumin and tetrahydrocurcumin in rat plasma and application to pharmacokinetic study of phospholipid complex of curcumin. *Journal of pharmaceutical and biomedical analysis* **2006**,*40* (3), 720-727.
89. Maiti, K.; Mukherjee, K.; Gantait, A.; Saha, B. P.; Mukherjee, P. K., Curcumin–phospholipid complex: preparation, therapeutic evaluation and pharmacokinetic study in rats. *International journal of pharmaceutics* **2007**,*330* (1-2), 155-163.
90. Li, J.; Wang, X.; Zhang, T.; Wang, C.; Huang, Z.; Luo, X.; Deng, Y., A review on phospholipids and their main applications in drug delivery systems. *Asian journal of pharmaceutical sciences* **2015**,*10* (2), 81-98.
91. Takahashi, M.; Uechi, S.; Takara, K.; Asikin, Y.; Wada, K., Evaluation of an oral carrier system in rats: bioavailability and antioxidant properties of liposome-encapsulated curcumin. *Journal of Agricultural and Food Chemistry* **2009**,*57* (19), 9141-9146.
92. Cabral, H.; Kataoka, K., Progress of drug-loaded polymeric micelles into clinical studies. *Journal of Controlled Release* **2014**,*190*, 465-476.
93. Reddy, B.; Yadav, H. K.; Nagesha, D. K.; Raizaday, A.; Karim, A., Polymeric micelles as novel carriers for poorly soluble drugs. *Journal of nanoscience and nanotechnology* **2015**,*15* (6), 4009-4018.
94. Zhao, L.; Du, J.; Duan, Y.; Zhang, H.; Yang, C.; Cao, F.; Zhai, G., Curcumin loaded mixed micelles composed of Pluronic P123 and F68: preparation, optimization and *in vitro* characterization. *Colloids and Surfaces B: Biointerfaces* **2012**,*97*, 101-108.
95. Valeur, B.; Berberan-Santos, M. N., A brief history of fluorescence and phosphorescence before the emergence of quantum theory. *Journal of Chemical Education* **2011**,*88* (6), 731-738.
96. Lakowicz, J. R., Principles of Fluorescence Spectroscopy. 3rd ed.; Springer: New York, 2006.
97. Pitto-Barry, A.; Barry, N. P., Pluronic® block-copolymers in medicine: from chemical and biological versatility to rationalisation and clinical advances. *Polymer Chemistry* **2014**,*5* (10), 3291-3297.
98. Chattopadhyay, A.; Harikumar, K., Dependence of critical micelle concentration of a zwitterionic detergent on ionic strength: implications in receptor solubilization. *Febs Letters* **1996**,*391* (1-2), 199-202.
99. Patra, D.; Ahmadi, D.; Aridi, R., Study on interaction of bile salts with curcumin and curcumin embedded in dipalmitoyl-sn-glycero-3-phosphocholine liposome. *Colloids and Surfaces B: Biointerfaces* **2013**,*110*, 296-304.
100. Brito, R. M.; Vaz, W. L., Determination of the critical micelle concentration of surfactants using the fluorescent probe N-phenyl-1-naphthylamine. *Analytical biochemistry* **1986**,*152* (2), 250-255.
101. Batrakova, E.; Lee, S.; Li, S.; Venne, A.; Alakhov, V.; Kabanov, A., Fundamental relationships between the composition of pluronic block copolymers and their hypersensitization effect in MDR cancer cells. *Pharmaceutical research* **1999**,*16* (9), 1373-1379.
102. Aydin, F.; Chu, X.; Uppaladadiam, G.; Devore, D.; Goyal, R.; Murthy, N. S.; Zhang, Z.; Kohn, J.; Dutt, M., Self-Assembly and Critical Aggregation Concentration Measurements of ABA Triblock Copolymers with Varying B Block Types: Model Development, Prediction, and Validation. *The Journal of Physical Chemistry B* **2016**,*120* (15), 3666-3676.
103. Holland, R. J.; Parker, E. J.; Guiney, K.; Zeld, F. R., Fluorescence probe studies of ethylene oxide/propylene oxide block copolymers in aqueous solution. *The Journal of Physical Chemistry* **1995**,*99* (31), 11981-11988.
104. Kunwar, A.; Barik, A.; Priyadarsini, K.; Pandey, R., Absorption and fluorescence studies of curcumin bound to liposome and living cells. *BARC newsletter* **2007**,*285*, 213.

105. Jain, N. J.; Aswal, V.; Goyal, P.; Bahadur, P., Micellar structure of an ethylene oxide–propylene oxide block copolymer: a small-angle neutron scattering study. *The Journal of Physical Chemistry B* **1998**,*102* (43), 8452-8458.
106. Zhou, Z.; Chu, B., Anomalous association behavior of an ethylene oxide/propylene oxide ABA block copolymer in water. *Macromolecules* **1987**,*20* (12), 3089-3091.
107. Mortensen, K.; Pedersen, J. S., Structural study on the micelle formation of poly (ethylene oxide)-poly (propylene oxide)-poly (ethylene oxide) triblock copolymer in aqueous solution. *Macromolecules* **1993**,*26* (4), 805-812.
108. Alexandridis, P.; Nivaggioli, T.; Hatton, T. A., Temperature effects on structural properties of Pluronic P104 and F108 PEO-PPO-PEO block copolymer solutions. *Langmuir* **1995**,*11* (5), 1468-1476.
109. Reddy, P. M.; Venkatesu, P., Influence of ionic liquids on the critical micellization temperature of a tri-block co-polymer in aqueous media. *Journal of colloid and interface science* **2014**,*420*, 166-173.
110. Sujatha, J.; Mishra, A., Phase transitions in phospholipid vesicles: Excited state prototropism of 1-naphthol as a novel probe concept. *Langmuir* **1998**,*14* (9), 2256-2262.
111. Mizusaki, M.; Morishima, Y.; Dubin, P. L., Interaction of pyrene-labeled hydrophobically modified polyelectrolytes with oppositely charged mixed micelles studied by fluorescence quenching. *The Journal of Physical Chemistry B* **1998**,*102* (11), 1908-1915.
112. Palit, D.; Sapre, A.; Mittal, J., Picosecond studies on the electron transfer from pyrene and perylene excited singlet states to N-hexadecyl pyridinium chloride. *Chemical physics letters* **1997**,*269* (3-4), 286-292.
113. Chebl, M.; Abiad, M. G.; Moussa, Z.; Patra, D., Two modes of associations of curcumin with pre- and nanoaggregated chitosan oligosaccharide lactate: ionic strength and hydrophobic bile salt modulate partition of drug and self-assembly process. *The Journal of Physical Chemistry C* **2016**,*120* (20), 11210-11224.
114. Barry, J.; Fritz, M.; Brender, J. R.; Smith, P. E.; Lee, D.-K.; Ramamoorthy, A., Determining the effects of lipophilic drugs on membrane structure by solid-state NMR spectroscopy: the case of the antioxidant curcumin. *Journal of the American Chemical Society* **2009**,*131* (12), 4490-4498.
115. Pérez-Lara, A.; Ausili, A.; Aranda, F. J.; de Godos, A.; Torrecillas, A.; Corbalán-García, S.; Gómez-Fernández, J. C., Curcumin disorders 1, 2-dipalmitoyl-sn-glycero-3-phosphocholine membranes and favors the formation of nonlamellar structures by 1, 2-dielaidoyl-sn-glycero-3-phosphoethanolamine. *The Journal of Physical Chemistry B* **2010**,*114* (30), 9778-9786.
116. Román, M. R. A. J. S., *Smart Polymers and Their Applications*. 1st ed.; Woodhead publishing: Cambridge, UK, 2014.
117. Shtykov, S.; Rusanova, T. Y., Nanomaterials and nanotechnologies in chemical and biochemical sensors: Capabilities and applications. *Russian Journal of General Chemistry* **2008**,*78* (12), 2521-2531.
118. Akiyoshi, K.; Deguchi, S.; Moriguchi, N.; Yamaguchi, S.; Sunamoto, J., Self-aggregates of hydrophobized polysaccharides in water. Formation and characteristics of nanoparticles. *Macromolecules* **1993**,*26* (12), 3062-3068.
119. Oh, J. K.; Lee, D. I.; Park, J. M., Biopolymer-based microgels/nanogels for drug delivery applications. *Progress in polymer science* **2009**,*34* (12), 1261-1282.
120. Bodratti, A. M.; Sarkar, B.; Alexandridis, P., Adsorption of poly (ethylene oxide)-containing amphiphilic polymers on solid-liquid interfaces: Fundamentals and applications. *Advances in colloid and interface science* **2017**,*244*, 132-163.

121. Sarkar, B.; Venugopal, V.; Bodratti, A. M.; Tsianou, M.; Alexandridis, P., Nanoparticle surface modification by amphiphilic polymers in aqueous media: Role of polar organic solvents. *Journal of colloid and interface science* **2013**,*397*, 1-8.
122. Yang, L.; Alexandridis, P., Physicochemical aspects of drug delivery and release from polymer-based colloids. *Current Opinion in Colloid & Interface Science* **2000**,*5* (1-2), 132-143.
123. Alexandridis, P., Gold nanoparticle synthesis, morphology control, and stabilization facilitated by functional polymers. *Chemical Engineering & Technology* **2011**,*34* (1), 15-28.
124. Tadros, T. F., *Interfacial Phenomena and Colloid Stability—Industrial Applications*. De Gruyter: Berlin, Germany, 2015.
125. Tadros, T., Viscoelastic properties of sterically stabilised emulsions and their stability. *Advances in colloid and interface science* **2015**,*222*, 692-708.
126. Dhillon, N.; Aggarwal, B. B.; Newman, R. A.; Wolff, R. A.; Kunnumakkara, A. B.; Abbruzzese, J. L.; Ng, C. S.; Badmaev, V.; Kurzrock, R., Phase II trial of curcumin in patients with advanced pancreatic cancer. *Clinical Cancer Research* **2008**,*14* (14), 4491-4499.
127. Sahu, A.; Kasoju, N.; Goswami, P.; Bora, U., Encapsulation of curcumin in Pluronic block copolymer micelles for drug delivery applications. *Journal of biomaterials applications* **2011**,*25* (6), 619-639.
128. Khalil, C.; Shebawy, W., UVB damage onset and progression 24 h post exposure in human-derived skin cells. *Toxicology reports* **2017**,*4*, 441-449.
129. Khalil, C.; Al Hageh, C.; Korfali, S.; Khnayzer, R. S., Municipal leachates health risks: Chemical and cytotoxicity assessment from regulated and unregulated municipal dumpsites in Lebanon. *Chemosphere* **2018**,*208*, 1-13.
130. Khalil, C., Human skin explants an *in vitro* approach for assessing UVB induced damage. *Toxicology in vitro : an international journal published in association with BIBRA* **2018**,*53*, 193-199.
131. Al Hageh, C.; Al Assaad, M.; El Masri, Z.; Samaan, N.; El-Sibai, M.; Khalil, C.; Khnayzer, R. S., A long-lived cuprous bis-phenanthroline complex for the photodynamic therapy of cancer. *Dalton transactions (Cambridge, England : 2003)* **2018**,*47* (14), 4959-4967.
132. Bakand, S.; Winder, C.; Khalil, C.; Hayes, A., Toxicity assessment of industrial chemicals and airborne contaminants: transition from *in vivo* to *in vitro* test methods: a review. *Inhalation toxicology* **2005**,*17* (13), 775-87.
133. Bakand, S.; Winder, C.; Khalil, C.; Hayes, A., An experimental *in vitro* model for dynamic direct exposure of human cells to airborne contaminants. *Toxicology letters* **2006**,*165* (1), 1-10.
134. Ayandele, E.; Sarkar, B.; Alexandridis, P., Polyhedral Oligomeric Silsesquioxane (POSS)-Containing Polymer Nanocomposites *nanomaterials* **2012**,*2*, 445-475.
135. Chidambaram, M.; Krishnasamy, K., Drug-Drug/Drug-Excipient Compatibility Studies on Curcumin using Non-Thermal Methods *Advanced Pharmaceutical Bulletin* **2014**,*4*, 309-312.
136. Patra, R. E. K. a. D., Tuning the surface of Au nanoparticles using poly(ethylene glycol)-block-poly(propylene glycol)-block-poly(ethylene glycol): enzyme free and label free sugar sensing in serum samples using resonance Rayleigh scattering spectroscopy. *Physical Chemistry Chemical Physics* **2018**,*20*, 9616-9629
137. Squires, M. S.; Hudson, E. A.; Howells, L.; Sale, S.; Houghton, C. E.; Jones, J. L.; Fox, L. H.; Dickens, M.; Prigent, S. A.; Manson, M. M., Relevance of mitogen activated protein kinase (MAPK) and phosphatidylinositol-3-kinase/protein kinase B (PI3K/PKB) pathways to induction of apoptosis by curcumin in breast cells. *Biochemical Pharmacology* **2003**,*65* (3), 361-376.
138. Amin, A. R. M. R.; Haque, A.; Rahman, M. A.; Chen, Z. G.; Khuri, F. R.; Shin, D. M., Curcumin Induces Apoptosis of Upper Aerodigestive Tract Cancer Cells by Targeting Multiple Pathways. *PLOS ONE* **2015**,*10* (4), e0124218.

139. Atsumi, T.; Tonosaki, K.; Fujisawa, S., Comparative cytotoxicity and ROS generation by curcumin and tetrahydrocurcumin following visible-light irradiation or treatment with horseradish peroxidase. *Anticancer research* **2007**,*27* (1a), 363-71.
140. Yao, J.; Yang, M.; Duan, Y., Chemistry, Biology, and Medicine of Fluorescent Nanomaterials and Related Systems: New Insights into Biosensing, Bioimaging, Genomics, Diagnostics, and Therapy. *Chemical Reviews* **2014**,*114*, 6130-6178.
141. Nafisi, S.; Adelzadeh, M.; Norouzi, Z.; Sarbolouki, M. N., Curcumin Binding to DNA and RNA. *DNA and Cell Biology* **2009**,*28* (4).
142. Kurdi, R. E.; Patra, D., Amplification of resonance Rayleigh scattering of gold nanoparticles by tweaking into nanowires: Bio-sensing of α -tocopherol by enhanced resonance Rayleigh scattering of curcumin capped gold nanowires through non-covalent interaction. *talanta* **2017**,*168*, 82-90.
143. Bisht, S.; Feldmann, G.; Soni, S.; Ravi, R.; Karikar, C.; Maitra, A.; Maitra, A., Polymeric nanoparticle-encapsulated curcumin ("nanocurcumin"): a novel strategy for human cancer therapy. *Nanobiotechnology* **2007**,*5*.
144. Ma, Z.; Haddadi, A.; Molavi, O.; Lavasanifar, A.; Lai, R.; Samuel, J., Micelles of poly(ethylene oxide)-*b*-poly(ϵ -caprolactone) as vehicles for the solubilization, stabilization, and controlled delivery of curcumin. *Biomedical Materials Research Part A* **2007**,*86* (2), 300-310.
145. Singla, P.; Chabba, S.; Mahajan, R. K., A systematic physicochemical investigation on solubilization and *in vitro* release of poorly water soluble oxcarbazepine drug in pluronic micelles. *Colloids and Surfaces A: Physicochemical and Engineering Aspects* **2016**,*504*, 479-488.
146. Nguyen-Kim, V.; Prévostac, S.; Seidel, K.; Maier, W.; Marguerre, A.-K.; Oetter, G.; Tadros, T.; Gradzielski, M., Solubilization of active ingredients of different polarity in Pluronic® micellar solutions – Correlations between solubilize polarity and solubilization site. *Colloid and Interface Science* **2016**,*477*, 94-102.
147. Bong, P.-H., Spectral and Photophysical Behaviors of Curcumin and Curcuminoids. *Bulletin of the Korean Chemical Society* **2000**,*21* (1), 81-86.
148. Alberts, B.; Johnson, A.; Lewis, J.; Raff, M.; Roberts, K.; Walter, P., Molecular Biology of the Cell. In *The Structure and Function of DNA* [Online] 4th ed.; Garland science: New York, 2002.
149. Sinden, R. R., DNA Structure and Function. Elsevier: 2012.
150. Karsten, U.; Wollenberger, A., Improvements in the ethidium bromide method for direct fluorometric estimation of DNA and RNA in cell and tissue homogenates. *Analytical Biochemistry* **1977**,*77* (2), 464-470.
151. Tanious, F. A.; Veal, J. M.; Buczak, H.; Ratmeyer, L. S.; Wilson, W. D., DAPI (4Z,6-Diamidino-2-phenylindole) Binds Differently to DNA and RNA: Minor-Groove Binding at AT Sites and Intercalation at AU Sites. *Biochemistry* **1992**,*31* (12), 3103-3112.
152. L.Singer, V.; J.Jones, L.; T.Yue, S.; P.Haugland, R., Characterization of PicoGreen Reagent and Development of a Fluorescence-Based Solution Assay for Double-Stranded DNA Quantitation. *Analytical Biochemistry* **1997**,*249* (2), 228-238.
153. Vitzthuma, F.; Geigera, G.; Bisswanger, H.; Brunner, H.; Bernhagen, J., A Quantitative Fluorescence-Based Microplate Assay for the Determination of Double-Stranded DNA Using SYBR Green I and a Standard Ultraviolet Transilluminator Gel Imaging System. *Analytical Biochemistry* **1999**,*276* (1), 59-64.